WEST VIRGINIA UNIVERSITY
College of Engineering



# ANALYSIS OF CIRCULATION CONTROLLED AIRFOILS

Edward H. Gibbs and Nathan Ness
June 1975

Prepared Under Contract
N00014-68-A-0512

for the

Office of Naval Research
Vehicle Technology, Code 211
(NR 215-163)



West Virginia University
Department of Aerospace Engineering
Morgantown, West Virginia

WEST VIRGINIA UNIVERSITY
College of Engineering

Aerospace
Engineering
TR-43

# ANALYSIS OF CIRCULATION CONTROLLED AIRFOILS

Edward H. Gibbs and Nathan Ness
June 1975

Prepared Under Contract
N00014-68-A-0512

for the

Office of Naval Research
Vehicle Technology, Code 211
(NR 215-163)



West Virginia University
Department of Aerospace Engineering
Morgantown, West Virginia

Unclassified
Security Classification

## DOCUMENT CONTROL DATA - R & D

*Security classification of title, body of abstract and indexing annotation must be entered when the overall report is classified)*

1. ORIGINATING ACTIVITY (Corporate author)

West Virginia University
Department of Aerospace Engineering
Morgantown, WV 26506

2a. REPORT SECURITY CLASSIFICATION

Unclassified

2b. GROUP

3. REPORT TITLE

Analysis of Circulation Controlled Airfoils

4. DESCRIPTIVE NOTES (Type of report and inclusive dates)

Scientific

5. AUTHOR(S) (First name, middle initial, last name)

Edward H. Gibbs and Nathan Ness

| 6. REPORT DATE | 7a. TOTAL NO. OF PAGES | 7b. NO. OF REFS |
|---|---|---|
| June 1975 | 200 | 33 |

| 8a. CONTRACT OR GRANT NO. | 9a. ORIGINATOR'S REPORT NUMBER(S) |
|---|---|
| N00014-68-A-0512 | |
| b. PROJECT NO. NR 215-163 | Aerospace Engineering TR-43 |
| c. | 9b. OTHER REPORT NO(S) (Any other numbers that may be assigned this report) |
| d. | None |

10. DISTRIBUTION STATEMENT

Approved for public release; distribution unlimited.

| 11. SUPPLEMENTARY NOTES | 12. SPONSORING MILITARY ACTIVITY |
|---|---|
| | Office of Naval Research<br>Vehicle Technology, Code 211<br>Arlington, Virginia 22217 |

13. ABSTRACT

A self-contained analysis for arbitrary circulation controlled airfoils in incompressible flow is developed. The analysis predicts the blowing slot conditions required to produce a specified lift coefficient on a given airfoil with given free stream conditions.

An iterative procedure is used to find the blowing slot conditions that allow the Thwaites condition of constant pressure in the separated region to be satisfied. With the input given, a potential flow analysis is performed using the Theodorsen method. Boundary layer analyses for the lower and upper surfaces then yield the separation pressure on the lower surface and the boundary layer properties at the slot on the upper surface. The flow is initially laminar and usually becomes turbulent. The Cebeci, Smith finite difference method is used and an eddy viscosity model is used for turbulent flow. Blowing slot values are assumed and a turbulent wall jet analysis is performed to determine the wall pressure at separation on the upper surface. If the two separation pressures, upper and lower, do not agree, new slot values are assumed and the wall jet analysis is repeated. Wall jet calculations include curvature effects on the jet and external flows, and approximate corrections for large pressure gradients. An eddy viscosity model is used but is modified to allow a negative shear stress at the velocity maximum. A fully developed laminar or turbulent channel flow is used for the slot profile. A finite difference method based on the Keller, Cebeci method is used for wall jet calculations.

Calculations are performed and compared to Kind's experimental data. Results are in good agreement for the blowing coefficient and local flow details.

DD FORM 1 NOV 65 1473 (PAGE 1)

S/N 0101-807-6801

Unclassified
Security Classification

| 14 KEY WORDS | LINK A | | LINK B | | LINK C | |
|---|---|---|---|---|---|---|
| | ROLE | WT | ROLE | WT | ROLE | WT |
| Circulation Controlled Airfoils | | | | | | |
| Incompressible Flow | | | | | | |
| Trailing Edge Wall Jet | | | | | | |
| Coefficient of Lift | | | | | | |
| Blowing Coefficient | | | | | | |
| Separated Flow | | | | | | |
| Theodorsen Potential Flow Analysis | | | | | | |
| Cebeci, Smith Boundary Layer Analysis | | | | | | |
| Modified Keller, Cebeci Wall Jet Analysis | | | | | | |
| Thwaites Wake Criterion | | | | | | |

# ABSTRACT

A self-contained analysis for arbitrary circulation controlled airfoils in incompressible flow is developed. The analysis predicts the blowing slot conditions required to produce a specified lift coefficient on a given airfoil with given free stream conditions.

An iterative procedure is used to find the blowing slot conditions that allow the Thwaites condition of constant pressure in the separated region to be satisfied. With the input given, a potential flow analysis is performed using the Theodorsen method. Boundary layer analyses for the lower and upper surfaces then yield the separation pressure on the lower surface and the boundary layer properties at the slot on the upper surface. The flow is initially laminar and usually becomes turbulent. The Cebeci, Smith finite difference method is used and an eddy viscosity model is used for turbulent flow. Blowing slot values are assumed and a turbulent wall jet analysis is performed to determine the wall pressure at separation on the upper surface. If the two separation pressures, upper and lower, do not agree, new slot values are assumed and the wall jet analysis is repeated. Wall jet calculations include curvature effects on the jet and external flows, and approximate corrections for large pressure gradients. An eddy viscosity model is used but is modified to allow a negative shear stress at the velocity maximum. A fully developed laminar or turbulent channel flow is used for the slot profile. A finite difference method based on the Keller, Cebeci method

is used for wall jet calculations.

Calculations are performed and compared to Kind's experimental data. Results are in good agreement for the blowing coefficient and local flow details.

# ACKNOWLEDGMENTS

This report represents the dissertation of the first author submitted to the Graduate School of West Virginia University in partial fulfillment of the requirements for the degree of Doctor of Philosophy. The first author wishes to acknowledge the guidance of Dr. Nathan Ness, his dissertation advisor, during the formulation of this work.

The authors wish to acknowledge Dr. Jerome B. Fanucci for his continued interest in this problem.

This work was funded in part by the Office of Naval Research, Mr. Tom L. Wilson, Contract Monitor to West Virginia University under Navy V/STOL Aerodynamics Contract N00014-68-A-0512.

TABLE OF CONTENTS

# LIST OF FIGURES

# LIST OF TABLES

# NOMENCLATURE

## English Symbols

$a$ Fig. 3; radius of circle in Theodorsen transformation

$A$ matrix in finite difference solution

$A_o$ a group of terms in $\epsilon_i^+$

$A_m$ Eq. (3-6a); Fourier coefficients

$b$ Eq. (3-1); coefficient in the complex transformation $\mathcal{Z}\mathcal{Z}'$; also $\ln 2$, a constant

$B$ matrix in finite difference solution

$B_m$ Eq. (3-6b); Fourier coefficients

$C$ chord length

$\mathcal{C}$ blowing slot thickness

$C$ matrix in finite difference solution

$C_f$ local skin friction coefficient

$C_\ell$ sectional lift coefficient

$C_{\dot{m}}$ Eq. (5-50); mass flow coefficient

$C_\mu$ Eq. (5-49); momentum coefficient

$C_p$ local pressure coefficient

$C_{p_{SEP_L}}$ pressure coefficient at separation on lower surface

$C_{p_{SEP_U}}$ pressure coefficient at separation on upper surface (at the wall)

$D$ matrix in finite difference solution

$E$ matrix in finite difference solution

$f$ dimensionless stream function

$F$ dimensionless stream function

$f(\xi)$ streamline curvature term

$f_\delta$ value of $f$ when $\eta = \eta_\delta$

$g$ Eq. (4-11); a general function of $\xi^*$; also Eq. (5-35); dimensionless curvature term

$G$ Eq. (5-35)

$\tilde{h}$ equation following Eq. (3-4b)

$H$ Eq. (5-36)

$\tilde{h}_j$ $\eta$ step size in finite difference grid

$K$ constant ratio between lengths of two adjacent intervals in the $\eta$ grid

$k_n$ $\xi$ step size in finite difference grid

$K_1$ constant in eddy viscosity expression

$K_2$ constant in eddy viscosity expression

$K_3$ constant in eddy viscosity expression

$\mathcal{L}$ Eq. (5-34); term in shear stress expression; also matrix in finite difference solution

$L_o$ Figs. 4, 5; a scale length

$N$ Eq. (5-15a); an exponent

$q$ Eq. (5-41); term in finite difference solution

$Q$ matrix in finite difference solution

$r$ Eq. (5-42); term in finite difference solution; also radial distance from axis of symmetry

$R$ surface radius of curvature; also Fig. 3; radial distance in $y$ plane

$R'$ Fig. 3; radial distance in $Z'$ plane

$R_{LE}$ Fig. 3; leading edge radius of curvature

$R_{TE}$ Fig. 3; trailing edge radius of curvature

$Re_{\delta^*}$ Eq. (4-24); displacement thickness Reynolds number

$Re_\theta$ Eq. (4-25); momentum thickness Reynolds number

$Re_T$ Eq. (5-16); turbulent Reynolds number

$Re_\infty$ $\frac{V_\infty C}{\nu}$; free stream Reynolds number

$s$ arc length along body surface; also Eq. (5-43); term in finite difference solution

$S$ Eq. (5-31); term for eddy viscosity expression

$t$ transverse curvature term; also Eq. (5-44); term in finite difference solution

$T$ Eq. (5-32); term for eddy viscosity expression

$u$ velocity in $x$ direction

$u'$ perturbation velocity in $x$ direction

$\mathcal{U}$ matrix in finite difference solution

$U_d$ Eq. (5-16); velocity deficit

$u_e$ potential flow velocity at surface, $u_e = V_b$

$U_e$ Figs. 4, 5; velocity at outer edge of wall jet

$u_{MIN}$ Fig. 5; minimum velocity

$u_z$ velocity in $x_c$ direction in $z$ plane

$u_\delta$ Figs. 4, 5; velocity

$u_\tau$ friction velocity, $\sqrt{\tau_w/\rho}$

$v$ velocity in $y$ direction

$v'$ perturbation velocity in $y$ direction

$V$ resultant velocity

$V_b$ resultant inviscid velocity at surface

$v_z$ velocity in $y_c$ direction in $z$ plane

$w$ complex potential function

$W$ general function

$x$ Fig. 1; curvilinear coordinate measured from front stagnation point

$x_c$ Fig. 3; chordwise coordinate in $\mathcal{Z}$ plane

$y$ Fig. 1; curvilinear coordinate normal to surface

$y_c$ Fig. 3; coordinate normal to chord in $\mathcal{Z}$ plane

$\mathcal{Z}$ Fig. 3; complex $\mathcal{Z}$ plane; also matrix in finite difference solution

$\mathcal{Z}'$ Fig. 3; complex $\mathcal{Z}'$ plane

Greek Symbols

$\alpha$ two dimensional angle of attack

$\alpha_m$ Eq. (3-5); real constants in Theodorsen transformation

$\beta$ Eq. (3-17b); pressure gradient parameter

$\beta_m$ Eq. (3-5); real constants in Theodorsen transformation

$\gamma$ Eq. (5-20); intermittency function; also coefficient in Eq. (5-44)

$\Gamma$ circulation

$\delta$ boundary layer thickness; also matrix in finite difference solution

$\Delta$ wall jet thickness

$\delta^*$ displacement thickness

$\delta()$ perturbation quantity in finite difference solution

$\epsilon$ Eq. (3-7); also $\epsilon = 0$ for two dimensional flows and $\epsilon = 1$ for axisymmetric flows

$\epsilon^+$ dimensionless eddy viscosity

$\epsilon_i^+$ dimensionless inner eddy viscosity

$\epsilon_o^+$ dimensionless outer eddy viscosity

$\epsilon_M^+$ Eq. (5-16); dimensionless eddy viscosity in outer region of wall jet

$\epsilon_{UBL}^+$ maximum value of dimensionless eddy viscosity in upstream boundary layer

$\zeta$ Fig. 3; complex $\zeta$ plane; also coefficient in Eq. (5-44)

$\eta$ Eq. (4-1b); transformed independent variable; also Eq. (5-7); dimensionless independent variable, $y/C$

$\eta_\delta$ value of $\eta$ when $f' = .995$

$\eta_\Delta$ value of $\eta$ at $y = \Delta$

$\eta_{L_o}$ $L_o/C$

$\Theta$ momentum thickness; also coefficient in Eq. (5-44)

$\lambda$ Fig. 3; independent variable in $\zeta$ plane; also coefficient in Eq. (5-44)

$\lambda_K$ a constant value of $\lambda$

$\mu$ coefficient of viscosity

$\nu$ kinematic viscosity

$\xi$ Eq. (4-1a); transformed streamwise independent variable; also Eq. (5-7); dimensionless independent variable, $x/C$

$\xi^*$ Eq. (3-17a); dimensionless transformed streamwise independent variable

$\xi_{SLOT} = \xi_1$ ; value of $\xi$ at the blowing slot location

$\pi$ group of terms in Eq. (5-29)

$\rho$ mass density

$\sigma$ standard deviation of intermittency function; also coefficient in Eq. (5-44)

$\tau$ shear stress

$\varphi$ Fig. 3; independent variable in $\zeta$ plane; also $\varphi$ is the angular inclination of the body; also $\varphi = f - \eta$ is a translated dimensionless stream function; also coefficient in Eq. (5-44)

$\Delta\varphi = \varphi - \varphi_0$ ; perturbation quantity

$\psi$ Eq. (3-2b); independent variable in $Z'$ plane; also $\psi$ is the stream function; also coefficient in Eq. (5-44)

$\omega$ Eq. (3-2b); independent variable in $Z'$ plane; also $\omega = 0$ or 1 if transverse curvature is neglected or included in the boundary layer analysis; also coefficient in Eq. (5-43)

Subscripts and Superscripts

$( )_{AVE}$ average value

$( )_{BL}$ Eq. (5-52); value in upstream boundary layer at slot

$( )_e$ at outer edge of boundary layer or wall jet

$( )^{(i)}$ value on $i$ th iteration

$( )_i$ value at $\eta_i$

$( )_{J_e}$ value at grid point where outer edge conditions are applied

$( )_m$ Figs. 4, 5; value at $y = y_m$ or $\eta = \eta_m$

$( )_{STAG}$ stagnation value

$( )_w$ value at wall

$( )_{y_m+L_0}$ Figs. 4, 5; value at $y = y_m + L_0$

$( )_{y_m+2.3L_0}$ Fig. 5; value at $y = y_m + 2.3L_0$

$( )^*$ dimensionless value

$( )_\infty$ free stream value; at infinity

# 1. INTRODUCTION

Interest in STOL flight has led to an interest in circulation controlled airfoils. A circulation controlled airfoil has a bluff trailing edge with a tangential blowing slot located slightly upstream of the trailing edge. Experiments by Kind (Refs. 4, 5, 15) and later by others have shown that such an airfoil can produce relatively high lift coefficients for relatively low blowing rates from the slot. Circulation controlled airfoils thus provide a relatively simple and efficient method of obtaining STOL flight.

The principle of a circulation controlled airfoil is based on the fact that there are any number of valid potential flow solutions (each with a different value of the circulation, and therefore lift) for an airfoil with a bluff trailing edge. In a real (viscous) fluid, the circulation that will actually develop depends on the separation characteristics on the upper and lower surfaces. By introducing blowing on the upper surface, separation on the upper surface is delayed. As the blowing is increased, the upper surface separation point moves further back around toward the lower surface. As this occurs, the potential flow rear stagnation point also moves down, and thus the front stagnation point and the circulation are altered. The blowing therefore causes the flow over the entire airfoil to be altered. A relatively small change in the location of the stagnation point results in a large change in the circulation, and therefore in the lift. Since the blowing is used only to delay separation, the amount required is small compared to that required for a jet flap.

The blowing is effective in delaying separation because of the Coanda effect. This effect (Ref. 2) refers to the ability of a plane wall jet to follow the contour of a convex curved boundary adjacent to it. Downstream of the blowing slot, a wall jet develops on the convex surface of the airfoil. Because of the Coanda effect, the wall jet tends to remain attached to the surface. Since the wall jet is considerably more energetic than the conventional boundary layer that would exist if the wall jet were not present, the wall jet can resist separation for a significantly longer distance.

The flow conditions on a circulation controlled airfoil are indicated in Fig. 1. Beginning at the front stagnation point, a boundary layer develops along the lower surface and eventually separates. Also beginning at the front stagnation point, a boundary layer develops along the upper surface and eventually reaches the blowing slot. Both the upper and lower surface boundary layer are initially laminar and then usually become turbulent. A turbulent wall jet develops downstream of the blowing slot and eventually separates. A typical wall jet development is illustrated in Fig. 2. A separation region exists between the wall jet separation point and the lower surface boundary layer separation point.

For a given airfoil with given free stream conditions, the upper surface separation point is determined by the amount of blowing used. A change in the airfoil shape or free stream conditions also results in a change in the separation point, so the circulation is a function of the airfoil shape, free stream conditions, and blowing rate.

The purpose of the present analysis is to obtain a self-contained procedure to predict the performance of arbitrary circulation controlled airfoils. An outline of the procedure is given in the next section.

## 2. OUTLINE OF THE THEORY

The purpose of the present analysis is to predict the blowing slot conditions required to produce a specified lift coefficient for a given circulation controlled airfoil with given free stream conditions. This section presents an outline of the calculation procedure and general considerations involved. The following three sections present details of the calculations along with a review of the pertinent literature.

Input for the present analysis consists of the airfoil geometry, the angle of attack $\alpha$, the free stream Reynolds number $R_{e_\infty}$, and the prescribed lift coefficient $C_\ell$. The airfoil geometry includes the location and thickness of the blowing slot, which is assumed to be tangential to the airfoil surface.

With the input given, a potential flow analysis is performed. The potential flow analysis provides the location of the front stagnation point, the rear (potential flow) stagnation point, and the velocity and pressure distribution around the airfoil. The velocity and pressure distributions are then converted to the form required for a boundary layer analysis.

A boundary layer analysis is then performed for the lower surface of the airfoil. The analysis starts at the front stagnation point and proceeds downstream until separation occurs. With the location of the separation point known, the pressure coefficient at separation on the lower surface $C_{P_{SEP_L}}$ is known from the potential flow analysis. The boundary layer flow is initially laminar, but

usually becomes turbulent before separation occurs. For low Reynolds numbers the flow may remain laminar, but in either case the analysis determines $C_{P_{SEP_L}}$.

A boundary layer analysis is also performed for the upper surface of the airfoil. The analysis starts at the front stagnation point and proceeds downstream to the blowing slot. In general, the last point at which boundary layer calculations are performed is slightly upstream of the blowing slot; however, the boundary layer properties at this point are used for the boundary layer properties at the blowing slot. The upper surface boundary layer is also initially laminar, but becomes turbulent before it reaches the blowing slot. Because of the prevailing pressure gradients, the upper surface boundary layer will normally become turbulent even for relatively low Reynolds numbers. If the boundary layer separates upstream of the blowing slot, calculations are terminated. If the boundary layer remains attached at the slot, the analysis provides the boundary layer properties at the slot.

A turbulent wall jet analysis is then performed. The analysis begins at the blowing slot and proceeds downstream until separation occurs. When separation occurs, the wall pressure coefficient at separation on the upper surface $C_{P_{SEP_U}}$ is known from the wall jet analysis. The correct blowing slot conditions are those conditions that result in a constant wall pressure in the separated region, i.e., $C_{P_{SEP_U}} = C_{P_{SEP_L}}$. This is known as the Thwaites condition (Ref. 10), and is also experimentally justified. Since it is nec-

essary to know the blowing slot conditions in order to perform the wall jet calculations to determine $C_{p_{SEP_U}}$, an iterative procedure is required. Blowing slot conditions are assumed and these conditions, along with the known upstream boundary layer properties, provide the starting conditions for the turbulent wall jet analysis. Wall jet calculations are then performed from the blowing slot downstream until separation occurs, yielding a value of $C_{p_{SEP_U}}$. In general, the calculated value of $C_{p_{SEP_U}}$ will not equal the previously determined value of $C_{p_{SEP_L}}$. New blowing slot conditions are then assumed and the wall jet calculations are repeated until $C_{p_{SEP_U}}$ and $C_{p_{SEP_L}}$ agree to within a prescribed tolerance. Then the Thwaites condition is satisfied, and the assumed blowing slot conditions are the correct ones for the prescribed input conditions.

The procedure described above constitutes a self-contained analysis of circulation controlled airfoils, provided the calculations can be performed for arbitrary airfoil shapes without the use of experimental data. Well developed and tested general methods are available for the potential flow and boundary layer calculations. The wall jet region is one of high complexity. Theories for this region are presently semi-empirical relying as they do on experimental data such as the surface pressure distribution. A major effort in this work involved the generation of a self-contained analysis for the wall jet region.

The potential flow is calculated by the Theodorsen method (Ref. 7) of conformal transformation. This is an exact method and applies to arbitrary airfoil shapes. It can also be used without difficulty in the present application where the lift coefficient is prescribed. Details of the method are given in Section 3.

Boundary layer calculations are performed using the Cebeci, Smith finite difference method (Ref. 8). For turbulent flow, the Reynolds stresses are evaluated using an eddy viscosity coefficient, while for laminar flow the eddy viscosity coefficient is set equal to zero. The method provides an exact numerical solution for laminar flow, and has been found to be one of the better methods for turbulent flow (Ref. 13). Transition from laminar to turbulent flow is assumed to occur when the momentum thickness Reynolds number is 640 for a favorable pressure gradient or 320 for an adverse pressure gradient. Gaster's (Ref. 9) experimental relations for the bursting of short laminar separation bubbles are also included in the transition cirteria if the flow is approaching laminar separation. If trip wires are used, transition is assumed to occur at the location of the trip wire (if transition has not already occurred upstream of the wire). Separation for either laminar or turbulent flow is determined by the wall shear stress becoming zero. Details of the method are given in Section 4.

There are several difficulties that complicate the wall jet analysis. The presence of the upstream boundary layer means that there is always a relative minimum in the velocity profile for some distance downstream of the blowing slot. For typical circulation con-

trolled airfoil applications, however, the velocity minimum is only significant for a relatively short distance downstream of the slot. The wall jet profile of most significance for circulation control applications is therefore one with a velocity maximum but no minimum. The inner portion (below the velocity maximum) of such a profile has features of a conventional turbulent boundary layer, while the outer portion (above the velocity maximum) has features of a free turbulent jet. These analogies are not exact, however, because the two regions develop simultaneously. Eddy viscosity models seem to give reasonable shear stress results for most of the inner and outer regions, but in general a somewhat arbitrary fairing is required to obtain a continuous eddy viscosity distribution. This is because the eddy viscosity in the outer region tends to be much larger (a difference of a factor of 10 is not uncommon). Of perhaps more fundamental importance is the fact that an eddy viscosity model does not seem to be accurate near the velocity maximum. Experiments show that the shear stress near the velocity maximum is usually negative, with a magnitude comparable to the wall shear stress. However, an eddy viscosity approach gives a zero shear stress at the velocity maximum. In the case of a flow with curvature an eddy viscosity approach gives a nonzero shear stress at the velocity maximum, but the magnitude of the shear stress is nowhere near large enough to agree with experiment.

For circulation control applications, additional direct and indirect difficulties arise because the streamlines have a small radius of curvature. This results from a small surface radius of curvature

plus the Coanda effect. A conventional order of magnitude analysis shows that the radius of curvature of a streamline is ( $\mathcal{R} + y$ ), where $\mathcal{R}$ is the surface radius of curvature and $y$ is the normal coordinate of the streamline. The normal pressure gradient is therefore no longer negligible and the pressure varies across the jet. From the irrotational flow results, which must also be corrected for curvature effects, the velocity and pressure are known at the outer edge of the jet. However, the pressure in the jet, including the wall pressure, must be calculated during the wall jet solution. These direct curvature effects can be handled without difficulty by retaining appropriate curvature terms in the equations; however, the indirect effects of curvature are more of a problem. The most significant indirect effect is that large potential flow velocity and pressure gradients are associated with a small surface radius of curvature. As a result of the sustained severe adverse pressure gradient, the wall jet thickens rapidly, and a streamline radius of curvature is no longer equal to ( $\mathcal{R} + y$ ). If this effect is not adequately accounted for, the calculated wall pressure will not be accurate, so separation cannot be determined accurately. Retaining additional terms in the $y$ momentum equation can account for this effect. Unfortunately, however, the significant additional term required cannot be handled exactly within boundary layer theory since it involves second order streamwise derivatives. Over the region where the above correction is required, an analogous correction to the potential flow velocity is required to obtain an accurate value for the outer edge of the jet.

Curvature also tends to increase the shear stress in the outer portion of the jet, and tends to decrease it in the inner portion. Corrections are available to account for this, but additional uncertainties are introduced since the outer turbulence spilling over into the inner region tends to offset the decrease in the inner region. A final difficulty, which is not inherent but is common, is that many circulation controlled airfoils have a discontinuous radius of curvature at the blowing slot. This results from truncating the airfoil at the blowing slot and adding a circular trailing edge in place of the truncated portion. In general, it is possible to do this and still maintain a continuous shape and slope, but the radius of curvature is normally discontinuous. For calculations, the radius can be faired in, but it seems one fairing is appropriate for the wall jet equations while another is appropriate for the outer edge conditions.

The basic formulation of the wall jet problem consists of the boundary layer equations for the case where the surface radius of curvature is the same order of magnitude as the thickness of the viscous region. The turbulent Reynolds stresses are evaluated in terms of an eddy viscosity coefficient. This basic formulation is altered to allow the shear stress to be negative at the velocity maximum, and to correct the $y$ momentum equation for streamline curvature effects that are not adequately described by conventional boundary layer approximations. These alterations were found to be necessary in order to obtain useful results, although the need for

them could probably be reduced by use of experimental data in the calculations. The shear stress modification applies near the velocity maximum and is based on an extension of mixing length theory. The curvature modification uses average values to approximate a term that is otherwise unmanageable. Both of these modifications are preliminary, but seem to be workable. To obtain the outer boundary conditions, the potential flow velocity is modified by a standard curvature correction along with an additional correction similar to that used in the wall jet. The pressure is obtained from the velocity and total pressure, where the total pressure allows for the remains of the upstream boundary layer. This procedure is used for the outer edge conditions downstream of the point where the velocity minimum essentially disappears. Upstream of that point, the wall jet calculations include the relative minimum velocity, and the outer edge conditions apply at a point corresponding to the outer edge of the upstream boundary layer. Outer edge conditions for this region are taken as the uncorrected potential flow velocity and pressure. The reasons for using different conditions for the two regions are to allow for the curvature discontinuity that typically occurs at the slot, and to switch smoothly from a profile with a relative minimum velocity to one without a minimum.

The wall jet equations are solved by a finite difference method based on the Keller, Cebeci method (Ref. 14). Details are given in Section 5. Although most wall jet analyses use integral methods, a finite difference method was selected since it offered some potential advantages, such as being able to determine separation by the wall

shear stress becoming zero, having the possibility of more flexability in handling profiles with a minimum velocity, and being able to start at the slot without requiring a separate mixing region analysis. A disadvantage is that more detailed information is required, but the more elaborate integral methods require almost the same information. Since the wall jet calculations are repeated during the iterative procedure, a relatively quick and efficient procedure is required. Also, the shape of a wall jet profile can require two to three times as many grid points as a conventional boundary layer in order to obtain comparable accuracy in the solution. Therefore, a method that is capable of reasonable accuracy with a relatively coarse grid is helpful. The Keller, Cebeci method satisfies these requirements and is relatively easy to use and was therefore selected.

## 3. POTENTIAL FLOW ANALYSIS

The potential flow is found by the Theodorsen method of conformal transformation. This is a direct method for finding the potential flow over a given arbitrary, closed two-dimensional body. The method is exact although in practice solutions must be obtained numerically. The Theodorsen method is reviewed herein in sufficient detail so that the computer program in the Appendix can be understood. Additional details may be found in Ref. 7.

It is well known from potential flow theory that the flow over a given airfoil can be found by conformally transforming the airfoil shape into a circle. The Theodorsen method transforms the given airfoil shape into a circle with the aid of an intermediate transformation as shown in Fig. 3. The reason for using the intermediate transformation and for taking the airfoil coordinate system as shown is that convergence of the final transformation is enhanced.

The first transformation maps the airfoil shape ( $Z$ plane) into a "nearly circular" curve $C'$ in the $Z'$ plane. The transformation is analogous to a Joukowski transformation, and is given by

$$Z = Z' + \frac{b^2}{Z'} \tag{3-1}$$

where

$$Z = x_c + i\, y_c \tag{3-2a}$$

$$Z' = b e^{\psi} e^{i\omega} \tag{3-2b}$$

The independent variables in the $Z'$ plane are taken as $(\psi, \omega)$. The constant $b$ is defined by

$$4b = C - \frac{R_{LE}}{2} - \frac{R_{TE}}{2}$$

where $R_{LE}$ and $R_{TE}$ are the leading and trailing edge radii of curvature of the airfoil.

Substituting (3-2) into (3-1) and equating real and imaginary parts gives

$$x_c = 2b \cos\omega \cosh\psi \qquad (3\text{-}3a)$$

$$y_c = 2b \sin\omega \sinh\psi \qquad (3\text{-}3b)$$

This transformation is unique if $\omega$ is restricted to $0 \leq \omega < 2\pi$. Eq. (3-3) is then inverted to give $\omega(x_c, y_c)$ and $\psi(x_c, y_c)$. Combining (3-3a) and (3-3b), and using trigonometric and hyperbolic function identities yields

$$\sin^2\omega = \frac{1}{2}\left[h + \sqrt{h^2 + \left(\frac{y_c}{b}\right)^2}\,\right] \qquad (3\text{-}4a)$$

and

$$\sinh^2\psi = \frac{1}{2}\left[-h + \sqrt{h^2 + \left(\frac{y_c}{b}\right)^2}\,\right] \qquad (3\text{-}4b)$$

where $h(x_c, y_c) = 1 - \left(\frac{x_c}{2b}\right)^2 - \left(\frac{y_c}{2b}\right)^2$

The correct sign for $\psi'$ , and the correct quadrant for $\omega$ follow by inspection of Eq. (3-3).

With $\psi'(x_c, y_c)$ and $\upsilon(x_c, y_c)$ known, the first transformation is complete. That is, for each airfoil input point $(x_c, y_c)$, a point $(\psi, \omega)$ is found. The resulting points $(\psi, \omega)$ are considered to form a function $\psi = \bar{\psi}(\omega)$. The curve $C'$ in the $Z'$ plane is then given by $Z' = b\, e^{\bar{\psi}(\omega)} e^{i\omega}$. The function $\bar{\psi}(\omega)$ is generally a slowly varying function (this is equivalent to saying $C'$ is "nearly circular") and is periodic with period $2\pi$ .

The transformation from the $Z'$ to the $\zeta$ plane is now considered. Polar coordinates as shown in Fig. 3 are used, where $(\lambda, \varphi)$ are taken as the independent variables. On the circle, which is centered at the origin, $\lambda = \lambda_K$ = constant, and the radius of the circle is therefore $r = b\, e^{\lambda_K}$.

The transformation used is

$$\ln \frac{Z'}{\zeta} = \sum_{n=1}^{\infty} \frac{\alpha_n + i\beta_n}{\zeta^n} \qquad (3\text{-}5)$$

where the constants $(\alpha_n, \beta_n)$ are real. Since $Z' \to \zeta$ as $\zeta \to \infty$ , the planes coincide at $\infty$ and the free stream conditions are the same in both. Substituting the respective polar coordinates for $Z'$ and $\zeta$ into (3-5) and equating real and imaginary parts of the resulting expression gives

$$\psi - \lambda = \sum_{n=1}^{\infty} \frac{e^{-n\lambda}}{b^n} \left(\alpha_n \cos n\varphi + \beta_n \sin n\varphi\right)$$

and

$$\omega - \varphi = \sum_{n=1}^{\infty} \frac{e^{-n\lambda}}{b^n} \left(\beta_n \cos n\varphi - \alpha_n \sin n\varphi\right)$$

The last two equations represent the mapping of any point in the $\mathcal{Z}'$ plane to the corresponding point in the $\zeta$ plane. The coefficients $(\alpha_n, \beta_n)$ are determined from the requirement that the curve $\mathcal{C}'$ maps into the circle. Therefore, from this point on the variables will be used in the restricted sense that $(\psi, \omega)$ define the curve $\mathcal{C}'$ and $(\lambda, \varphi)$ define the circle. Then, since $\lambda = \lambda_k$ on the circle,

$$\psi = \lambda_k + \sum_{n=1}^{\infty} (A_n \cos n\varphi + B_n \sin n\varphi) \qquad (3\text{-}6a)$$

and

$$\omega - \varphi = \sum_{n=1}^{\infty} (B_n \cos n\varphi - A_n \sin n\varphi) \qquad (3\text{-}6b)$$

where

$$A_n = \frac{e^{-n\lambda_k}}{b^n} \alpha_n$$

$$B_n = \frac{e^{-n\lambda_k}}{b^n} \beta_n$$

Eq. (3-6a) is the standard form of a Fourier series, and it follows that the coefficients are given by

$$\lambda_k = A_0 = \frac{1}{2\pi} \int_0^{2\pi} \psi(\varphi)\, d\varphi$$

$$A_n = \frac{1}{\pi} \int_0^{2\pi} \psi(\varphi) \cos n\varphi \, d\varphi$$

$$B_n = \frac{1}{\pi} \int_0^{2\pi} \psi(\varphi) \sin n\varphi \, d\varphi$$

Eqs. (3-6a) and (3-6b) give $\psi$ and $\omega$ as functions of $\varphi$, and the resulting points $[\psi(\varphi), \omega(\varphi)]$ represent points on the curve $C'$. From the $Z Z'$ transformation it is known that $\bar{\psi}(\omega)$ also represents the curve $C'$; therefore, $\psi$ and $\bar{\psi}$ represent the same dependent variable, but considered as a function of different independent variables. The solution for the $Z' \zeta$ transformation then requires a solution for the functions satisfying (3-6a) and (3-6b) where $\bar{\psi}(\omega)$ is a known function.

It is convenient to introduce a variable $\epsilon$ defined by

$$\epsilon = \omega - \varphi \tag{3-7}$$

Like $\psi$, $\epsilon$ may be considered a function of either $\omega$ or $\varphi$, and a similar notation is employed, i.e., $\epsilon = \epsilon(\varphi) = \bar{\epsilon}(\omega)$. It follows from (3-6b) that $\epsilon$ is periodic with period $2\pi$. Applying (3-6b) to a specific point on the circle $\varphi = \varphi'$ and using the definition of the Fourier coefficients gives

$$\epsilon(\varphi') = \sum_{n=1}^{\infty} \left\{ \frac{1}{\pi} \int_0^{2\pi} \psi(\varphi) \sin n\varphi \cos n\varphi' \, d\varphi \right.$$

$$\left. - \frac{1}{\pi} \int_0^{2\pi} \psi(\varphi) \cos n\varphi \sin n\varphi' \, d\varphi \right\}$$

Interchanging the order of summation and integration, and using a trigonometric identity then yields

$$\epsilon(\varphi') = \frac{1}{\pi} \int_0^{2\pi} \psi(\varphi) \sum_{n=1}^{\infty} \sin n(\varphi - \varphi') \, d\varphi$$

Introducing the rather obscure identity

$$\sum_{N=1}^{N} \sin N(\varphi-\varphi') = \frac{1}{2}\cot\frac{\varphi-\varphi'}{2} - \frac{1}{2}\frac{\cos\left[(2N+1)\frac{\varphi-\varphi'}{2}\right]}{\sin\frac{\varphi-\varphi'}{2}}$$

then yields

$$\epsilon(\varphi') = \lim_{N\to\infty}\left\{\frac{1}{2\pi}\int_0^{2\pi}\psi(\varphi)\cot\frac{\varphi-\varphi'}{2}\,d\varphi - \frac{1}{2\pi}\int_0^{2\pi}\psi(\varphi)\,\frac{\cos\left[(2N+1)\frac{\varphi-\varphi'}{2}\right]}{\sin\frac{\varphi-\varphi'}{2}}\,d\varphi\right\}$$

The first integral is independent of $N$, while the second is zero in the limit. The equation then becomes

$$\epsilon(\varphi') = \frac{1}{2\pi}\int_0^{2\pi}\psi(\varphi)\cot\frac{\varphi-\varphi'}{2}\,d\varphi \qquad (3\text{-}8)$$

The integral in (3-8) is singular, and the Cauchy principle value must be used. The integral is usually called Poisson's integral.

If the function $\psi(\varphi)$ were known, (3-8) would be a definite integral for $\epsilon(\varphi')$. However, what is known is $\bar{\psi}(\omega)$, where $\varphi = \omega - \epsilon$, and (3-8) is therefore an integral equation in $\epsilon$. The integral equation is solved by the method of successive approximations. Convergence of this method ultimately depends only on the function $\bar{\psi}(\omega)$ and the initial approximation $\epsilon_0$ for the function $\epsilon$. For most airfoil shapes, $\bar{\psi}(\omega)$ is a slowly varying function, $\epsilon_0 = 0$ is a good initial guess, and only one step in the iteration is sufficient for very good results. In this case, (3-8) can be reduced to

$$\bar{\epsilon}(\omega') \simeq \bar{\epsilon}_1(\omega') = \frac{1}{2\pi}\int_0^{2\pi} \cot\frac{\omega-\omega'}{2}\cdot\bar{\psi}(\omega)\,d\omega \qquad (3\text{-}9)$$

Eq. (3-9) gives $\bar{\epsilon}_1(\omega')$ as a definite integral since $\bar{\psi}(\omega)$ is known. In general the integral must be evaluated numerically since $\bar{\psi}(\omega)$ is only known numerically. This is done by prescribing a value of $\omega'$, performing the integration, and repeating this process until a sufficient number of points are obtained to define the $\bar{\epsilon}(\omega)$ function. With $\bar{\epsilon}(\omega)$ known, $\varphi(\omega) = \omega - \bar{\epsilon}(\omega)$ is known, $\psi(\varphi)$ is therefore known, and the second transformation is complete.

The velocity $V$ on the surface of the airfoil is obtained from the complex potential function. Since

$$\left[\frac{dw(z)}{dz}\right]_{\text{airfoil}} = \left(u_z - i v_z\right)_{\text{airfoil}}$$

it follows that

$$V = \left|\frac{dw(z)}{dz}\right|_{\text{airfoil}} = \left|\frac{dw(\zeta)}{d\zeta}\right|_{\text{circle}} \cdot \left|\frac{d\zeta}{d\bar{z}'}\right|_{c} \cdot \left|\frac{dz'}{dz}\right|_{\text{airfoil}} \qquad (3\text{-}10)$$

The complex potential for flow over a circle of radius $a$ is

$$w(\zeta) = V_\infty\left(\zeta e^{-i\alpha} + \frac{a^2 e^{i\alpha}}{\zeta}\right) + \frac{i\Gamma}{2\pi}\ln\frac{\zeta e^{-i\alpha}}{a}$$

Therefore

$$\frac{dw(\zeta)}{d\zeta} = V_\infty\left(e^{-i\alpha} - \frac{a^2 e^{i\alpha}}{\zeta^2}\right) + \frac{i\Gamma}{2\pi\zeta}$$

The lift coefficient $C_\ell$ is related to the circulation $\Gamma$ by the Kutta-Joukowski theorem, which gives

$$\Gamma = \frac{C_\ell C V_\infty}{2}$$

Then

$$\left| \frac{d[U(\zeta)]}{d\zeta} \right|_{\text{circle}} = 2V_\infty \left| \sin(\varphi - \alpha) + \frac{C_\ell C}{8\pi z} \right| \qquad (3\text{-}11)$$

Taking differentials of $z'$ and $\zeta$ (with $\lambda = \lambda_K$) gives

$$\frac{dz'}{z'} = \left( i + \frac{d\bar{\psi}}{d\omega} \right) d\omega$$

and

$$\frac{d\zeta}{\zeta} = i \left( 1 - \frac{d\bar{\epsilon}}{d\omega} \right) d\omega$$

Then, since $\zeta = b e^{\lambda_K} e^{i\varphi}$ on the circle

$$\left| \frac{d\zeta}{dz'} \right|_{c'} = \frac{b e^{\lambda_K} \left| 1 - \frac{d\bar{\epsilon}}{d\omega} \right|}{|z'|_{c'} \sqrt{1 + \left( \frac{d\bar{\psi}}{d\omega} \right)^2}} \qquad (3\text{-}12)$$

Differentiating (3-1) gives

$$\frac{dz}{dz'} = \frac{1}{z'} \left( z' - \frac{b^2}{z'} \right)$$

Using $z' = b e^{\bar{\psi}} e^{i\omega}$ in the terms in parenthesis then yields

$$\left| \frac{dz'}{dz} \right|_{\text{airfoil}} = \frac{|z'|_{c'}}{2b} \frac{1}{\sqrt{\sinh^2 \bar{\psi} + \sin^2 \omega}} \qquad (3\text{-}13)$$

Eqs. (3-10) through (3-13) then give the velocity on the airfoil sur-

face as

$$\frac{V_b}{V_\infty} = \frac{e^{\lambda\kappa}\left|\sin(\varphi-\alpha) + \frac{C_\ell C}{8\pi a}\right| \cdot \left|1 - \frac{d\bar{\epsilon}}{d\omega}\right|}{\sqrt{\left[\sinh^2\bar{\psi} + \sin^2\omega\right]\left[1 + \left(\frac{d\bar{\psi}}{d\omega}\right)^2\right]}} \qquad (3\text{-}14)$$

Eq. (3-14) applies to airfoils with either sharp or blunt trailing edges. For an airfoil with a sharp trailing edge, ( $\psi = 0$, $\omega = 0$) at the trailing edge, and the Kutta condition becomes

$$\left|\sin(\varphi-\alpha) + \frac{C_\ell C}{8\pi a}\right| = 0 \quad \text{at} \quad \omega = 0$$

Since $\varphi(0) = -\bar{\epsilon}(0)$ , the Kutta condition becomes

$$C_\ell = \frac{8\pi a}{C}\sin\left(\bar{\epsilon}(0) + \alpha\right) \qquad (3\text{-}15)$$

The pressure coefficient on the airfoil surface follows from the Bernoulli equation, and is given by

$$C_p = 1 - \left(\frac{V_b}{V_\infty}\right)^2 \qquad (3\text{-}16)$$

The potential flow is then known since $V_b$ and $C_p$ on the airfoil surface are known. A different form of the potential flow is required as input to the boundary layer program, however, and this is considered next. Curvilinear coordinates shown in Fig. 1 are used, and $V_b$ becomes $u_e$. The curvilinear coordinate $\chi$ is measured along the body surface from the front stagnation point, and it is therefore necessary to determine the arc length along the airfoil.

The arc length $\Delta s$ between two given points ( $x_{c_j}$ , $y_{c_j}$ ) and ( $x_{c_{j+1}}$ , $y_{c_{j+1}}$ ) is

$$\Delta s = \int_{x_{c_j}}^{x_{c_{j+1}}} \sqrt{1 + \left(\frac{dy_c}{dx_c}\right)^2}\, dx_c = \int_{y_{c_j}}^{y_{c_{j+1}}} \sqrt{1 + \left(\frac{dx_c}{dy_c}\right)^2}\, dy_c$$

The first form of this equation is used for all increments except those adjacent to the leading edge (and trailing edge, if the trailing edge is blunt), where $\frac{dy_c}{dx_c} \to \infty$ . For these increments, the second form is used, but not directly since $\frac{dx_c}{dy_c}$ is usually known as a function of $x_c$ instead of $y_c$ . The square root term is expanded to give

$$\sqrt{1 + \left(\frac{dx_c}{dy_c}\right)^2} = 1 + \frac{1}{2}\left(\frac{dx_c}{dy_c}\right)^2 + O\left(\frac{dx_c}{dy_c}\right)^4$$

Then

$$\int_{y_{c_j}}^{y_{c_{j+1}}} \sqrt{1 + \left(\frac{dx_c}{dy_c}\right)^2}\, dy_c \simeq \left| (y_{c_{j+1}} - y_{c_j}) + \frac{1}{2}\int_{x_{c_j}}^{x_{c_{j+1}}} \frac{dx_c}{\left(\frac{dy_c}{dx_c}\right)} \right|$$

Each integral is evaluated numerically. With the arc lengths known, the value of $x$ is calculated for each output point (i.e., each point at which the velocity $V_b = u_e$ is known).

The functions $\xi^*$ and $\beta$ defined by (3-17) are also required.

$$\xi^*\left(\frac{x}{c}\right) = \int_0^{x/c} u_e^*\, d\left(\frac{x}{c}\right) \qquad \text{(3-17a)}$$

$$\beta\left(\frac{x}{c}\right) = \frac{2\xi^*}{u_e^{*2}} \frac{du_e^*}{d\left(\frac{x}{c}\right)} \qquad (3\text{-}17b)$$

where $u_e^* = u_e / V_\infty$.

Both $\xi^*$ and $\beta$ are evaluated at each output point by evaluating the required integrals and derivatives numerically. The derivatives are evaluated using least-square parabolas for five consecutive nonequally spaced points.

## 4. BOUNDARY LAYER ANALYSIS

The boundary layer properties for both laminar and turbulent flow are calculated using the Cebeci, Smith finite difference method. The turbulent Reynolds' shear stresses are eliminated by using an eddy viscosity expression. For laminar flow, the eddy viscosity is set equal to zero, and the equations reduce to the classical laminar boundary layer equations. Both the streamwise and normal derivatives are replaced by finite difference expressions, and the resulting algebraic equations are then solved by a matrix factorization method. The Cebeci, Smith method has been extensively developed and tested against experiments and other theories and has been found to be accurate (Ref. 8). The method also predicts either laminar or turbulent separation. The Cebeci, Smith method is reviewed herein in sufficient detail so that the computer program in the Appendix can be understood.

The method has been developed for either two dimensional or axisymmetric flows (with or without transverse curvature effects). For incompressible turbulent boundary layers, the conservation equations are:

Continuity:

$$\frac{\partial}{\partial x}\left(r^{\epsilon}\rho u\right)+\frac{\partial}{\partial y}\left(r^{\epsilon}\rho v\right)=0$$

Momentum:

$$\rho u\frac{\partial u}{\partial x}+\rho v\frac{\partial u}{\partial y}+\frac{\partial P}{\partial x}-\frac{1}{r^{\epsilon}}\frac{\partial}{\partial y}\left[r^{\epsilon}\left(\mu\frac{\partial u}{\partial y}-\rho\overline{u'v'}\right)\right]=0$$

where $\epsilon = 0$ for two dimensional flows, and $\epsilon = 1$ for axisymmetric flows. The quantity $r(x,y)$ is the radius from the axis of symmetry to the point being considered in the boundary layer. In terms of the body geometry

$$r(x,y) = r_w(x) + \omega y \cos\varphi(x)$$

where $r_w(x)$ is the body radius, $\varphi(x)$ is the angular inclination of the body, $\omega = 1$ if transverse curvature effects are included, and $\omega = 0$ if transverse curvature is neglected.

The boundary conditions considered are

$$u(x,0) = 0$$
$$v(x,0) = v_w(x) \qquad \text{(suction or injection permitted)}$$
$$u(x,\infty) = u_e(x)$$

Defining an eddy viscosity $\epsilon^+$ by

$$-\rho\overline{u'v'} = \rho\nu\epsilon^+\frac{\partial u}{\partial y}$$

and using the Bernoulli equation for $\frac{\partial P}{\partial x}$ then yields

Momentum: [Eulers

$$\rho u\frac{\partial u}{\partial x} + \rho v\frac{\partial u}{\partial y} - \rho u_e\frac{du_e}{dx} - \frac{u}{r^\epsilon}\frac{\partial}{\partial y}\left[r^\epsilon(1+\epsilon^+)\frac{\partial u}{\partial y}\right] = 0$$

The continuity equation is identically satisfied by introducing the stream function $\psi$, defined by

$$\rho u r^\epsilon = \left(\frac{\partial\psi}{\partial y}\right)_x$$

$$\rho v r^{\epsilon} = -\left(\frac{\partial \psi}{\partial x}\right)_y$$

The independent variables are transformed from $(x,y)$ to $(\xi, \eta)$, where

$$\xi(x) = \rho\mu \int_0^x u_e r_w^{2\epsilon}\, dx \tag{4-1a}$$

$$\eta(x,y) = \frac{\rho u_e}{\sqrt{2\xi}} \int_0^y r^{\epsilon}\, dy \tag{4-1b}$$

and a dimensionless stream function $f(\xi,\eta) = \frac{\psi}{\sqrt{2\xi}}$ is introduced. Then $\frac{u}{u_e} = \frac{\partial f}{\partial \eta}$, and the momentum equation becomes

$$\frac{\partial}{\partial \eta}\left[(1+t)^{2\epsilon}(1+\epsilon^+)\frac{\partial^2 f}{\partial \eta^2}\right] + \beta(\xi)\left[1-\left(\frac{\partial f}{\partial \eta}\right)^2\right] + f\frac{\partial^2 f}{\partial \eta^2} + 2\xi\left[\frac{\partial f}{\partial \xi}\frac{\partial^2 f}{\partial \eta^2} - \frac{\partial f}{\partial \eta}\frac{\partial^2 f}{\partial \xi \partial \eta}\right] = 0 \tag{4-2}$$

where

$$\beta(\xi) = \frac{2\xi}{u_e}\frac{du_e}{d\xi}$$

and

$$(1+t)^{2\epsilon} = \left(\frac{r}{r_w}\right)^{2\epsilon} = 1 + 2\epsilon\omega\,\frac{\sqrt{2\xi}\,\cos\phi\;\eta}{\rho u_e r_w^{2\epsilon}}$$

The quantity $t(\xi,\eta)$ is the transverse curvature term.

The boundary conditions transform to

$$\frac{\partial f}{\partial \eta}(\xi, 0) = 0 \tag{4-3a}$$

$$\frac{d\xi}{dx}\left[\frac{1}{2\xi}f''(\xi,0)+\frac{\partial f}{\partial\eta}(\xi,0)\right]=-\frac{\rho\lambda_w^{\epsilon}U_w}{\sqrt{2\xi}} \qquad (4\text{-}3b)$$

$$\frac{\partial f}{\partial\eta}(\xi,\infty)=1 \qquad (4\text{-}3c)$$

Eq. (4-3a) is used in obtaining (4-3b). Eq. (4-3b) can be further simplified by solving it as an ordinary differential equation in $f(\xi,0)$ . Then (4-3d) replaces (4-3b).

$$f(\xi,0)=\frac{-1}{\mu\sqrt{2\xi}}\int_0^{\xi}\frac{U_w\,d\xi}{U_e\,\lambda_w^{\epsilon}} \qquad (4\text{-}3d)$$

The Cebeci, Smith eddy viscosity model consists of an inner representation $\epsilon_i^+$ near the wall and an outer representation $\epsilon_o^+$ away from the wall. The inner expression is

$$\epsilon_i^+=\frac{K_1^2y^2}{\nu}\left(1-e^{-\frac{y}{A_o}}\right)^2\cdot\left|\frac{\partial u}{\partial y}\right|$$

where $K_1$ is a constant and, for an impermeable wall*,

$$A_o=\frac{26\,\nu}{\sqrt{\frac{\tau_w}{\rho}+\frac{dP_e}{dx}\frac{y}{\rho}}}$$

*See footnote on next page

The outer expression is

$$\epsilon_o^+ = \frac{K_2 u_e}{\nu} \frac{\int_o^\delta (1 - \frac{u}{u_e}) dy}{1 + 5.5 (\frac{y}{\delta})^6}$$

where $K_2$ is a constant. The boundary layer thickness $\delta$ is taken as the value of $y$ where $\frac{u}{u_e} = 0.995$. With this definition of $\delta$, the values for the constants are taken* as $K_1 = 0.4$ and $K_2 = 0.0168$. The inner and outer expressions are used as follows (for a given value of $x$): The eddy viscosity $\epsilon^+$ is taken as $\epsilon_i^+$ for $0 \le y \le y_c$, and is taken as $\epsilon_o^+$ for $y_c \le y \le \delta$. The value of $y_c$ is the value of $y$ at which $\epsilon_i^+ = \epsilon_o^+$. The eddy viscosity $\epsilon^+$ is thus continuous, but in general its derivative has a finite discontinuity at $y = y_c$. In terms of $(\xi, \eta)$, the eddy viscosity expressions become

$$\epsilon_i^+ = K_1^2 (1+t)^\epsilon \frac{\sqrt{2\xi}}{\mu R_w^\epsilon} Y^2 |f''| \cdot$$

$$\cdot \left\{ 1 - \exp\left[ -\frac{\sqrt{2\xi}}{\mu R_w^{\epsilon/2}} \frac{Y}{26} \left| \frac{\mu}{\sqrt{2\xi}} (f_w'' - \beta Y) \right|^{1/2} \right] \right\}^2 \qquad (4\text{-}4a)$$

where

$$Y(\xi, \eta) = \int_o^\eta \frac{d\eta}{(1+t)^\epsilon} \quad , \quad f'' \equiv \frac{\partial^2 f}{\partial \eta^2} \quad , \quad f_w'' \equiv f''(\xi, 0)$$

*More recent expressions for $K_1$, $K_2$, and $A_o$, are given in Section 5. They should also be used here, but became available too late to make the necessary changes.

$$\epsilon_o^+ = \frac{K_2\sqrt{2\xi}}{\mu R_w^{\epsilon}} \frac{\int_0^{\eta_\delta} (1-f')(1+t)^{-\epsilon} d\eta}{1 + 5.5\left[\dfrac{\int_0^{\eta} (1+t)^{-\epsilon} d\eta}{\int_0^{\eta_\delta} (1+t)^{-\epsilon} d\eta}\right]^6} \qquad (4\text{-}4b)$$

For two dimensional flow or axisymmetric flow without transverse curvature, $t=0$, and these simplify to

$$\epsilon_i^+ = K_1^2 \frac{\sqrt{2\xi}}{\mu R_w^{\epsilon}} \eta^2 |f''| \cdot$$

$$\cdot \left\{ 1 - \exp\left[ -\frac{\sqrt{2\xi}\,\eta}{26\mu R_w^{\epsilon/2}} \left| \frac{\mu}{\sqrt{2\xi}} (f_w'' - \beta\eta) \right|^{1/2} \right] \right\}^2 \qquad (4\text{-}5a)$$

$$\epsilon_o^+ = \frac{K_2\sqrt{2\xi}}{\mu R_w^{\epsilon}} \frac{\eta_\delta - (f_\delta - f_w)}{1 + 5.5\left(\dfrac{\eta}{\eta_\delta}\right)^6} \qquad (4\text{-}5b)$$

In the present application, only two dimensional airfoils are considered, and the simpler forms (4-5) are used (with $\epsilon = 0$ also).

It is convenient to nondimensionalize $\xi(x)$. This is done by defining $\xi^*\left(\frac{x}{c}\right)$ as

$$\xi^*\left(\frac{x}{c}\right) = \int_0^{x/c} u_e^* \left(\frac{R_w}{c}\right)^{2\epsilon} d\left(\frac{x}{c}\right) \qquad (4\text{-}6)$$

where $u_e^* = u_e/V_\infty$. Then $\xi = \mu^2 c^{2\epsilon} Re_\infty \xi^*$ where $Re_\infty = \rho V_\infty c / \mu$. The momentum equation (4-2) then becomes

$$\frac{\partial}{\partial \eta}\left[(1+t)^{2\epsilon}\,(1+\epsilon^{+})\,\frac{\partial^2 f}{\partial \eta^2}\right] + \beta(\xi^*)\left[1-\left(\frac{\partial f}{\partial \eta}\right)^2\right]$$

$$+ f\,\frac{\partial^2 f}{\partial \eta^2} + 2\xi^*\left[\frac{\partial f}{\partial \xi^*}\,\frac{\partial^2 f}{\partial \eta^2} - \frac{\partial f}{\partial \eta}\,\frac{\partial^2 f}{\partial \xi^* \partial \eta}\right] = 0 \qquad (4\text{-}7)$$

where

$$\beta(\xi^*) = \frac{2\xi^*}{u_e^*}\,\frac{d u_e^*}{d \xi^*} \qquad (4\text{-}8)$$

and

$$(1+t)^{2\epsilon} = 1 + 2\epsilon\omega\left(\frac{c}{\lambda_w}\right)^{2\epsilon}\,\frac{\sqrt{2\xi^*}\,\cos\phi}{\sqrt{Re_\infty}\,u_e^*}\,\eta$$

The eddy viscosity expressions (4-5) become

$$\epsilon_i^{+} = K_1^2\left(\frac{c}{\lambda_w}\right)^{\epsilon}\sqrt{Re_\infty}\,\sqrt{2\xi^*}\;\eta^2\,|f''|\cdot$$

$$\cdot\left\{1 - \exp\left[-\left(\frac{c}{\lambda_w}\right)^{\epsilon/2}\,\frac{Re_\infty^{1/4}\,(2\xi^*)^{1/4}}{26}\,\eta\,\left|f_w'' - \beta\eta\right|^{\frac{1}{2}}\right]\right\}^2 \qquad (4\text{-}9a)$$

$$\epsilon_o^{+} = K_2\left(\frac{c}{\lambda_w}\right)^{\epsilon}\sqrt{Re_\infty}\,\sqrt{2\xi^*}\,\frac{\eta_\delta + f_w - f_\delta}{1 + 5.5\left(\frac{\eta}{\eta_\delta}\right)^6} \qquad (4\text{-}9b)$$

The boundary conditions become

$$\frac{\partial f}{\partial \eta}(\xi, 0) = f_w' = 0 \qquad (4\text{-}10a)$$

$$\frac{\partial f}{\partial \eta}(\xi, \infty) = f_\infty' = 1 \qquad (4\text{-}10b)$$

$$f(\xi, 0) = f_w = -\frac{\sqrt{Re_\infty}}{\sqrt{2\xi^*}}\int_0^{\xi^*}\frac{v_w^*}{u_e^*\left(\frac{\lambda_w}{c}\right)^{\epsilon}}\,d\xi^* \qquad (4\text{-}10c)$$

For two dimensional flow ($\epsilon = 0$), $u_e^*$ follows from (3-14), and $\xi^*$ and $\beta$ reduce to the definitions given in (3-17). The output from the potential flow program therefore provides all the potential flow input needed for the boundary layer program.

Eq. (4-7) subject to the boundary conditions (4-10) is solved by a finite difference procedure (Ref. 8). First, the $\xi^*$ derivatives are replaced by finite difference expressions. For a general function $g(\xi^*)$, a three point Lagrange polynomial gives

$$\left.\frac{dg}{d\xi^*}\right|_{\xi^*_m} = A_1\, g(\xi^*_m) + A_2\, g(\xi^*_{m-1}) + A_3\, g(\xi^*_{m-2}) \qquad (4\text{-}11)$$

where

$$A_1 = \frac{1}{\xi^*_m - \xi^*_{m-1}} + \frac{1}{\xi^*_m - \xi^*_{m-2}}$$

$$A_2 = \frac{-(\xi^*_m - \xi^*_{m-2})}{(\xi^*_m - \xi^*_{m-1})(\xi^*_{m-1} - \xi^*_{m-2})}$$

$$A_3 = \frac{(\xi^*_m - \xi^*_{m-1})}{(\xi^*_{m-1} - \xi^*_{m-2})(\xi^*_m - \xi^*_{m-2})}$$

The $\xi^*$ increments do not have to be equally spaced. For a two point formula, (4-11) still holds, with

$$A_1 = \frac{1}{(\xi_m^* - \xi_{m-1}^*)}$$

$$A_2 = \frac{-1}{(\xi_m^* - \xi_{m-1}^*)}$$

$$A_3 = 0$$

With the $\xi^*$ derivatives replaced by finite difference expressions, the momentum equation (4-7) becomes

$$\left[(1+t)_m^{2\epsilon}\,(1+\epsilon^+)_m\, f_m''\right]' + \beta_m\,(1 - f_m'^2) + f_m f_m''$$

$$+ 2\xi_m^* \left[f_m''(A_1 f_m + A_2 f_{m-1} + A_3 f_{m-2}) - f_m'(A_1 f_m' + A_2 f_{m-1}' + A_3 f_{m-2}')\right] = 0$$

where primes denote $\eta$ derivatives. If solutions are known at $\xi_{m-1}^*$ and $\xi_{m-2}^*$, this is an ordinary differential equation for $f_m(\eta)$.

Cebeci, Smith noted that round-off errors could be reduced by introducing a "translated stream function" $\varphi$ defined by

$$\varphi = f - \eta$$

Since $A_1 + A_2 + A_3 = 0$, the momentum equation in terms of $\varphi$ is

$$\left[ (1+t)_m^{2\epsilon} (1+\epsilon^+)_m \varphi'' \right]' - \beta_m (2\varphi' + \varphi'^2)$$

$$+ \varphi'' (\varphi + \eta)$$

$$+ 2\xi_m^* \left[ \varphi'' (A_1 \varphi + A_2 \varphi_{m-1} + A_3 \varphi_{m-2}) \right.$$

$$\left. - (\varphi'+1)(A_1 \varphi' + A_2 \varphi'_{m-1} + A_3 \varphi'_{m-2}) \right] = 0 \qquad (4\text{-}12)$$

where $\varphi \equiv \varphi_m$. Eq. (4-12) will be solved by an iterative procedure. It is first linearized by assuming certain terms that make it nonlinear are known from a previous iteration (denoted by $\varphi_o$). No terms are neglected, however, and as the iteration converges the solution of the full nonlinear Eq. (4-12) is obtained.

The linear equation is

$$\left[ (1+t)_m^{2\epsilon} (1+\epsilon^+)_{o_m} \varphi'' \right]' - \beta_m (2\varphi' + \varphi'\varphi_o) + \varphi''(\varphi_o + \eta)$$

$$+ 2\xi_m^* \left[ \varphi_o'' (A_1 \varphi + A_2 \varphi_{m-1} + A_3 \varphi_{m-2}) \right.$$

$$\left. - (\varphi_o'+1)(A_1 \varphi' + A_2 \varphi'_{m-1} + A_3 \varphi'_{m-2}) \right] = 0 \qquad (4\text{-}13)$$

Cebeci, Smith found that round-off errors could be further reduced by writing (4-13) in terms of $\Delta\varphi = \varphi - \varphi_o$. The equation then becomes

$$E_1 \Delta\varphi''' + E_2 \Delta\varphi'' + E_3 \Delta\varphi' + E_4 \Delta\varphi = E_5 \qquad (4\text{-}14)$$

where

$$E_1 = (1+t)_m^{2\epsilon} \; (1+\epsilon^+)_{0_m}$$

$$E_2 = \left[ (1+t)_m^{2\epsilon} \; (1+\epsilon^+)_{0_m} \right]' + \varphi_0 + \eta$$

$$E_3 = -\beta_m (\varphi_0' + 2) - 2\xi_m^* (\varphi_0' + 1) A_1$$

$$E_4 = 2\xi_m^* \varphi_0'' A_1$$

$$E_5 = -(E_1 \varphi_0''' + E_2 \varphi_0'' + E_3 \varphi_0' + E_4 \varphi_0)$$
$$+ 2\xi_m^* \left[ (\varphi_0' + 1)(A_2 \varphi_{m-1}' + A_3 \varphi_{m-2}') \right.$$
$$\left. - \varphi_0'' (A_2 \varphi_{m-1} + A_3 \varphi_{m-2}) \right]$$

With values of $E_i$ known from the previous iteration, Eq. (4-14) is a linear equation for $\Delta\varphi$ . It is solved by replacing $\eta$ derivatives by finite difference expressions. The finite difference expressions are obtained from the five point Lagrange polynomial

$$g(\eta) = L_{i-2}(\eta)\, g_{i-2} + L_{i-1}(\eta)\, g_{i-1} + L_i(\eta)\, g_i$$
$$+ L_{i+1}(\eta)\, g_{i+1} + L_{i+2}(\eta)\, g_{i+2}$$

where

$$L_i(\eta) = \frac{\prod_{\substack{K=i-2 \\ K\neq j}}^{i+2} (\eta - \eta_K)}{\prod_{\substack{K=i-2 \\ K\neq j}}^{i+2} (\eta_j - \eta_K)}$$

Then

$$g' = L'_{i-2}\, g_{i-2} + L'_{i-1}\, g_{i-1} + L'_i\, g_i + L'_{i+1}\, g_{i+1} + L'_{i+2}\, g_{i+2}$$

with similar results for the higher derivatives.

A constant step size $h$ in the $\eta$ direction can generally be used for laminar flow. For turbulent flow, however, a constant step size results in an excessive number of points. This is because turbulent boundary layers have large gradients near the wall (which require small step sizes), but may be many times thicker than laminar boundary layers. A simple variable-step grid was therefore developed by Cebeci, Smith. In this grid the ratio of lengths of any two adjacent intervals is constant. Then

$$h_i = K h_{i-1} \qquad , \qquad K = \text{constant}$$

The step size then grows progressively larger away from the wall. Taking $\eta_1 = 0$ and $\eta_2 = h_1$ , the distance to a grid point is

$$\eta_{i+1} = h_1 \frac{K^i - 1}{K - 1}$$

The variable grid involves the three parameters $h_1$, $K$, and the number of steps $N$. Table 1/2 in Ref. 8 gives suitable combinations of these parameters.

Applying the finite difference formulas to this grid and to (4-14) gives

$$\Delta\varphi_{i+2} + F_i \Delta\varphi_{i+1} + G_i \Delta\varphi_i + I_i \Delta\varphi_{i-1} + M_i \Delta\varphi_{i-2} = N_i \qquad (4\text{-}15)$$

for $i = 3, \ldots, N-2$

where

$$F_i = \frac{B_4}{R_i} \left\{ 6 (a_1 + K - K^2 a_1) \right.$$

$$\left. + 2 h_{i-1} \frac{E_2}{E_1} K a_1 (1 - K a_1 - K^2) - h_{i-2} \frac{E_3}{E_1} K^3 a_1^2 \right\}$$

$$G_i = \frac{B_3}{R_i} \left\{ 6 (a_1 + K - K^2 - K^2 a_1) \right.$$

$$+ 2 \frac{E_2}{E_1} h_{i-2} K (K^3 a_1 - K^2 a_1 - K^2 - K a_1^2 - K a_1 + a_1)$$

$$\left. + \frac{E_3}{E_1} h_{i-2}^2 K^3 a_1 (K^2 + K a_1 - a_1 - 1) + \frac{E_4}{B_3 E_1 h_{i-2}} \right\}$$

$$I_i = \frac{B_2}{R_i}\left\{ 6\,(a_1 - K^2 - K^2 a_1) + 2\,\frac{E_2}{E_1}\,R_{i-2}\,K^2 a_1\,(K^2 - a_1 - 1) + \frac{E_3}{E_1}\,R_{i-2}^2\,K^4 a_1^2 \right\}$$

$$M_i = \frac{B_1}{R_i}\left\{ 6K\,(1 - K - K a_1) + 2\,\frac{E_2}{E_1}\,R_{i-2}\,K^3 (K a_1 - a_1 - 1) + \frac{E_3}{E_1}\,R_{i-2}^2\,K^5 a_1 \right\}$$

$$N_i = \frac{E_5}{E_1\,R_{i-2}\,R_i}$$

$$R_i = B_5\left\{ 6\,(a_1 + K - K^2) + 2\,R_{i-2}\,\frac{E_2}{E_1}\,K\,(a_1 - a_1 K - K^2) - R_{i-2}^2\,\frac{E_3}{E_1}\,K^3 a_1 \right\}$$

$$a_1 = 1 + K \quad , \quad a_2 = 1 + K + K^2 \quad , \quad a_3 = 1 + K + K^2 + K^3$$

$$B_1 = \frac{1}{a_1 a_2 a_3 R_{i-2}^4} \quad , \quad B_2 = \frac{-1}{a_1 a_2 K^3 R_{i-2}^4} \quad , \quad B_3 = \frac{1}{a_1^2 K^5 R_{i-2}^4}$$

$$B_4 = \frac{-1}{a_1 a_2 K^6 R_{i-2}^4} \quad , \quad B_5 = \frac{1}{a_1 a_2 a_3 K^6 R_{i-2}^4}$$

A similar procedure for the point $N-1$ gives

$$\Delta\varphi_N + F_{N-1}\Delta\varphi_{N-1} + G_{N-1}\Delta\varphi_{N-2} + I_{N-1}\Delta\varphi_{N-3} + M_{N-1}\Delta\varphi_{N-4} = N_{N-1} \quad (4\text{-}16)$$

where $$R_{N-1} = B_5\left\{6(a_2 + Ka_1 + K^2) + 2\frac{E_2}{E_1}\rho_{N-4}K \cdot \right.$$

$$\left. \cdot (i_1 i_2 + a_2 K + a_1 K^2) + \frac{E_3}{E_1}\rho_{N-4}^2 K^3 a_1 a_2\right\}$$

$$F_{N-1} = \frac{B_4}{R_{N-1}}\left\{6(a_2 + Ka_1 + K^2 - K^3) + 2\frac{E_2}{E_1}\rho_{N-4}K \cdot \right.$$

$$\cdot (a_1 a_2 + a_2 K - a_2 K^2 + a_1 K^2 - a_1 K^3 - K^4)$$

$$\left. + \frac{E_3}{E_1}\rho_{N-4}^2 K^3 (a_1 a_2 - K a_1 a_2 - K^2 a_2 - K^3 a_1) + \frac{E_4}{E_1 B_4 \rho_{N-4}}\right\}$$

$$G_{N-1} = \frac{B_3}{R_{N-1}}\left\{6(a_2 + Ka_1 - K^3) + 2\frac{E_2}{E_1}\rho_{N-4}K \cdot \right.$$

$$\left. \cdot (a_1 a_2 - K^2 a_2 - a_1 K^3) - \frac{E_3}{E_1}\rho_{N-4}^2 K^4 a_1 a_2\right\}$$

$$I_{N-1} = \frac{B_2}{R_{N-1}}\left\{6(a_2 + K^2 - K^3) + 2\frac{E_2}{E_1}\rho_{N-4}K^2(a_2 - a_2 K - K^3)\right.$$

$$\left. - \frac{E_3}{E_1}\rho_{N-4}^2 K^5 a_2\right\}$$

$$M_{N-1} = \frac{B_1}{R_{N-1}}\left\{6K(a_1 + K - K^2) + 2\frac{E_2}{E_1}\rho_{N-4}K^3 \cdot \right.$$

$$\left. \cdot (a_1 - K a_1 - K^2) - \frac{E_3}{E_1}\rho_{N-4}^2 K^6 a_1\right\}$$

$$N_{N-1} = \frac{E_5}{E_1 R_{N-4} R_{N-1}}$$

The boundary conditions (4-10) in terms of $\varphi$ become

$$\varphi(\xi^*, 0) = -\frac{\sqrt{Re_\omega}}{\sqrt{2\xi^*}} \int_0^{\xi^*} \frac{U_w \, d\xi^*}{u_e^* \left(\frac{\rho_w}{C}\right)^{\epsilon}} \tag{4-17a}$$

$$\varphi'(\xi^*, 0) = -1 \tag{4-17b}$$

$$\varphi'(\xi^*, \eta_\infty) = 0 \tag{4-17c}$$

Each iteration for $\varphi$ satisfies these boundary conditions, so the boundary conditions for $\Delta\varphi$ are

$$\Delta\varphi_w = 0 \;, \quad \Delta\varphi'_w = 0 \;, \quad \Delta\varphi'_\delta = 0$$

In the finite difference scheme the subscript $(\,)_w$ is identical to the subscript $(\,)_1$ hence the first boundary condition provides

$$\Delta\varphi_1 = 0 \tag{4-18a}$$

Applying the finite difference procedure to the second boundary condition and using Eq. (4-18a) gives

$$\Delta\varphi_5 + F_2 \, \Delta\varphi_4 + G_2 \, \Delta\varphi_3 + I_2 \, \Delta\varphi_2 = 0 \tag{4-18b}$$

where

$$F_2 = \frac{B_4 \, a_1 \, a_3}{R_2}$$

$$G_2 = \frac{B_3 \, a_2 \, a_3}{R_2}$$

$$I_2 = \frac{B_2 a_1 a_2 a_3}{R_2}$$

$$R_2 = B_5 a_1 a_2$$

Applying the finite difference procedure to the last boundary condition gives

$$\Delta\varphi_N + F_N \Delta\varphi_{N-1} + G_N \Delta\varphi_{N-2} + I_N \Delta\varphi_{N-3} + M_N \Delta\varphi_{N-4} = 0 \quad (4\text{-}18c)$$

where

$$F_N = \frac{B_4}{R_N} a_1 a_2 a_3$$

$$G_N = \frac{B_3}{R_N} K a_2 a_3$$

$$I_N = \frac{B_2}{R_N} K^2 a_1 a_3$$

$$M_N = \frac{B_1}{R_N} K^3 a_1 a_2$$

$$R_N = B_5 \left( K^3 a_1 a_2 + K^2 a_1 a_3 + K a_2 a_3 + a_1 a_2 a_3 \right)$$

With $\Delta\varphi_1 = 0$ known, there are N-1 unknowns $\Delta\varphi_i$, $i = 2, \ldots, N$. Eq. (4-15) yields N-4 equations (one for each point $i = 3, \ldots, N-2$). Eqs. (4-16), (4-18b), (4-18c) each yield one equation, so there are N-1 equations.

This system of equations can be rewritten in matrix form

$$[A][\Delta\varphi] = [N] \quad (4\text{-}19)$$

where $[A]$ is an (N-1) x (N-1) matrix consisting of the $F_i$, $G_i$, $I_i$, $M_i$ values, $[N]$ is an (N-1) x 1 matrix consisting of the $N_i$ values, and $[\Delta\varphi]$ is an (N-1) x 1 matrix consisting of the unknown $\Delta\varphi_i$ values. Eq. (4-19) is solved by a matrix factorization technique. Details are given in Ref. 8. Once (4-19) is solved for $\Delta\varphi_i$, new values of $\varphi$ are calculated, and the procedure is repeated until convergence is obtained. The convergence criteria is based on $\varphi''_w$ for laminar flow and on $\varphi''_w$ and $\delta^*$ for turbulent flow.

Once convergence is obtained the boundary layer properties at the station $\xi^* = \xi^*_m$ are known. The velocity profile is known from $\frac{u}{u_e} = f' = \varphi' + 1$. Other parameters (assuming $t = 0$) follow from

$$c_f = \frac{2\tau_w}{\rho u_e^2} = \frac{2}{\sqrt{Re_\infty}} \left(\frac{\rho_w}{\rho}\right)^{\epsilon} \frac{\varphi''_w}{\sqrt{2\xi^*}} \qquad (4\text{-}20)$$

$$\delta^* = -\frac{C\sqrt{2\xi^*}}{\sqrt{Re_\infty}\, u_e^* \left(\frac{\rho_w}{\rho}\right)^{\epsilon}} (\varphi_\delta - \varphi_w) \qquad (4\text{-}21)$$

$$\theta = -\frac{C\sqrt{2\xi^*}}{\sqrt{Re_\infty}\, u_e^* \left(\frac{\rho_w}{\rho}\right)^{\epsilon}} \int_0^{\eta_\delta} \varphi'(\varphi'+1)\, d\eta \qquad (4\text{-}22)$$

$$\delta = \frac{c\sqrt{2\xi^*}\,\eta_\delta}{\sqrt{Re_\infty}\,u_e^*\left(\frac{\Omega\omega}{c}\right)^\epsilon} \qquad (4\text{-}23)$$

$$Re_{\delta^*} = \rho u_e \delta^*/\mu = Re_\infty u_e^* \frac{\delta^*}{c} \qquad (4\text{-}24)$$

$$Re_\theta = \rho u_e \theta/\mu = Re_\infty u_e^* \frac{\theta}{c} \qquad (4\text{-}25)$$

In general the integrals are evaluated numerically. The value of $\eta_\delta$ is the value of $\eta$ for which $f' = .995$ ( $\varphi' = -.005$).

Boundary Layer Solution

The solution begins at the stagnation point where the flow is laminar. A suitable $\eta$ grid for laminar flow is $\eta_\infty = 6$ with $h_1 = .025$. A solution is then obtained for the stagnation point. Since $\xi^* = 0$ at the stagnation point, (4-14) shows that the $\xi^*$ dependent terms drop out. The solution is not completely self-starting however, since the $\varphi_0$ terms are required. A good initial guess for $\varphi_0'$ was found to be

$$\varphi_0' = -\left(\frac{\eta}{3}\right)^4 + 4\left(\frac{\eta}{3}\right)^3 - 6\left(\frac{\eta}{3}\right)^2 + 4\left(\frac{\eta}{3}\right) - 1 \qquad (0 \le \eta \le 3)$$

and

$$\varphi_0' \doteq 0 \qquad (3 \le \eta \le 6)$$

Values of $\varphi_0$, $\varphi_0''$, $\varphi_0'''$ are found by differentiation and integration of $\varphi_0'$. The iteration continues until convergence is ob-

tained (the stagnation point solution converges to the Falkner-Skan solution). With the stagnation point solution known, the first downstream point ( $\xi^* = \xi_1^*$ ) is calculated. Two point $\xi^*$ formulas are used for this point, while three point formulas are used for all subsequent points. For the first solution at a new downstream station, the solution for the previous station is used for $\varphi_o$, $\varphi_o'$, $\varphi_o''$, $\varphi_o'''$. When a solution is obtained for a given point, the program continues to the next downstream point. This is continued until separation or transition occurs. Separation is determined by $\varphi_w'' \rightarrow 0$ (i.e., $\frac{\partial u}{\partial y}\Big|_w \rightarrow 0$ ). A variety of transition criteria could be used. Those considered for this analysis are

$$Re_\theta = 640 \qquad \text{for} \qquad \frac{dP_e}{dx} \leq 0$$

$$Re_\theta = 320 \qquad \text{for} \qquad \frac{dP_e}{dx} > 0$$

and a criteria due to Gaster (Ref. 9). Gaster obtained a method for determining whether laminar separation results in complete separation or a short "laminar separation bubble" followed by a reattached turbulent boundary layer. If the laminar boundary layer is approaching separation and Gaster's criteria for "short bubble" separation is satisfied, transition to turbulent flow is assumed.

When transition occurs, the $\eta$ grid is redefined for turbulent flow. Values of the laminar solution at the previous $\xi^*$ station are obtained at the turbulent grid points by interpolation. The solution

for the first turbulent $\xi^{**}$ station is obtained using two point $\xi^{**}$ formulas, while subsequent stations use three point formulas. The turbulent solutions are obtained in the same manner as the laminar ones except that $\epsilon^{+}$ is finite and the convergence criteria also includes $\delta^{*}$. After the first iteration (only) at a new downsteam location for turbulent flow, the old and new solutions are averaged. Cebeci, Smith found this necessary to obtain convergence. The turbulent calculations continue downstream until separation occurs. Turbulent separation is also determined by the condition $\varphi_w'' \to 0$.

In actual calculations, laminar or turbulent separation is demined when $\varphi_w''$ becomes zero or negative during an iteration. This is both more reliable and more convenient than the procedure initially used (Ref. 3). This procedure cannot be used with the Gaster criteria, however, since additional iterations or downstream calculations cannot be performed. Therefore, the Gaster criteria is used if the flow is laminar and $\varphi_w'' \leq .2$. For a boundary layer that is not near separation, typical values of $\varphi_w''$ are $> 1$.

# 5. WALL JET ANALYSIS

The turbulent wall jet properties are calculated using a finite difference method based on the Keller, Cebeci method (Ref. 14). Two dimensional incompressible flow is assumed, and a typical wall jet development is sketched in Fig. 2. Wall jet calculations are a reasonably straightforward application of boundary layer theory, but there are two difficulties. The first is that, as with any turbulent flow, semi-empirical expressions are required to evaluate the Reynolds stresses. Such expressions are available, but the amount of data available is quite limited in comparison to the case of conventional boundary layers, and the available data are not always in agreement with each other. This situation leads to uncertainties in the shear stress model, but an apparently reasonable model can be formulated. The second is that on circulation controlled airfoils, the wall jet develops in a region with a small surface radius of curvature. Boundary layer theory can account for this, but the boundary layer approximations for streamline radii of curvature begin to break down over the latter portion of the jet as the jet thickens rapidly. If this effect is not adequately accounted for, the wall pressure distribution, and therefore the separation prediction, will not be accurate. An exact accounting for this effect is difficult since a required correction term contains second order streamwise derivatives, which do not fit into boundary layer theory.

During development of the wall jet analysis, calculations were performed for a flow denoted as Kind's Flow II (Ref. 15). This flow

was selected as a test case because measured wall jet profiles along with a measured boundary layer profile upstream of the blowing slot were available for it. The effective two dimensional angle of attack was also known. This flow has a moderate momentum blowing coefficient and a relatively small trailing edge radius of curvature, and should be a reasonable test case. It was originally intended to perform calculations for other flows also, including those of Ref. 11, but time did not permit this.

Before developing the wall jet equations, the boundary conditions are presented since they are simpler but illustrate similar curvature effects. The outer boundary conditions require that the jet flow match the existing external flow. When the surface radius of curvature $R$ is small, the known potential flow surface values do not apply directly at the outer edge of the jet. The potential flow is unaffected by the jet according to boundary layer theory, so the following analysis yields the outer edge conditions. The irrotationality and continuity equations for incompressible two dimensional flow are, respectively

$$\frac{\partial}{\partial y}\left(\frac{R+y}{R}u\right) - \frac{\partial v}{\partial x} = 0$$

$$\frac{\partial u}{\partial x} + \frac{\partial}{\partial y}\left(\frac{R+y}{R}v\right) = 0$$

Integrating the irrotationality equation from the wall to the edge of the jet gives

$$\frac{R+\Delta}{R}\, u_e - u_e = \int_0^{\Delta} \frac{\partial v}{\partial x}\, dy$$

where $u_e$ is the known potential flow velocity at the surface and $U_e$ is the desired outer edge velocity. In the usual analysis, as in Ref. 16 for example, $v$ terms are neglected since $v = 0$ at the wall and the region considered is thin. In this case, the continuity equation is also neglected, and the outer edge velocity is

$$U_e = \frac{R}{R+\Delta}\, u_e \qquad (5\text{-}1)$$

Eq. (5-1) is the standard curvature correction and is accurate within a limited distance of the wall. For large velocity gradients and relatively thick jets, $v$ begins to become significant and Eq. (5-1) begins to become inaccurate. A higher order term can be calculated. Using the irrotationality equation with $\frac{\partial v}{\partial x} = 0$ gives an expression for $u$, which is used in the continuity equation to obtain an expression for $v$. This expression for $v$ is then used in the irrotationality equation to obtain a new expression for $u$. For $R$ = constant, the results of this analysis give the outer edge irrotational values as

$$U_e = \frac{R}{R+\Delta}\left[u_e - \frac{R^2}{2}\frac{d^2 u_e}{dx^2}\left(\ln\frac{R+\Delta}{R}\right)^2\right] \qquad (5\text{-}2)$$

and

$$v_\Delta = -\frac{R^2}{R+\Delta}\frac{du_e}{dx}\ln\frac{R+\Delta}{R} \qquad (5\text{-}3)$$

According to conventional order of magnitude estimates, both $V_\Delta$ and the second term in the brackets in Eq. (5-2) should be insignificant. This is true for most of the jet region, but a combination of large $\frac{dU_e}{dx}$ and increasing $\Delta$ result in $V_\Delta$ eventually becoming comparable to $U_e$. The term $\frac{d^2U_e}{dx^2}$ in Eq. (5-2) is difficult to evaluate accurately since $U_e$ is only known numerically. It is calculated by fitting a least - squares straight line to three points where $\frac{dU_e}{dx}$ is known and using the slope for $\frac{d^2U_e}{dx^2}$.

The pressure $P_e$ at the outer edge of the jet is determined from

$$P_e = P_{e_{STAG}} - \frac{\rho}{2}\left(U_e^2 + V_\Delta^2\right) \qquad (5\text{-}4)$$

where $P_{e\,STAG}$ is the total pressure at the outer edge of the jet and $U_e$ and $V_\Delta$ are known from Eqs. (5-2) and (5-3). For irrotational flow, $P_{e\,STAG}$ is of course equal to the known free stream total pressure. However, the remains of the upstream boundary layer can result in a total pressure deficit, and this can be accounted for by allowing $P_{e\,STAG}$ to vary from one streamline to another. This variation is relatively minor, and will be discussed shortly.

The above analysis is used for the outer edge conditions for wall jets without a velocity minimum, i.e., after the minimum has been essentially entrained. Theoretically, it could also be used at the outer edge of jets with a velocity minimum, and this would be somewhat simpler since $P_{e\,STAG}$ would be equal to the free stream value. For typical circulation controlled airfoils, however, there are prac-

tical difficulties that suggest a different approach. The difficulties arise because the upstream boundary layer is normally several times thicker than the blowing slot, which means that the curvature corrections would have to be applied much further from the wall. This would be no problem if the surface radius of curvature did not change abruptly.

However, most circulation controlled airfoils have a discontinuous radius of curvature at the blowing slot. Applying Eq. (5-1) or (5-2) at such a point would result in a sudden decrease in $U_e$ (by about 30% for Kind's Flow II, for example). The radius of curvature could be faired in, but there is little information to suggest the proper fairing, so the result would be somewhat arbitrary. For this reason, and others discussed below, the following procedure is used.

The initial wall jet calculations include the velocity minimum, and the outer edge conditions apply at a point corresponding to the outer edge of the upstream boundary layer. The outer edge conditions are taken as the uncorrected potential flow surface values

$$U_e = u_e \quad , \quad P_e = p_e \tag{5-5}$$

To compensate for the lack of a curvature correction for the pressure, the normal pressure gradient in the wall jet equations is set equal to zero for the portion of the flow above the velocity minimum. The normal pressure gradient is actually set equal to zero slightly above the minimum instead of at the minimum, but the difference is not great. Then for the initial wall jet development, the pressure at

the velocity minimum is essentially the potential flow surface pressure $P_e$ , and the velocity $u_{MIN}$ is determined during the wall jet solution. The minimum velocity $u_{MIN}$ is zero at the slot, and the ratio $u_{MIN} / u_e$ increases as the jet procedes downstream. This ratio increases rapidly at first, and more slowly downstream. As the jet proceeds downstream, the point of minimum velocity moves further away from the wall. At each downstream location, the known value of $u_{MIN}$ is compared to a velocity calculated by applying Eq. (5-2) at the location of the minimum velocity. Initally $u_{MIN}$ is less than this velocity, but eventually the two values become approximately equal. When the two velocities become approximately equal, wall jet calculations switch over to the case of a wall jet without a minimum velocity, i.e., the flow above the minimum is dropped from wall jet calculations. At the switching point, the known velocity profile for the portion of the jet above the minimum is used to tabulate streamline constants and their corresponding total pressures. These tabulated values are then used in Eq. (5-4) to determine $P_{e\,STAG}$ for the downstream calculations.

This procedure allows a smooth transition from profiles with a minimum velocity to those without, and allows the remains of the upstream boundary layer to be accounted for approximately. By the time the switch is made to profiles without a minimum, the velocity above the minimum is nearly constant and the shear stress is thus essentially zero. The total pressure is therefore nearly constant along a streamline, although it varies somewhat from one streamline to another. A more straightforward analysis would be to continue to per-

form wall jet calculations out to the irrotational flow, i.e., to the streamline corresponding to the outer edge of the upstream boundary layer. This would require that calculations be performed out to a point further from the wall, and would not be difficult if $\frac{dU_e}{dx}$ were sufficiently small. However, $\frac{dU_e}{dx}$ eventually becomes large enough for the boundary layer approximations for streamline radii of curvature to begin to break down. As this occurs, uncertainties in the outer edge conditions and in the wall jet equations increase, and these uncertainties increase as the distance from the wall increases. This effect is severe enough to justify calculating only as far from the wall as is necessary. Therefore, the present procedure is adopted.

Fortunately, the inner boundary conditions are simpler to use and to describe. At the wall, the no slip condition and an impermeable surface result in

$$u = 0 \quad , \quad v = 0 \qquad @ \quad y = 0 \tag{5-6}$$

The boundary layer equations for the time-mean values for two dimensional incompressible turbulent flow with a small surface radius of curvature are

Continuity

$$\frac{\partial u}{\partial x} + \frac{R+y}{R}\frac{\partial v}{\partial y} + \frac{v}{R} = 0$$

or

$$\frac{\partial u}{\partial x} + \frac{\partial}{\partial y}\left(\frac{R+y}{R} v\right) = 0$$

$$\overline{u' \frac{\partial v'}{\partial y}} -$$

Momentum x

$$\rho\left(\frac{R}{R+y} u \frac{\partial u}{\partial x} + v \frac{\partial u}{\partial y} + \frac{uv}{R+y}\right) + \frac{R}{R+y} \frac{\partial P}{\partial x} - \frac{\partial \tau}{\partial y} - \frac{2\tau}{R+y} = 0$$

or

$$\frac{\partial}{\partial x}\left(\frac{P}{\rho} + \frac{u^2}{2}\right) + \frac{R+y}{R} v \left(\frac{\partial u}{\partial y} + \frac{u}{R+y}\right) - \frac{1}{R(R+y)} \frac{\partial}{\partial y}\left[(R+y)^2 \frac{\tau}{\rho}\right] = 0$$

where $\tau = \nu\rho \frac{R+y}{R} \frac{\partial}{\partial y}\left(\frac{R}{R+y} u\right) - \rho\overline{u'v'}$ is the shear stress.

Momentum y

$$\frac{1}{\rho} \frac{\partial P}{\partial y} - \frac{u^2}{R+y} = 0$$

This form of the momentum $y$ equation results from the customary boundary layer approximations, and is equivalent to assuming a streamline radius of curvature equal to $(R+y)$. This is adequate over most of the jet region, but begins to break down over the latter portion where the jet thickens rapidly due to the strong adverse pressure gradient. Experimental results indicate that the pressure change across the jet tends to zero as separation is approached. However, the above equation predicts a finite pressure change across the jet. This means that if the pressure at the outer edge of the jet is correct and the above equation is used, the pressure gradient at the wall will be too mild, which means that the predicted separation point will be too optimistic, i.e., too far downstream. The effect on calculated results can be severe enough that separation is not predicted at all, even though upstream calculated values are in good agreement

with experiment. It is necessary to obtain a more suitable form of the momentum $y$ equation.

Observation of various calculated results indicates that the pressure change across the jet must be accurately predicted, but that the form of the momentum $y$ equation used to do this is not particularly important. In other words, the pressure distribution at the wall is much more important than the details of the streamline curvature. However, in order to predict the wall pressure accurately without resorting to experimental data for each case, it is necessary to consider the streamline curvature.

The momentum $y$ equation with all convection terms retained but all stress terms neglected is

$$\frac{1}{\rho}\frac{\partial P}{\partial y} - \frac{u^2}{R+y} + v\frac{\partial v}{\partial y} + \frac{R}{R+y}u\frac{\partial v}{\partial x} = 0$$

According to boundary layer order of magnitude estimates, the last two terms are two orders of magnitude less than the first two terms. Also, some of the neglected stress terms are the same order of magnitude as the last two terms, so this form of the equation is not entirely consistent. However, the effect that needs to be accounted for in calculations seems to be due to streamline curvature rather than additional stress terms, so the above equation should be an adequate starting point. The $v\frac{\partial v}{\partial y}$ term could be included in exact form without difficulty. However, including it but not the $\frac{\partial v}{\partial x}$ term results in a negligible improvement. The $\frac{\partial v}{\partial x}$ term is more difficult since it results in a second order streamwise derivative. It is not difficult to write a finite difference expression for the

second derivative, although the expression must be centered one grid point upstream, but the resulting calculations become unstable at an incredible rate. An exact curvature correction is therefore untenable.

The second order streamwise partial derivative can be reduced to ordinary second derivatives of profile parameters if an approximate velocity profile is used, or if local similarity is assumed. If an approximate velocity profile is used, the result would be equivalent to that of Kind (Ref. 17), although the procedure is somewhat different. However, in using this procedure in conjunction with an integral method, Kind (Ref. 18) found that stability problems resulted as separation was approached, and the method had to be abandoned over the latter portion of the flow. A closely related but somewhat simpler method is to assume local similarity of the velocity profiles. This is equivalent to using an approximate velocity profile, but ignoring some of the resulting terms.

Including the $\frac{\partial v}{\partial x}$ term in exact or quasi-exact form tends to produce stability problems, while ignoring the term tends to produce an insignificant correction and therefore inaccurate wall pressure calculations. An approximate but plausible treatment of the term thus seems in order. Examining Kind's measured velocity profiles, which seem reasonably typical, suggests a possibility. For $y \leq y_m$, $\frac{\partial u}{\partial x}$ has a large negative value, while for $y > y_m$, $\frac{\partial u}{\partial x}$ may be positive or negative, but tends to have a much smaller magnitude. It follows from the continuity equation that $v$ increases fairly rap-

idly from the wall to $y_m$, then changes more slowly. Therefore, $v_m$ should be a reasonably representative value for the outer portion of the jet, where most of the pressure change across the jet occurs. If so, $\frac{dv_m}{dx}$ should provide a reasonable average value of $\frac{\partial v}{\partial x}$, and a workable form of the momentum $y$ equation should be obtainable.

Using the definition

$$u_m \delta^* = \int_0^{y_m} (u_m - u)\, dy$$

along with Leibnitz's rule and the continuity equation gives

$$\frac{R+y_m}{R} \cdot v_m = \frac{d}{dx}(u_m \delta^*) - \frac{du_m}{dx} y_m$$

Since the definition of $\delta^*$ is not modified for curvature, the $\frac{R+y_m}{R}$ term should probably be set equal to one, but the difference tends to be minor. From this,

$$\frac{dv_m}{dx} = \frac{d^2}{dx^2}(u_m \delta^*) - \frac{d^2 u_m}{dx^2} y_m - \frac{du_m}{dx}\frac{dy_m}{dx}$$

Dropping the second derivatives gives

$$\frac{dv_m}{dx} = -\frac{du_m}{dx}\frac{dy_m}{dx}$$

Using this as an average value of $\frac{\partial v}{\partial x}$ in the momentum $y$ equation produced good results for a test run, but the procedure is not entirely satisfactory as it stands. The reason is that calculations can tend to ignore the term. If $u_m$ happens to be too large during an iteration, $\frac{du_m}{dx}$ is too small, and $\frac{dy_m}{dx}$ tends to be too small

also. Thus the correction term tends to be too small. If $u_m$ is too large, the pressure change across the jet tends to be too large, and the correction term being too small tends to reinforce the problem.

Including second derivatives would tend to give a larger $\frac{dv_m}{dx}$, but can cause stability problems and probably should be used only as a last resort. At least part of the stability problem encountered with second derivatives was due to a convergence problem (described later) which tended to cause oscillations. This problem was later corrected, but by then approaching deadlines did not permit re-evaluation of various procedures.

The full momentum $y$ equation, with the aid of the continuity equation, can be written as

$$\frac{1}{\rho}\frac{\partial P}{\partial y} - \frac{u^2}{R+y}\left[1 - R\frac{\partial}{\partial x}\left(\frac{v}{u}\right)\right] - \frac{v^2}{R+y} = 0$$

Dropping the $v^2$ term and using an average value for $\frac{\partial}{\partial x}\left(\frac{v}{u}\right)$ gives

$$\frac{1}{\rho}\frac{\partial P}{\partial y} - \frac{u^2}{R+y}\left[1 - f(x)\right] = 0$$

where $f(x) = R\left[\frac{\partial}{\partial x}\left(\frac{v}{u}\right)\right]_{AVE}$. As discussed above, there is a reasonable hope of finding a suitable expression for $f(x)$ based on average values. Because of time limitations, a simple order of magnitude value determined from the potential flow values is used.

Using $\frac{v}{u} \simeq -\frac{y}{u_e}\frac{du_e}{dx}$ gives

$$\frac{\partial}{\partial x}\left(\frac{v}{u}\right) \simeq -\frac{y}{u_e}\frac{d^2u_e}{dx^2} + \frac{y}{u_e^2}\left(\frac{du_e}{dx}\right)^2$$

An average value is taken as

$$\left[\frac{\partial}{\partial x}\left(\frac{v}{u}\right)\right]_{AVE} = \frac{\Delta}{2}\left(\frac{1}{u_e}\frac{du_e}{dx}\right)^2$$

which gives

$$f(x) = \frac{R\Delta}{2}\left(\frac{1}{u_e}\frac{du_e}{dx}\right)^2$$

This approximate procedure at least allows useful calculations to be performed without the use of experimental data. Also, as mentioned previously, the normal pressure gradient is set equal to zero above the velocity minimum. This can be accomplished by setting $f = 1$ above the velocity minimum, and doing so does not result in any difficulty in the calculations.

The continuity equation is identically satisfied by introducing a stream function $\psi$ defined by

$$\rho u = \left(\frac{\partial \psi}{\partial y}\right)_x$$

$$\rho v \frac{R+y}{R} = -\left(\frac{\partial \psi}{\partial y}\right)_y$$

For the wall jet, there is no particular advantage in introducing a transformation similar to that used for the boundary layer calculations - Eq. (4-1). The independent variables are therefore retained as $(x, y)$. The dependent and independent variables are nondimensionalized and made of 0 (1) by use of the following definitions

$$\xi = \frac{x}{c} \quad , \quad \eta = \frac{y}{\mathcal{C}}$$

$$C_P = \frac{P - P_\infty}{\frac{1}{2}\rho V_\infty^2} \quad , \quad F = \frac{\psi}{\rho U_e \mathcal{C}} \quad , \quad \tau^* = \frac{\tau}{\frac{1}{2}\rho V_\infty^2}$$

$$g = \mathcal{C}/R \quad , \qquad \mathcal{C} = \text{slot thickness} \qquad (5\text{-}7)$$

Velocities nondimensionalized by $V_\infty$, and lengths nondimensionalized by $C$, are denoted by an asterisk, such as $U_e^* = U_e / V_\infty$ and $\mathcal{C}^* = \mathcal{C}/C$.

With these definitions, $u^* = U_e^* \frac{\partial F}{\partial \eta}$ , $v^* = \frac{-\mathcal{C}^*}{1+g\eta} \frac{\partial}{\partial \xi}(U_e^* F)$ and the equations become

Momentum x

$$\frac{\partial}{\partial \xi}\left[ C_P + \left( U_e^* \frac{\partial F}{\partial \eta} \right)^2 \right] - 2U_e^* \left[ \frac{\partial^2 F}{\partial \eta^2} + \frac{g}{1+g\eta} \frac{\partial F}{\partial \eta} \right] \frac{\partial}{\partial \xi}(U_e^* F)$$

$$- \frac{1}{\mathcal{C}^*} \frac{1}{1+g\eta} \frac{\partial}{\partial \eta}\left[ (1+g\eta)^2 \tau^* \right] = 0 \qquad (5\text{-}8)$$

Momentum y

$$\frac{\partial C_P}{\partial \eta} - \frac{2g[1 - f(\xi)]}{1+g\eta} U_e^{*2} \left( \frac{\partial F}{\partial \eta} \right)^2 = 0 \qquad (5\text{-}9)$$

The inner boundary conditions (5-6) become

$$F = 0 \quad , \quad \frac{\partial F}{\partial \eta} = 0 \qquad at \qquad \eta = 0 \tag{5-10}$$

The condition $U = 0$ at $y = 0$ results in the condition $U_e^* F$ = constant at $\eta = 0$ , and the first condition in Eq. (5-10) therefore results by setting the constant equal to zero. The outer boundary conditions are asymptotic but in practice are applied at a finite location $y = \Delta \quad (\eta = \eta_\Delta)$. They become

$$\frac{\partial F}{\partial \eta} = 1 \quad , \quad C_P = C_{P_e} \qquad at \qquad \eta = \eta_\Delta \tag{5-11}$$

Eqs. (5-2) to (5-4) give

$$U_e^* = \frac{1}{1+g\eta_\Delta}\left[ U_e^* - \frac{R^{*2}}{2} \frac{d^2 U_e^*}{d\xi^2} \left( \ln[1+g\eta_\Delta] \right)^2 \right] \tag{5-12a}$$

$$C_{P_e} = C_{P_{e_{STAG}}} - U_e^{*2} - \left( \frac{R^*}{1+g\eta_\Delta} \frac{dU_e^*}{d\xi} \ln[1+g\eta_\Delta] \right)^2 \tag{5-12b}$$

For the case where Eq. (5-5) is used, the values are

$$U_e^* = U_e^* \quad , \quad C_{P_e} = C_{P_e} = 1 - U_e^{*2} \tag{5-13}$$

If an eddy viscosity model is used, the shear stress is

$$\tau = \nu \rho \left(1 + \epsilon^+\right) \frac{R+Y}{R} \frac{\partial}{\partial Y} \left( \frac{R+Y}{R} u \right)$$

or

$$\tau = \nu\rho\,(1+\epsilon^+)\left(\frac{\partial u}{\partial y} - \frac{u}{R+y}\right)$$

where $\epsilon^+$ is the dimensionless eddy viscosity coefficient. As developed shortly, an eddy viscosity model is used, but with a modification to allow the shear stress to be negative at the velocity maximum. The shear stress is therefore taken as

$$\tau = \nu\rho\,(1+\epsilon^+)\left[\frac{\partial u}{\partial y} - \frac{u}{R+y} - \frac{\zeta^*}{\ell}(u-u_e)\right]$$

where $\zeta^*$ is related to the mixing length. In dimensionless form this becomes

$$\tau^* = \frac{2U_e^*}{\ell^* Re_\infty}(1+\epsilon^+)\left[\frac{\partial^2 F}{\partial \eta^2} - \frac{g}{1+g\eta}\frac{\partial F}{\partial \eta} - \zeta^*\left(\frac{\partial F}{\partial \eta} - 1\right)\right] \qquad (5\text{-}14)$$

Different eddy viscosity expressions are required for different portions of the wall jet profile. These expressions are developed below. For some of the development, it is necessary, or at least convenient, to know the approximate velocity profile shape, so this is considered first. Sketches of profiles showing notation are given in Figs. 4 and 5. One of the better integral methods for calculating wall jet development is that of Gartshore and Newman (Ref. 19), which is also used with modifications for curvature by Kind (Ref. 18). The velocity profiles used in these analyses are

$$u = u_m\left(\frac{y}{y_m}\right)^N \qquad (y \le y_m) \qquad (5\text{-}15a)$$

and

$$u = u_\delta + U_d\, e^{-b\left(\frac{y-y_m}{L_0}\right)^2} \qquad (y_m \le y \le y_\delta) \quad \text{(5-15b)}$$

where $U_d = u_m - u_\delta$, $u_\delta = U_e$ for profiles without a minimum velocity and $u_\delta = u_{MIN}$ for profiles with a minimum velocity. The constant $b = \ln 2$. The exponent $N$ varies from about 1/11 to 1/2, with N = 1/2 typically taken as a separation criteria. Eq. (5-15b) predicts an asymptotic velocity decay, but experiment (Ref. 20) and calculated values when intermittency is included indicate that $u = u_\delta$ at about $(y - y_m)/L_0 = 2.3$. The above expressions are used anytime approximate velocity profiles are required.

The eddy viscosity in the region $y \ge y_m$ is determined from Dvorak's model (Ref. 21). The data used for this region are from profiles without a velocity minimum, but the results (excluding the intermittency profile) are assumed to apply for profiles with a minimum also. Dvorak's model is based on measurements by Wygnanski and Fiedler for a variety of turbulent shear flows. An eddy Reynolds number $R_{e_T}$ is defined as in Eq. (5-16) and found to have a constant value of about 15.

$$R_{e_T} = \frac{U_d\, \sigma}{\nu \epsilon^+_m} = 15 \qquad \text{(5-16)}$$

In general, $U_d$ is a velocity deficit and $\sigma$ is the standard deviation of the intermittency profile, and thus is a measure of the size of the large eddies (Ref. 22). For a wall jet, $U_d = u_m - u_\delta$ is known, and if a suitable expression for $\sigma$ is available Eq. (5-16)

provides an eddy viscosity model. Dvorak gives results for $\sigma$ based on data by Gartshore, but as discussed below the results do not seem to be general since they essentially prescribe a wall jet thickness that is not always in agreement with experiment. The reference Dvorak cites (Gartshore's dissertation) was not available to the author, but another paper by Gartshore (Ref. 22) contains apparently the same data. In Ref. 22, Gartshore uses measured intermittency profiles for a wall jet in still air and three wall jet flows in specialized pressure gradients for which self-similar solutions exist to provide an experimental verification of Townsend's large eddy equilibrium hypothesis (Ref. 23). The data in Ref. 22 can also be used to check Eq. (5-16), and the results are in good agreement, giving a value of $R_{e_T}$ that varies between 14.5 and 17. The data for $\sigma$ can be put into different forms, and the method used here is to determine $\sigma/L_o$ as a function of $U_\delta / U_d$ . The following curves are used to do this

$$\frac{\sigma}{L_o} = .471 \qquad \left(\frac{U_\delta}{U_d} \geq 3.04\right) \tag{5-17a}$$

$$\frac{\sigma}{L_o} = .403 + .035\left(\frac{U_\delta}{U_d} - 1.1\right) \qquad \left(1.1 < \frac{U_\delta}{U_d} < 3.04\right) \tag{5-17b}$$

$$\frac{\sigma}{L_o} = .541\left(\frac{U_\delta}{U_d} - .52\right)\left(\frac{U_\delta}{U_d} - 1.1\right) - 1.114\,\frac{U_\delta}{U_d}\left(\frac{U_\delta}{U_d} - 1.1\right)$$

$$+ .632\,\frac{U_\delta}{U_d}\left(\frac{U_\delta}{U_d} - .52\right) \qquad \left(0 \leq \frac{U_\delta}{U_d} \leq 1.1\right) \tag{5-17c}$$

The mean location of the intermittency profile $\bar{y}$ is also determined

by curve fitting the data of Ref. 22 to obtain

$$\frac{\bar{y}}{L_o} = \frac{y_m}{L_o} + 1.4 \qquad \left(\frac{u_\delta}{u_d} \geq 3.04\right) \tag{5-18a}$$

$$\frac{\bar{y}}{L_o} = \frac{y_m}{L_o} + 1.59 - .098\left(\frac{u_\delta}{u_d} - 1.1\right) \qquad \left(1.1 < \frac{u_\delta}{u_d} < 3.04\right) \tag{5-18b}$$

$$\frac{\bar{y}}{L_o} = \frac{y_m}{L_o} + 3.65\left(\frac{u_\delta}{u_d} - .52\right)\left(\frac{u_\delta}{u_d} - 1.1\right) - 5.71\,\frac{u_\delta}{u_d}\left(\frac{u_\delta}{u_d} - 1.1\right) \tag{5-18c}$$

$$+ 2.49\,\frac{u_\delta}{u_d}\left(\frac{u_\delta}{u_d} - .52\right) \qquad \left(0 \leq \frac{u_\delta}{u_d} \leq 1.1\right)$$

For a given velocity profile, $u_\delta$, $u_d$ and $L_o$ are known. Eq. (5-17) then provides $\sigma$ and Eq. (5-16) then provides $\epsilon_m^+$. The value of $\bar{y}$ is determined from Eq. (5-18). The value of $\epsilon_m^+$ is multiplied by a curvature correction $K_c$ described later. For a wall jet profile without a velocity minimum. the eddy viscosity for $y \geq y_m$ is taken as

$$\epsilon^+ = K_c\,\epsilon_m^+\,\gamma \tag{5-19}$$

where

$$\gamma = \frac{1}{2}\left[1 - \operatorname{erf}\left(\frac{y-\bar{y}}{\sqrt{2}\,\sigma}\right)\right] \tag{5-20}$$

is the intermittency function.

For a profile with a minimum velocity, the eddy viscosity distribution for $y \geq y_m$ is taken as follows.

$$\epsilon^+ = K_c\,\epsilon_m^+ \qquad \left(y_m \leq y \leq y_m + L_o\right) \tag{5-21}$$

$$\epsilon^+ = \epsilon^+_{UBL} \cdot \gamma \qquad \left(Y \geq Y_m + 2.3L_o\right) \qquad (5\text{-}22)$$

where $\bar{y} = .8\Delta$ , $\sigma = .127\,\Delta$ and $\gamma$ is given by Eq. (5-20)

$$\epsilon^+ = \epsilon^+_{Y_m+L_o} + \left(\epsilon^+_{Y_m+2.3L_o} - \epsilon^+_{Y_m+L_o}\right) \cdot \qquad (5\text{-}23)$$

$$\cdot \left\{1 - \cos\left[\frac{\pi}{2}\,\frac{Y-(Y_m+L_o)}{1.3\,L_o}\right]\right\} \qquad \left(Y_m+L_o < Y < Y_m+2.3L_o\right)$$

The value in Eq. (5-21) is the same as in Eq. (5-19) except that the intermittency function is excluded. Values for Eq. (5-21) are determined the same as for Eq. (5-19). The region in which each of the above expressions is used is somewhat arbitrary but seems reasonable. Eq. (5-15b) shows that the maximum negative shear stress occurs at about $Y_m + .85\,L_o$ so the region for Eq. (5-21) extends somewhat above that point. This allows a smooth switch to profiles without a minimum. The region in which Eq. (5-22) is used corresponds approximately with the portion of the flow above the velocity minimum. In Eq. (5-22), $\epsilon^+_{UBL}$ is the maximum value in the upstream boundary layer at the slot, and is known from the known boundary layer properties. The approximate values for $\bar{y}$ and $\sigma$ in Eq. (5-22) are given by Dvorak as asymptotic values for a boundary layer with a large shape factor. They also give reasonable agreement with the intermittency distribution used in the upstream boundary layer calculations. Eq. (5-23) is an arbitrary fairing to connect the other two expressions.

For wall jets on convex surfaces, the radial gradient of momentum in the outer region is negative, and this tends to produce additional turbulence in the outer region. The curvature correction $K_c$ is used to account for this. Kind (Ref. 18) derives a curvature correction based on data for the growth of a curved wall jet in still air. Kind uses the Gartshore and Newman (Ref. 19) expression for eddy viscosity, which is essentially the same as Eq. (5-16) except that $R_{e_T}$ is determined as the sum of two terms. Kind corrects both terms for curvature, and an identical procedure does not apply with Eq. (5-16). However, the major portion of this correction is retained by taking

$$K_c = \left[1 + 4.48\ \frac{y_m + L_o}{R} - 1.34\left(\frac{y_m + L_o}{R}\right)^2\right]^2 \cdot$$

$$\cdot \left[1 + 1.34\left(\frac{y_m + L_o}{R}\right)^2\right]^{-1} \cdot \left[1 + .3\ \frac{y_m + L_o}{R}\right]^{-1} \qquad (5\text{-}24)$$

This correction can be quite significant since it can easily increase the eddy viscosity by a factor of two or more.

Eqs. (5-17) and (5-18) are used in place of those given by Dvorak since Dvorak's expressions, when used with Eq. (5-20), result in the eddy viscosity becoming zero at about the middle of Kind's measured wall jet profiles. A similar difficulty also arises for Jones' measured measured profiles (Ref. 24). This apparently is related to the fact that experiments often show different wall jet growth rates, especially near the blowing slot. Use of Eqs. (5-17) and (5-18) allows the jet thickness to be determined during the cal-

culations, and calculated results indicate that the thickness of the outer portion of the jet is essentially determined by the maximum value of the eddy viscosity. As would be expected, increasing the eddy viscosity increases the thickness of the jet. Dvorak uses a diffusion equation to allow the actual eddy viscosity to lag behind $\epsilon_m^+$, and this procedure was used initially. However, for Kind's Flow II, this procedure seemed to limit the eddy viscosity to too small a value, while use of $\epsilon_m^+$ resulted in good agreement with experiment. Therefore, the local value $\epsilon_m^+$ is used in the calculations.

The inner region ($y < y_m$) of a wall jet profile resembles a conventional turbulent boundary layer, and the conventional eddy viscosity model for a boundary layer thus seems to be a reasonable starting point for the wall jet formulation. In general, however, such a model will not match the eddy viscosity in the outer region without the aid of a somewhat arbitrary fairing. The conventional boundary layer model near the wall is

$$\epsilon_i^+ = \frac{K_1^2 y^2}{\nu} \left(1 - e^{-\frac{y}{A_0}}\right)^2 \left|\frac{\partial u}{\partial y}\right| \qquad (5\text{-}25)$$

where

$$A_0 = \frac{K_3 \nu}{\sqrt{\tau/\rho}}$$

while away from the wall the conventional model is

$$\epsilon_o^+ = \frac{K_2 u_m}{\nu} \int_0^{y_m} \left(1 - \frac{u}{u_m}\right) dy \qquad (5\text{-}26)$$

The matching condition for the two expressions is that the eddy viscosity be continuous. Common values for the constants are $K_1 = .4$, $K_2 = .0168$ and $K_3 = 26$. For low Reynolds numbers, Cebeci (Refs. 25 and 26) recommends the values

$$K_1 = .40 + \frac{.19}{1 + .49 \times 10^{-6} Re_\theta^2} \qquad (5\text{-}27)$$

$$K_3 = 26 + \frac{14}{1 + 10^{-6} Re_\theta^2} \qquad (5\text{-}28)$$

$$K_2 = \frac{.0168\ (1.55)}{1 + \Pi} \qquad (5\text{-}29)$$

where $$\Pi = .55\left\{1 - \exp\left[-.243\sqrt{\frac{Re_\theta}{425} - 1} - .298\left(\frac{Re_\theta}{425} - 1\right)\right]\right\}$$

Eqs. (5-27) and (5-28) apply for $Re_\theta \geq 300$, while Eq. (5-29) applies for $Re_\theta \geq 425$, where

$$Re_\theta = \frac{u_m}{\nu} \int_0^{y_m} \frac{u}{u_m}\left(1 - \frac{u}{u_m}\right) dy$$

The above values are used here, and if $Re_\theta$ is less than the given limiting values the expressions are evaluated for the limiting values. The $\frac{\tau}{\rho}$ term in the expression for $A_o$ is evaluated in terms of $\frac{\tau_w}{\rho}$ and the pressure gradient by the usual procedure. Near the wall the convective terms are neglected, and the momentum $X$ equation is

$$\frac{\partial}{\partial x}\left(\frac{p}{\rho}\right) = \frac{1}{R(R+y)}\frac{\partial}{\partial y}\left[(R+y)^2\frac{\tau}{\rho}\right]$$

Evaluating the pressure gradient at the wall and integrating gives

$$\frac{\tau}{\rho} = \left(\frac{R}{R+y}\right)^2\left[\frac{\tau_w}{\rho} + \frac{\partial}{\partial x}\left(\frac{p}{\rho}\right)\Big|_w \frac{y}{R}\left(R+\frac{y}{2}\right)\right]$$

This expression could be used as is, but for conventional boundary layers Cebeci (Ref. 28) recommends evaluating it at

$$y_s = \frac{11.8\,\nu}{\sqrt{\tau_w/\rho}} \qquad (5\text{-}30a)$$

The expression was used with $y$ as a variable and also with $y$ evaluated at various fixed locations, and the difference in the solution was insignificant. The form used gives

$$A_o = K_3\,\nu\,\frac{R+y_s}{R}\left[\frac{\tau_w}{\rho} + \frac{\partial}{\partial x}\left(\frac{p}{\rho}\right)\Big|_w \frac{y_s}{R}\left(R+\frac{y_s}{2}\right)\right]^{-1/2} \qquad (5\text{-}30b)$$

were $y_s$ is given by Eq. (5-30a). For a convex radius of curvature, both the inner and outer eddy viscosity expressions can be corrected by multiplying by $S^2$, where (Ref. 27)

$$S = \left(1 + \frac{14u}{R\frac{\partial u}{\partial y}}\right) \qquad (5\text{-}31)$$

Gartshore and Newman (Ref. 19) use a correction to the outer eddy viscosity to allow for the turbulence in the outer portion of the wall jet. This correction is equivalent to multiplying Eq. (5-26)

by the factor $T$ , where

$$T = 50 \Big/ \left\{ 15 + 35\, e^{-\left(\frac{\tau_{y_m+L_o}}{\tau_w}\right)^2} \right\} \qquad (5\text{-}32)$$

Gartshore and Newman use this expression in conjunction with an integral method to determine the shear stress at $y = \frac{1}{2} y_m$ , and how it applies in the present formulation should probably depend on where the fairing to join the outer region begins.

The eddy viscosity distribution is taken as follows. Near the wall, Eqs. (5-25, 27, 28, 30) are used to evaluate $\epsilon_i^+$ . This expression is used until $\epsilon_i^+ = \epsilon_o^+$, where $\epsilon_o^+$ is determined from Eqs. (5-26, 29). Matching occurs at about $y = .2\, y_m$. From the matching point to $y_m$ , the eddy viscosity is determined from the somewhat arbitrary fairing

$$\epsilon^+ = \epsilon_o^+ + \frac{K_c \epsilon_m^+ - \epsilon_o^+}{2} \left[ 1 - erf\left(\frac{y - .65\, y_m}{.175\, y_m}\right) \right] \qquad (5\text{-}33)$$

A typical eddy viscosity distribution as determined by the above procedure is shown in Fig. 4, and is drawn to scale for one of the calculated velocity profiles. A lack of detailed information for the inner region along with the difference in magnitude between $\epsilon_o^+$ and $K_c \epsilon_m^+$ leads to some uncertainty in the formulation. Several variations for $\epsilon_i^+$, $\epsilon_o^+$ and the fairing were used during development of the analysis. These variations were made while attempting to sort out development difficulties that were related to a convergence anomaly and, eventually, the inaccurate pressure gradient

over the latter portion of the jet. Most of the variations were made before these difficulties were sorted out, so conclusions concerning them are somewhat tentative, but are probably reasonable. The expressions used for $\epsilon_c^+$ and the fairing seem to have only a minor effect on calculated velocity profiles. The value of $\epsilon_o^+$ can have more of an effect, and its streamwise variation is of significance. If $\epsilon_o^+$ increases too slowly in the streamwise direction, the velocity gradient near the wall tends to remain too high. Since the value of $\epsilon_o^+$ is of some significance, a fairing that allows the eddy viscosity to remain essentially equal to $\epsilon_o^+$ for a short distance seems appropriate. Otherwise, the value of $\epsilon_o^+$ may be effectively lost since the calculations may fail to distinguish where the $\epsilon_c^+$ expression stops and the fairing begins.

Eq. (5-31) was included in the formulation at one time, but tended to reinforce an oscillation that was occurring in the solution, and was therefore dropped. The oscillation was later eliminated, but use of Eq. (5-31) was not reconsidered. For the fairing used, the value of $\epsilon^+$ at $y = \frac{1}{2} y_m$ depends on $\epsilon_o^+$ and $K_c \epsilon_m^+$ . The value of $\epsilon^+$ is increasing very rapidly with $y$ for this portion of the profile, and the value at $y = \frac{1}{2} y_m$ is in reasonable agreement with Eq. (5-32).

Turbulent wall jets typically have a negative shear stress at $y = y_m$ . The explanation for this is that the turbulence from the outer region can spill over into the inner region, and vice versa, but the large eddies in the outer region tend to dominate the

flow at $y = y_m$. Gartshore and Newman (Ref. 19) use the empirical expression

$$\tau_m = \tau_{y_m + L_o} \cdot \left[ .15 + .30 \left( \frac{y_m}{L_o} \right)^2 \right]$$

for the magnitude of $\tau$ at $y = y_m$. Kind (Ref. 18) uses the same expression but with a modification for curvature. According to the above expression, $\tau_m$ is of the order of 20% of the maximum negative shear stress in the outer region, and thus can have a magnitude comparable to or greater than the wall shear stress. Gartshore and Newman found that using $\tau_m = 0$ in their integral method resulted in $y_m$ being too small, i.e., the velocity maximum remaining too close to the wall, and a similar result was obtained in the present method using a conventional eddy viscosity model. A method to allow $\tau_m$ to be negative was therefore devised.

Following the usual mixing length analysis (Ref. 29), but retaining second derivatives in the Taylor series and applying the analysis near the velocity maximum gives

$$\overline{|u'|} \cdot \frac{\ell^2}{2} \left| \frac{\partial^2 u}{\partial y^2} \right|$$

where $\ell$ is the mixing length. By analogy with usual mixing length procedure, the shear stress is taken as

$$\frac{\tau}{\rho} = \nu \epsilon^+ \frac{\ell}{2} \frac{\partial^2 u}{\partial y^2}$$

This result only applies near the velocity maximum and it is not desirable to retain the second derivative, so the approximate velocity profiles given by Eq. (5-15) are used to evaluate the term. From Eq. (5-15b) assuming a profile without a minimum velocity

$$\frac{\partial u}{\partial y} = \left[ -\frac{2b}{L_o} \quad \frac{y-y_m}{L_o} \right] (u-u_e)$$

$$\frac{\partial^2 u}{\partial y^2} = -\frac{2b}{L_o^2}\left[ 1 - 2b\left(\frac{y-y_m}{L_o}\right)^2 \right] (u-u_e)$$

where $2b = 2\ln 2 = 1.387$. Using the mixing length expression $\nu\epsilon^+ = \ell^2 \left|\frac{\partial u}{\partial y}\right|$, Eq. (5-16) for $\nu\epsilon^+$, the above expression for $\frac{\partial u}{\partial y}$ evaluated at $y = y_m + L_o$, and $\tau = .4 L_o$ as typical values gives $\ell \simeq .2 L_o$. Therefore, the shear stress correction term is taken as

$$\frac{\tau}{\rho} = -\nu(1+\epsilon^+) \frac{.1387}{L_o}\left[ 1 - 1.387\left(\frac{y-y_m}{L_o}\right)^2 \right] (u-u_e)$$

This yields $\tau_m = .2\,\tau_{y_m + L_o}$, which is in reasonable agreement with experiment. The maximum negative shear stress is unchanged by the above term since the term vanishes at about $y_m + .85 L_o$.

Use of Eq. (5-15a) gives

$$\frac{\partial u}{\partial y} = \frac{N u_m}{y_m}\left(\frac{y}{y_m}\right)^{N-1} = \frac{N u}{y_m}\left(\frac{y_m}{y}\right)$$

$$\frac{\partial^2 u}{\partial y^2} = \frac{N(N-1) u_m}{y_m^2}\left(\frac{y}{y_m}\right)^{N-2} = \frac{N(N-1) u}{y_m^2}\left(\frac{y_m}{y}\right)^2$$

Neither of these expressions match the outer expressions at $y = y_m$ Also, the form is different, and $\frac{\partial^2 u}{\partial y^2}$ does not become zero at a convenient point as it does for the outer portion. The result for $\frac{\partial^2 u}{\partial y^2}$ is therefore used as a guide, but is altered so that it matches the outer expression to give

$$\frac{\tau}{\rho} = -\nu (1+\epsilon^+) \frac{.1387}{L_o} \left(\frac{y_m}{y}\right)^2 (u - u_e)$$

the $\left(\frac{y_m}{y}\right)^2$ term is replaced by a linear fairing from the wall to the somewhat arbitrarily selected point $y = .6 y_m$. Reasonable variations in this matching point have little effect on calculated results. Results of the above analysis are added to the conventional eddy viscosity model, giving Eq. (5-14), where

$$\mathcal{L}^* = \frac{.1387}{\eta_{L_o}} \left[\frac{\eta}{.216 \eta_m}\right] \qquad (0 \le \eta < .6\eta_m) \qquad (5\text{-}34a)$$

$$\mathcal{L}^* = \frac{.1387}{\eta_{L_o}} \left(\frac{\eta_m}{\eta}\right)^2 \qquad (.6\eta_m \le \eta \le \eta_m) \qquad (5\text{-}34b)$$

$$\mathcal{L}^* = \frac{.1387}{\eta_{L_o}} \left[1 - 1.387 \left(\frac{\eta - \eta_m}{\eta_{L_o}}\right)^2\right] \qquad (5\text{-}34c)$$
$$(\eta_m < \eta \le \eta_m + .85\eta_{L_o})$$

$$\mathcal{L}^* = 0 \qquad (\eta > \eta_m + .85\eta_{L_o}) \qquad (5\text{-}34d)$$

Eq. (5-14) along with Eq. (5-34) is used for profiles with or without a minimum velocity. No direct modification is made for curvature.

The equations are solved by a finite difference method based on the Keller, Cebeci method (Ref. 14). This method applies to a system

of first order differential equations, and the present equations are rewritten as such a system by defining

$$G = \frac{\partial F}{\partial \eta} \tag{5-35}$$

$$H = \frac{\partial G}{\partial \eta} \tag{5-36}$$

With these definitions, Eqs. (5-8, 9, 10, 11, 14) become

Momentum x

$$\frac{\partial}{\partial \xi}\left[C_{\mathcal{I}} + (U_e^* G)^2\right] - 2U_e^*\left[H + \frac{g}{1+g\eta} G\right]\frac{\partial}{\partial \xi}(U_e^* F)$$

$$- \frac{2U_e^*}{\mathcal{L}^{*2} Re_\infty} \frac{1}{1+g\eta} \frac{\partial}{\partial \eta}\left\{(1+g\eta)^2 (1+\epsilon^+)\cdot\right.$$

$$\left.\cdot\left[H - \frac{g}{1+g\eta} G - \mathcal{L}^*(G-1)\right]\right\} = 0 \tag{5-37}$$

Momentum y

$$\frac{\partial C_{\mathcal{I}}}{\partial \eta} - \frac{2g[1-f(\xi)]}{1+g\eta} U_e^{*2} G^2 = 0 \tag{5-38}$$

Inner Boundary Conditions

$$F = 0\,,\ G = 0 \quad at \quad \eta = 0 \tag{5-39}$$

Outer Boundary Conditions

$$G = 1\,,\ C_{\mathcal{I}} = C_{\mathcal{I}_e} \quad at \quad \eta = \eta_\Delta \tag{5-40}$$

The finite difference procedure applies to the arbitrary grid

$$\xi_1 = \xi_{SLOT} \;, \quad \xi_m = \xi_{m-1} + \ell_m \qquad m = 2, .., N$$

$$\eta_1 = 0 \;, \quad \eta_j = \eta_{j-1} + h_j \qquad j = 2, .., J$$

Values at a grid point $(\xi_m, \eta_j)$ are denoted as $F_j^m$, and the notation

$$\xi_{m-1/2} = \frac{1}{2}(\xi_m + \xi_{m-1}) \;, \quad \eta_{j-1/2} = \frac{1}{2}(\eta_j + \eta_{j-1})$$

is used for averages of grid points. Averages are taken as

$$F_j^{m-1/2} = \frac{1}{2}(F_j^m + F_j^{m-1}) \;, \quad F_{j-1/2}^m = \frac{1}{2}(F_j^m + F_{j-1}^m)$$

$$F_{j-1/2}^{m-1/2} = \frac{1}{2}(F_{j-1/2}^m + F_{j-1/2}^{m-1}) = \frac{1}{2}(F_j^{m-1/2} + F_{j-1}^{m-1/2})$$

The finite difference procedure uses first order centered difference formulas for derivatives, and average values for algebraic terms. Such a procedure is inherently stable in the sense that no extraneous solutions to the difference equations can be present and grow as calculations proceed downstream. Other types of instabilities are possible, but can be avoided. Streamwise derivatives are taken as

$$\frac{\partial w}{\partial \xi} \rightarrow (w_{j-1/2}^m - w_{j-1/2}^{m-1}) / \ell_m$$

An equivalent expression for normal derivatives is

$$\frac{\partial w}{\partial \eta} \rightarrow \left( w_j^{m-1/2} - w_{j-1}^{m-1/2} \right) / h_j$$

Because of the form of the equations, some simplification without loss of accuracy results by taking

$$\frac{\partial w}{\partial \eta} \rightarrow \left( w_j^{m} - w_{j-1}^{m} \right) / h_j$$

Eqs. (5-35, 36) are taken as

$$\left( F_j^m - F_{j-1}^m \right) / h_j = G_{j-1/2}^m$$

$$\left( G_j^m - G_{j-1}^m \right) / h_j = H_{j-1/2}^m$$

This is the form used by Keller, Cebeci. It results in no loss of accuracy since satisfying the above equations at each $\xi_m$ also results in averages at $\xi_{m-1/2}$ being satisfied. Eq. (5-38) is taken as

$$\left( C_{\frac{p}{2}_j}^m - C_{\frac{p}{2}_{j-1}}^m \right) / h_j = \frac{2 g_m \left( 1 - f_m \right)}{1 + g_m \eta_{j-1/2}} L e_m^{k^2} \left( G_{j-1/2}^m \right)^2$$

This equation could also be written for $\xi_{m-1/2}$ instead of $\xi_m$, and initially it was. The difference in the solution was insignificant, so the simpler form above is used. Eq. (5-37) is taken as

$$\left\{\left[C_F + (U_e^* G)^2\right]_{j-1/2}^{m} - \left[C_F + (U_e^* G)^2\right]_{j-1/2}^{m-1}\right\} / R_{e_m}$$

$$-\left\{\left[U_e^* H + \frac{g}{1+g\eta} U_e^* G\right]_{j-1/2}^{m} + \left[U_e^* H + \frac{g}{1+g\eta} U_e^* G\right]_{j-1/2}^{m-1}\right\} \cdot$$

$$\cdot \left[U_{e_m}^* F_{j-1/2}^{m} - U_{e_{m-1}}^* F_{j-1/2}^{m-1}\right] / R_{e_m} - \frac{2 U_{e_m}^*}{\mathcal{L}^{*2} Re_\infty} \frac{1}{1+g_m \eta_{j-1/2}} \cdot$$

$$\cdot \left[\left\{(1+g\eta)^2 (1+\epsilon^+)\left[H - \frac{g}{1+g\eta} G - \mathcal{L}^* (G-1)\right]\right\}_j^{m}\right.$$

$$\left. - \left\{(1+g\eta)^2 (1+\epsilon^+)\left[H - \frac{g}{1+g\eta} G - \mathcal{L}^* (G-1)\right]\right\}_{j-1}^{m}\right] / h_j = 0$$

In the above form, the shear stress term is the only $\eta$ derivative, and is treated in the form

$$\frac{\partial W}{\partial \eta} \rightarrow \left(W_j^m - W_{j-1}^m\right) / h_j$$

Because of the other terms in the equation, it would seem better to treat it in the form

$$\frac{\partial W}{\partial \eta} \rightarrow \left(W_j^{m-1/2} - W_{j-1}^{m-1/2}\right) / h_j$$

as Keller, Cebeci do. However, the second form results in a difficulty if the calculations begin at the slot, as they do in the present solution. As discussed later, the initial wall jet profile is taken as a fully developed slot profile plus the known upstream boundary layer profile. For fully developed slot flow, the shear

stress decreases linearly from the wall and its slope depends on the pressure gradient in the slot. The wall jet adapts to the external pressure gradient, which in general is much different than that in the slot, so the shear stress gradient near the wall is considerably different for the first downstream point. Use of the second finite difference form therefore results in drastic oscillations as the calculations try to make the average shear stress gradient correct. The first form avoids this difficulty. It would be possible to switch from the first to the second form at some point downstream of the slot. At one time this was done, but it resulted in an insignificant difference, so the first form is retained throughout for simplicity.

In the calculations, a solution is known at a station $\xi_{m-1}$, and the equations are used to find the solution at $\xi_m$. Use of the finite difference expressions results in the above system of nonlinear algebraic equations. An iterative procedure is required to solve these equations, and the Keller, Cebeci procedure is used. The superscript $m$ is dropped, and the $i$ th iteration is denoted as $F_j^{(i)}$. Also, $F_j^{(i+1)} = F_j^{(i)} + \delta F_j^{(i)}$ with similar expressions for the other variables. The $\delta F_j^{(i)}$ is a perturbation term which is solved for in each iteration. Substituting the above expressions into the finite difference equations and neglecting products of perturbation terms. From Eq. (5-35)

$$\delta F_j^{(i)} - \frac{h_j}{2}\delta G_j^{(i)} - \delta F_{j-1}^{(i)} + \frac{h_j}{2}\delta G_{j-1}^{(i)} = g_{j-1/2}^{(i)} \qquad (5\text{-}41)$$

where $$g_{j-1/2}^{(i)} = -F_j^{(i)} + F_{j-1}^{(i)} + h_j \, G_{j-1/2}^{(i)}$$

From Eq. (5-36)

$$\delta G_j^{(i)} - \frac{h_j}{2}\delta H_j^{(i)} - \delta G_{j-1}^{(i)} + \frac{h_j}{2}\delta H_{j-1}^{(i)} = r_{j-1/2}^{(i)} \qquad (5\text{-}42)$$

where $$r_{j-1/2}^{(i)} = -G_j^{(i)} + G_{j-1}^{(i)} + h_j \, H_{j-1/2}^{(i)}$$

From Eq. (5-38)

$$\omega_j^{(i)}\delta G_j^{(i)} + \delta C_{E_j}^{(i)} + \omega_j^{(i)}\delta G_{j-1}^{(i)} - \delta C_{E_{j-1}}^{(i)} = s_{j-1/2}^{(i)} \qquad (5\text{-}43)$$

where

$$s_{j-1/2}^{(i)} = -C_{E_j}^{(i)} + C_{E_{j-1}}^{(i)} + h_j \frac{2g_m(1-f_m)\,U_{e_m}^{*2}}{1+g_m\eta_{j-1/2}}\left[G_{j-1/2}^{(i)}\right]^2$$

From Eq. (5-37)

$$\gamma_j^{(i)}\delta F_j^{(i)} + \beta_j^{(i)}\delta G_j^{(i)} + \theta_j^{(i)}\delta H_j^{(i)} + \lambda_j^{(i)}\delta C_{E_j}^{(i)} \qquad (5\text{-}44)$$

$$+\gamma_j^{(i)}\delta F_{j-1}^{(i)} + \overline{\beta}_j^{(i)}\delta G_{j-1}^{(i)} + \varphi_j^{(i)}\delta H_{j-1}^{(i)} + \lambda_j^{(i)}\delta C_{E_{j-1}}^{(i)} = t_{j-1/2}^{(i)}$$

where

$$\gamma_j^{(i)} = -\frac{h_j}{k_n}\frac{U_{e_m}^*}{2}\left\{U_{e_m}^*\left[H_{j-1/2}^{(i)} + \frac{g_m}{1+g_m\eta_{j-1/2}}G_{j-1/2}^{(i)}\right]\right.$$

$$\left. + U_{e_{m-1}}^*\left[H_{j-1/2}^{m-1} + \frac{g_{m-1}}{1+g_{m-1}\eta_{j-1/2}}G_{j-1/2}^{m-1}\right]\right\}$$

$$\varphi_j^{(i)} = \frac{R_j}{R_m} U_{e_m}^* \left\{ U_{e_m}^* G_{j-1/2}^{(i)} - \frac{1}{2} \frac{g_m}{1+g_m \eta_{j-1/2}} \cdot \right.$$

$$\left. \cdot \left[ U_{e_m}^* F_{j-1/2}^{(i)} - U_{e_{m-1}}^* F_{j-1/2}^{m-1} \right] \right\} + U_{e_m}^* E_j^{(i)} \left[ \frac{g_m}{1+g_m \eta_j} + \mathcal{L}_j^{*(i)} \right]$$

$$\theta_j^{(i)} = - \frac{R_j}{R_m} \frac{U_{e_m}^*}{2} \left[ U_{e_m}^* F_{j-1/2}^{(i)} - U_{e_{m-1}}^* F_{j-1/2}^{m-1} \right] - U_{e_m}^* E_j^{(i)}$$

$$\lambda_j^{(i)} = \frac{1}{2} \frac{R_j}{R_m}$$

$$\sigma_j^{(i)} = \frac{R_j}{R_m} \left\{ U_{e_m}^{*2} G_{j-1/2}^{(i)} - \frac{U_{e_m}^*}{2} \frac{g_m}{1+g_m \eta_{j-1/2}} \cdot \right.$$

$$\left. \cdot \left[ U_{e_m}^* F_{j-1/2}^{(i)} - U_{e_{m-1}}^* F_{j-1/2}^{m-1} \right] \right\} - U_{e_m}^* E_{j-1}^{(i)} \left[ \frac{g_m}{1+g_m \eta_{j-1}} + \mathcal{L}_{j-1}^{*(i)} \right]$$

$$\varphi_j^{(i)} = - \frac{R_j}{R_m} \frac{U_{e_m}^*}{2} \left[ U_{e_m}^* F_{j-1/2}^{(i)} - U_{e_{m-1}}^* F_{j-1/2}^{m-1} \right] + U_{e_m}^* E_{j-1}^{(i)}$$

$$t_{j-1/2}^{(i)} = \frac{R_j}{R_m} \left\{ - \left[ C_{I_{j-1/2}}^{(i)} + \left( U_{e_m}^* G_{j-1/2}^{(i)} \right)^2 \right] + \left[ C_{I_{j-1/2}}^{m-1} + \left( U_{e_{m-1}}^* G_{j-1/2}^{m-1} \right)^2 \right] \right.$$

$$+ \left[ U_{e_m}^* \left( H_{j-1/2}^{(i)} + \frac{g_m}{1+g_m \eta_{j-1/2}} G_{j-1/2}^{(i)} \right) + U_{e_{m-1}}^* \left( H_{j-1/2}^{m-1} + \frac{g_{m-1}}{1+g_{m-1} \eta_{j-1/2}} G_{j-1/2}^{m-1} \right) \right] \cdot$$

$$\left. \cdot \left[ U_{e_m}^* F_{j-1/2}^{(i)} - U_{e_{m-1}}^* F_{j-1/2}^{m-1} \right] \right\}$$

$$+ U_{e_m}^* E_j^{(i)} \left[ H_j^{(i)} - \frac{g_m}{1+g_m \eta_j} G_j^{(i)} - \mathcal{L}_j^{*(i)} \left( G_j^{(i)} - 1 \right) \right]$$

$$- U_{e_m}^* E_{j-1}^{(i)} \left[ H_{j-1}^{(i)} - \frac{g_m}{1+g_m \eta_{j-1}} G_{j-1}^{(i)} - \mathcal{L}_{j-1}^{*(i)} \left( G_{j-1}^{(i)} - 1 \right) \right]$$

$$E_j^{(i)} = \frac{2 \left( 1+g_m \eta_j \right)^2 \left( 1+\epsilon^+ \right)_j^{(i)}}{C^{*2} Re_\infty \left( 1+g_m \eta_{j-1/2} \right)} \quad , \quad E_{j-1}^{(i)} = \frac{2 \left( 1+g_m \eta_{j-1} \right)^2 \left( 1+\epsilon^+ \right)_{j-1}^{(i)}}{C^{*2} Re_\infty \left( 1+g_m \eta_{j-1/2} \right)}$$

Eq. (5-44) neglects terms resulting from $\delta\epsilon^+$ since there is no simple way to handle such terms. Keller, Cebeci also neglected such terms and found that doing so did not damage convergence.

The boundary conditions (5-39) and (5-40) are enforced for each iteration. Since $\eta_1 = 0$, Eq. (5-39) results in

$$\delta F_1^{(i)} = 0 \tag{5-45a}$$

$$\delta G_1^{(i)} = 0 \tag{5-45b}$$

The thickness of the jet at a station $\xi_m$ is determined during the solution. A basic grid is selcted, and the outer point $\eta_J$ in the grid should be far enough from the wall to allow for the maximum jet thickness that will be encountered. Over much of the jet region, the jet will be much thinner than this, so the entire grid is not used in all calculations. The outer boundary conditions are handled as follows. A grid point $J_\epsilon \leq J$, corresponding approximately to $\eta_{J\epsilon} = 1.2\,\eta_{\Delta m-1}$, is selected as the outer point. Eq. (5-12) or (5-13) is applied to obtain $U_e^*$ and $C_{\ell_e}$ at $\eta_{J\epsilon}$. Eq. (5-40) is enforced at $\eta_{J\epsilon}$ for each iteration, and this gives

$$\delta G_{J\epsilon}^{(i)} = 0 \tag{5-46a}$$

$$\delta C_{\ell_{J\epsilon}}^{(i)} = 0 \tag{5-46b}$$

The actual thickness $\eta_\Delta$ of the jet may be less than $\eta_{J\epsilon}$.

The system of equations is solved by a matrix factorization procedure analogous to that used by Keller, Cebeci. The equations are written in a particular order and then considered in groups of four to obtain the desired form. The first group consists of Eqs. (5-45a) (5-45b), (5-44) for $j = 2$, and (5-43) for $j = 2$, in that order. The second group (in order) consists of Eqs. (5-41) for $j = 2$, (5-42) for $j = 2$, (5-44) for $j = 3$, and (5-43) for $j = 3$. Subsequent groups, except for the last group, are analogous to the second group, but with $j$ increased by one for each group. The last group (in order) consists of Eqs. (5-41) for $j = J_E$, (5-42) for $j = J_E$, (5-46a), and (5-46b). This system of equations in matrix form is then

$$[A^{(i)}][\delta^{(i)}] = [\varphi^{(i)}]$$

where

$$[\delta^{(i)}] = \begin{bmatrix} \delta_1^{(i)} \\ \delta_2^{(i)} \\ \vdots \\ \delta_j^{(i)} \\ \vdots \\ \delta_{J_E}^{(i)} \end{bmatrix} \qquad [\varphi^{(i)}] = \begin{bmatrix} \varphi_1^{(i)} \\ \varphi_2^{(i)} \\ \vdots \\ \varphi_j^{(i)} \\ \vdots \\ \varphi_{J_E}^{(i)} \end{bmatrix}$$

$$\left[A^{(i)}\right] = \begin{bmatrix} A_1^{(i)} & C_1^{(i)} & & & & & \\ B_2^{(i)} & A_2^{(i)} & C_2^{(i)} & & & & \\ & B_3^{(i)} & A_3^{(i)} & C_3^{(i)} & & 0 & \\ & & \ddots & \ddots & \ddots & & \\ & & & B_j^{(i)} & A_j^{(i)} & C_j^{(i)} & \\ & & & & \ddots & \ddots & \ddots \\ & & 0 & & & B_{J_E-1}^{(i)} & A_{J_E-1}^{(i)} & C_{J_E-1}^{(i)} \\ & & & & & B_{J_E}^{(i)} & A_{J_E}^{(i)} \end{bmatrix}$$

where

$$\delta_j^{(i)} = \begin{bmatrix} \delta F_j^{(i)} \\ \delta G_j^{(i)} \\ \delta H_j^{(i)} \\ \delta C_{E_j}^{(i)} \end{bmatrix} \quad (j = 1, \ldots, J_E) \quad , \quad Q_j^{(i)} = \begin{bmatrix} g_{j-1/2}^{(i)} \\ \ell_{j-1/2}^{(i)} \\ t_{j+1/2}^{(i)} \\ \ell_{j+1/2}^{(i)} \end{bmatrix} \quad (j = 2, \ldots, J_E - 1)$$

$$Q_1^{(i)} = \begin{bmatrix} 0 \\ 0 \\ t_{3/2}^{(i)} \\ \ell_{3/2}^{(i)} \end{bmatrix} \qquad Q_{J_E}^{(i)} = \begin{bmatrix} g_{J_E-1/2}^{(i)} \\ \ell_{J_E-1/2}^{(i)} \\ 0 \\ 0 \end{bmatrix}$$

$$A_1^{(i)} = \begin{bmatrix} 1 & 0 & 0 & 0 \\ 0 & 1 & 0 & 0 \\ \gamma_2^{(i)} & \sigma_2^{(i)} & \varphi_2^{(i)} & \lambda_2^{(i)} \\ 0 & \omega_2^{(i)} & 0 & -1 \end{bmatrix}$$

$$A_{J_E}^{(i)} = \begin{bmatrix} 1 & -\frac{h_{J_E}}{2} & 0 & 0 \\ 0 & 1 & -\frac{h_{J_E}}{2} & 0 \\ 0 & 1 & 0 & 0 \\ 0 & 0 & 0 & 1 \end{bmatrix}$$

$$A_j^{(i)} = \begin{bmatrix} -1 & -\frac{h_j'}{2} & 0 & 0 \\ 0 & 1 & -\frac{h_j'}{2} & 0 \\ \gamma_{j+1}^{(i)} & \sigma_{j+1}^{(i)} & \varphi_{j+1}^{(i)} & \lambda_{j+1}^{(i)} \\ 0 & \omega_{j+1}^{(i)} & 0 & -1 \end{bmatrix} \quad (j = 2, J_E - 1)$$

$$B_j^{(i)} = \begin{bmatrix} -1 & -\frac{h_j'}{2} & 0 & 0 \\ 0 & -1 & -\frac{h_j'}{2} & 0 \\ 0 & 0 & 0 & 0 \\ 0 & 0 & 0 & 0 \end{bmatrix} \quad (j = 2, J_E)$$

$$C_j^{(i)} = \begin{bmatrix} 0 & 0 & 0 & 0 \\ 0 & 0 & 0 & 0 \\ \gamma_{j+1}^{(i)} & \sigma_{j+1}^{(i)} & \theta_{j+1}^{(i)} & \lambda_{j+1}^{(i)} \\ 0 & \omega_{j+1}^{(i)} & 0 & 1 \end{bmatrix} \quad (j = 1, J_E - 1)$$

The system $[A^{(i)}][\delta^{(i)}] = [Q^{(i)}]$ can be solved efficiently by matrix factorization, and this is the procedure used by Keller, Cebeci. Let $[A^{(i)}] = [\mathcal{L}^{(i)}][\mathcal{U}^{(i)}]$

where

$$[\mathcal{L}^{(i)}] = \begin{bmatrix} D_1^{(i)} & & & & & \\ B_2^{(i)} & D_2^{(i)} & & & 0 & \\ & \ddots & \ddots & & & \\ & & B_j^{(i)} & D_j^{(i)} & & \\ & & & \ddots & \ddots & \\ 0 & & & & B_{J_E-1}^{(i)} & D_{J_E-1}^{(i)} \\ & & & & B_{J_E}^{(i)} & D_{J_E}^{(i)} \end{bmatrix}$$

$$[\mathcal{U}^{(i)}] = \begin{bmatrix} 1 & E_1^{(i)} & & & & \\ & 1 & E_2^{(i)} & & 0 & \\ & & \ddots & \ddots & & \\ & & & 1 & E_j^{(i)} & \\ & & & & \ddots & \ddots \\ 0 & & & & 1 & E_{J_E-2} \\ & & & & & 1 \quad E_{J_E-1} \\ & & & & & 1 \end{bmatrix}$$

where $D_1^{(i)} = A_1^{(i)}$

$$D_j^{(i)} = A_j^{(i)} - B_j^{(i)} E_{j-1}^{(i)} \qquad (j = 2, J_E)$$

$$E_j^{(i)} = \left[D_j^{(i)}\right]^{-1} \cdot C_j^{(i)} \qquad (j = 1, J_E - 1)$$

The $(4 \times 4)$ matrices $A_j^{(i)}$, $B_j^{(i)}$, $C_j^{(i)}$ have been given previously, and the $(4 \times 4)$ matrices $D_j^{(i)}$ and $E_j^{(i)}$ can be calculated sequentially from them as shown above. The matrix $\left[D_j^{(i)}\right]^{-1}$ is the inverse matrix of $D_j^{(i)}$. The matrix inversion is performed using a standard matrix factorization technique (Ref. 30). It is necessary that $A_1^{(i)}$ be nonsingular, and the equations were arranged in the order used to accomplish this.

With $\left[\mathcal{L}^{(i)}\right]$ and $\left[\mathcal{U}^{(i)}\right]$ known, the matrix equation can be written as

$$\left[\mathcal{L}^{(i)}\right]\left[Z^{(i)}\right] = \left[\varphi^{(i)}\right]$$

and solved for $\left[Z^{(i)}\right]$ where $\left[Z^{(i)}\right] = \left[\mathcal{U}^{(i)}\right]\left[\delta^{(i)}\right]$.

With

$$\left[Z^{(i)}\right] = \begin{bmatrix} Z_1^{(i)} \\ Z_2^{(i)} \\ \vdots \\ Z_j^{(i)} \\ \vdots \\ Z_{J_E}^{(i)} \end{bmatrix}$$

where

$$Z_j^{(i)} = \begin{bmatrix} Z_{j,1}^{(i)} \\ Z_{j,2}^{(i)} \\ Z_{j,3}^{(i)} \\ Z_{j,4}^{(i)} \end{bmatrix}$$

the solution is

$$Z_1^{(i)} = \left[D_1^{(i)}\right]^{-1} Q_1^{(i)}$$

$$Z_{j'}^{(i)} = \left[D_{j'}^{(i)}\right]^{-1} \left[Q_{j'}^{(i)} - B_{j'}^{(i)} Z_{j'-1}^{(i)}\right] \quad (j' = 2, J_E)$$

With $\left[Z^{(i)}\right]$ known, $\left[\delta^{(i)}\right]$ is found from

$$\left[\mathcal{A}^{(i)}\right]\left[\delta^{(i)}\right] = \left[Z^{(i)}\right]$$

The solution is

$$\delta_{J_E}^{(i)} = Z_{J_E}^{(i)}$$

$$\delta_{j'}^{(i)} = Z_{j'}^{(i)} - E_{j'}^{(i)} \delta_{j'+1}^{(i)} \quad (j' = J_E - 1, 1)$$

With $\left[\delta^{(i)}\right]$ known, new values $\left(F_j^{(i)}, G_j^{(i)}, H_j^{(i)}, C_{\bar{E}_j}^{(i)}\right)$ are determined, and the procedure is repeated until convergence occurs. When convergence occurs, the solution for $\xi_m$ is known, and calculations proceed to $\xi_{m+1}$. Convergence criteria are taken as $\delta H_1^{(i)}$ and $\delta C_{\bar{E}_1}^{(i)}$ becoming less than some prescribed tolerance. This is equivalent to the velocity gradient at the wall and the integral of the velocity profile squared not changing significantly for the $i$th iteration.

Separation is determined by the calculated value of $H_w$ becoming zero or negative. For the initial guess for the velocity profile at a station $\xi_m$, $H_1^{(1)}$ (i.e., $H_w$) is positive. Subsequent iterations give $H_1^{(i+1)} = H_1^{(i)} + \delta H_1^{(i)}$ until convergence occurs or $H_1^{(i+1)} \leq 0$. If $H_1^{(i+1)} \leq 0$, iterations terminate and separation is assumed to have occurred.

Wall jet calculations begin at the blowing slot. A velocity profile for the flow in the slot is assumed, and the boundary layer profile above the slot is known from the upstream boundary layer calculations. The flow in the slot is assumed to be a fully developed incompressible channel flow. For such a flow (Ref. 31)

$$\frac{d\tau}{dy} = \frac{dP}{dx} = \text{constant}$$

Assuming symmetry about the slot centerline, this gives

$$\tau = \tau_w \left(1 - \frac{2y}{\ell}\right) \tag{5-47}$$

where $\mathcal{C}$ = slot thickness. For laminar flow, $\tau = \nu\rho \frac{du}{dy}$, and the velocity profile corresponding to Eq. (5-47) is

$$u = \frac{\tau_w}{\nu\rho} y \left(1 - \frac{y}{\mathcal{C}}\right)$$

If a suitable eddy viscosity distribution is known for turbulent flow, a similar procedure can be used to obtain

$$\frac{du}{dy} = \frac{\tau_w}{\rho\nu(1+\epsilon^+)} \left(1 - \frac{2y}{\mathcal{C}}\right)$$

The eddy viscosity model developed by Mei and Squire (Refs. 32, 33) gives

$$\epsilon^+ = \frac{.4\, y^{+3}}{(y^{+2} + 324)\left(1 + 3.4 \frac{y^+}{R^+}\right)}$$

where

$$y^+ = \frac{y u_\tau}{\nu}, \quad u_\tau = \sqrt{\frac{\tau_w}{\rho}}, \quad R^+ = \frac{\mathcal{C}}{2} \frac{u_\tau}{\nu}$$

This expression along with Eq. (5-47) gives

$$H = \frac{H_w}{1+\epsilon^+} (1 - 2\eta) \qquad (5\text{-}48)$$

where

$$H_w = \mathcal{C}^* Re_\infty u_\tau^{*2} / u_e^*$$

$$1 + \epsilon^+ = 1 + \frac{.4 (\mathcal{C}^* Re_\infty u_\tau^*)^3 \eta^3}{\left[(\mathcal{C}^* Re_\infty u_\tau^*)^2 \eta^2 + 324\right]\left[1 + 6.8\eta\right]}$$

Integrating Eq. (5-48) gives G and F. All terms in Eq. (5-48) are known except $u_e^*$, which must be prescribed. Prescribing $u_e^*$ thus prescribes the blowing slot values. Eq. (5-48) can be integrated in closed form (Refs. 32, 33) but for the present purpose it is more convenient to do the integration numerically. Either a turbulent slot flow or a laminar slot flow can be prescribed. For the laminar case, the eddy viscosity is set equal to zero. For all calculations performed so far, a turbulent slot flow has been assumed.

Blowing slot values are normally given in terms of a momentum coefficient $C_\mu$ and a mass flow coefficient $C_{\dot{m}}$, where

$$C_\mu = \frac{\rho_j \int_0^\ell u^2 dy}{\frac{1}{2}\rho V_\infty^2 c} = 2\frac{\rho_j}{\rho}\ell^* u_e^{*2}\int_0^1 G^2 d\eta \qquad (5\text{-}49)$$

$$C_{\dot{m}} = \frac{\rho_j \int_0^\ell u\, dy}{c\rho V_\infty} = \ell^* u_e^* \frac{\rho_j}{\rho} F_{\eta=1} \qquad (5\text{-}50)$$

In Eqs. (5-49,50) $\rho_j$ is the density of the flow in the slot. Since the wall jet analysis is for incompressible flow, it is assumed that $\rho_j = \rho$. Eq. (5-49) is the appropriate form for the case where the velocity in the slot is not uniform. For most cases, however, experimental values of $C_\mu$ are based on an average velocity. An average velocity $u_{AVE}^*$ for the slot is

$$u_{AVE}^* = \frac{1}{\ell}\int_0^\ell u^* dy = u_e^* F_{\eta=1}$$

Defining a momentum coefficient $C_{\mu\,AVE}$ in terms of the average velocity gives

$$C_{\mu_{AVE}} = \frac{\rho_j U_{AVE}^2 \mathcal{C}}{\frac{1}{2}\rho V_\infty^2 C} = 2\frac{\rho_j}{\rho}\mathcal{C}^* U_e^{*2} F^{-1}_{\eta=1} \qquad (5\text{-}51)$$

The values predicted by Eqs. (5-49) and (5-51) are reasonably close but not identical. For Kind's Flow II, assuming a turbulent slot flow, the value of $C_\mu$ is about 10% higher than $C_{\mu_{AVE}}$.

With $U_e^*$ for the slot prescribed, the velocity profile and thus $C_\mu$ and $C_{jn}$ are known. The upstream boundary layer profile is also known, but in terms of a different coordinate system. Letting the subscript $(\,)_{BL}$ denote quantities in the upstream boundary layer coordinates (evaluated at the slot), the values in the wall jet coordinates become

$$F = F_{\eta=1} + \frac{\sqrt{2\xi^*_{BL}}}{\mathcal{C}^*\sqrt{Re_\infty}\ U_e^*} f_{BL} \qquad (5\text{-}52a)$$

$$G = f'_{BL} \qquad (5\text{-}52b)$$

$$H = \frac{\mathcal{C}^*\sqrt{Re_\infty}\ U_e^*}{\sqrt{2\xi^*_{BL}}} f''_{BL} \qquad (5\text{-}52c)$$

$$\eta = \frac{\sqrt{2\xi^*_{BL}}}{\mathcal{C}^*\sqrt{Re_\infty}\ U_e^*}\eta_{BL} \qquad (5\text{-}52d)$$

$$C_p = 1 - U_e^{*2} \qquad (5\text{-}52e)$$

Neither the upstream boundary layer calculations nor the slot flow analysis include normal pressure gradients, so the initial pressure distribution is taken as $C_p = 1 - u_e^{*2}$. For the form used for the finite difference expressions, this does not cause any difficulty, and neither does the fact that $H$ is discontinuous at $\eta = 1$.

Large gradients are associated with the sharp velocity minimum at the slot, so a finer grid is necessary near the slot. From results presented by Keller, Cebeci (Ref. 14), 40 $\eta$ grid points seemed a reasonable number for a conventional boundary layer profile. The shape of the initial wall jet profile requires tripling this number, so a maximum of 121 $\eta$ grid points was selected. The $\eta$ grid for the initial calculations is taken as follows. For the region $0 \le \eta \le \frac{1}{2}$, the Cebeci, Smith grid $h_j = K h_{j-1}$ is used, but the value of $K$ is altered occasionally. For $\frac{1}{2} \le \eta \le 1$, the grid is a mirror image of the grid for $\eta \le \frac{1}{2}$. Selected points in the upstream boundary layer grid are used for the remaining wall jet grid points. The first streamwise step size is taken as 1/3 of the slot thickness, and the second step size is taken as 1 slot thickness. After the solution is obtained at this location, the grid is altered to a more suitable one for downstream calculations. The Cebeci, Smith grid $h_j = K h_{j-1}$ is used, again with $K$ altered occasionally. The streamwise step size can be varied as desired, but unless output at specific points is desired the step size is taken as follows. A maximum step size (such as 5 slot thicknesses) is prescribed. This is taken as the step size unless it results in $u_e^*$ changing by more than .1 between successive locations. If $u_e^*$ changes by more than .1, the

step size is reduced so as to make the change in $u_e^*$ approximately .1. However, the step size is not reduced to less than half the prescribed maximum value. The values of $K$ were selected on a trial and error basis, and general recommendations on how to pick values would require additional study. Calculations were performed with different grid parameters to insure that the grid used is adequate for the present calculations.

The grid used for the wall jet calculations is quite coarse compared to that used for the boundary layer calculations. Preliminary calculations indicate that an even coarser grid would be acceptable, although oscillations in the solution very near the wall can result if the $\eta$ grid is too coarse near the wall. Convergence of the finite difference method was found to be fast and reliable. However, a convergence anomaly existed during much of the development, and its presence was not directly obvious. The initial guess for the velocity profile at a new downstream location is taken as the solution from the previous location, and this seems to be satisfactory. However, unless some precaution is used, this can result in the initial guess for $\epsilon_o^+$ — from Eq. (5-26) — being too small while $\epsilon_i^+$ — from Eq. (5-25) — increases too rapidly. This results in a qualitatively poor initial eddy viscosity distribution, and subsequent iterations do not seem to be able to compensate even though convergence appears to be normal. Providing a qualitatively reasonable initial eddy viscosity distribution eliminates the problem, and the final solution is not sensitive to the initial guess used.

Summary Of Wall Jet Calculations

Wall jet calculations begin at the blowing slot. A value of $u_c^*$ for the slot is assumed, and the velocity profile for the slot is determined from Eq. (5-48). The rest of the initial velocity profile is determined from the known upstream boundary layer profile and is given by Eq. (5-52). The slot location is denoted as $\xi_1$ . The solution proceeds downstream from the slot. The solution at $\xi_2$ and $\xi_3$ is determined using a finite difference grid appropriate to a velocity profile with a sharp minimum. After the solution at $\xi_3$ is obtained, the grid is altered to a form more appropriate for downstream calculations, and the solution at the new grid points is obtained by interpolation. The solution then proceeds downstream. The initial wall jet calculations are for a profile with a relative minimum velocity. For such a profile, the outer edge conditions (at a point corresponding to the outer edge of the upstream boundary layer) are determined from Eq. (5-13). To compensate for the lack of a curvature correction for Eq. (5-13), the normal pressure gradient in the wall jet equations is set equal to zero above the velocity minimum. The eddy viscosity distribution is determined from Eqs. (5-25, 26, 33, 21, 22, 23).

Calculations retain the minimum velocity until they can switch smoothly to a profile without a minimum. For profiles without a velocity minimum, the outer edge conditions are determined from Eq. (5-12). The eddy viscosity distribution is determined from Eqs. (5-25, 26, 33, 19, 20). Calculations proceed downstream until sep-

aration is determined by the wall shear stress becoming zero or negative.

For all wall jet calculations, the outer boundary conditions are applied at a grid point corresponding approximately to $1.2\,\eta_{\Delta_{M-1}}$ The actual jet thickness is determined during the solution and may be less than $1.2\,\eta_{\Delta_{M-1}}$. The solution for $\eta' > J_E$ is taken as $F = F_{J_E} + (\eta - \eta_{J_E})$, $G=1$, $H=0$, $C_I = C_{I_e}$. The initial guess for $(F, G, H)$ at a station $\xi_M$ is taken as the corresponding values at $\xi_{M-1}$. The initial guess for $C_{I_M}$ is taken as $C_{I_{M-1}} + \Delta C_I$ where $\Delta C_I$ is determined so as to give the correct outer edge pressure. After the first iteration (only) at a station $\xi_M$, the old and new solutions are averaged. This did not seem to be necessary, but helped reduce over-shooting of the next iteration. A reasonable eddy viscosity distribution is provided for the first iteration.

An iterative procedure is required to determine the correct blowing slot values. Such a procedure should not be difficult to set up, but at present calculations are simply performed for a given number of assumed slot conditions.

# 6. RESULTS

Calculations are performed for Kind's Flow II (Refs. 4, 5, 15). Briefly, Kind's airfoil is a 20% thick ellipse with the trailing edge replaced by a circular section with a radius of 9/16 inches. The chord length is 14 5/8 inches, and the blowing slot is located at the location where the modified trailing edge joins the airfoil. Kind performed downwash corrections by comparing calculated and measured pressure distributions and estimates the accuracy of the resulting effective two dimensional angle of attack as $\pm$ 1/2°. Kind's experimental values for Flow II are $\mathcal{R}_{e_\infty}$ = 750000, $\alpha$ = -0.7°, $C_\ell$ = 1.82, $C_\mu$ = .055, $\mathcal{C}^*$ = .0012, $\mathcal{R}^*$ = .0378.

Using this input, calculations are performed as described previously. Results of the wall jet calculations are given for two different sets of blowing slot conditions in order to illustrate the effects of the assumed slot conditions. Results of the present calculations are shown in Figs. 6 through 15 and are discussed below.

Fig. 6 shows the calculated potential flow surface pressure distribution. Unfortunately, Kind does not give the measured distribution for Flow II, so a comparison is impossible. The same potential flow program used here has been used in other applications, such as in Ref. 3, where calculated values were found to be in good agreement with experiment for a cambered ellipse with a modified trailing edge.

Fig. 7 shows calculated and measured boundary layer profiles upstream of the blowing slot, and the agreement is good. The measured profile is .055C upstream of the slot, while the calculated profile

is .007C upstream and is the profile used for the wall jet calculations. The difference in location could cause some difference in the profiles, but there seems to be little upstream influence of the blowing slot for this flow (Potential flow calculations give a at the slot of about -2.3, while Kind's measured values give about -2.5 at the slot exit). Other potential sources of difference are the relatively low Reynolds number and the fact that Kind used two trip wires on both the upper and lower surfaces of the airfoil. As mentioned previously, the boundary layer eddy viscosity expressions were not updated by the newer expressions for low Reynolds number. In calculations, transition was assumed at the first trip wire, and the second wire was ignored.

Fig. 8 shows calculated and measured velocities at the outer edge of the wall jet, along with the calculated potential flow velocity. Calculated values shown are for $C_\mu$ = .054, but values for $C_\mu$ = .046 are virtually the same. Calculations include a velocity minimum up to $\xi - \xi_{SLOT}$ = .011, and the dashed line indicates the calculated value of $\alpha^*_{MIN}$ . Calculated values are in excellent agreement with experiment up to about $\xi - \xi_{SLOT}$ = .05, and then decrease in agreement, but are still useable. The discrepancy begins at about the same place where the normal velocity becomes comparable to the streamwise velocity, and other difficulties in the wall jet calculations begin at about the same location. Eqs. (5-1) and (5-2) give virtually the same result up to $\xi - \xi_{SLOT}$ = .05, with Eq. (5-2) giving some improvement downstream. The discrepancy in the

outer edge velocity forces some discrepancy in calculated velocity profiles (G) also. Fortunately, however, it seems that the effects on the velocity ( $U_e^* G$ ) in the inner portion of the jet are not great. This is discussed later.

Fig. 9 shows calculated and measured pressure distributions in the wall jet region. The experimental outer edge pressures were calculated by Kind using his measured velocities and the assumption that the total pressure remained constant along a streamline. Calculated values are shown for $C_\mu$ = .054. Values for $C_\mu$ = .046 are slightly different but are close enough that the curve is somewhat difficult to read if they are included. Calculated outer edge pressures are for the point in the wall jet finite difference grid where the outer boundary conditions are applied.

Calculated and measured pressures are in reasonable agreement with each other. The calculated wall pressure gradient is in good agreement with experiment for portions of the jet region, but is higher in places and lower in others. The difference is of the order of 30% for some of the latter portion of the jet, and this has some observable effects on the velocity profiles. However, the results are still reasonably good. In contrast to this is the case indicated for $f(\xi)$ = 0. The calculations for this case are identical except that the approximate streamline curvature correction is not included. Up to about $\xi - \xi_{slot}$ = .05, the results for this case are indistinguishable from the previous case. However, the results then begin to diverge at an increasing rate. As the wall pressure gradient remains too mild, the maximum velocity in the wall jet remains

too large, and these effects reinforce each other. The end result of this is that the calculations become useless.

The rapid change in wall pressure near the slot is a result of fairing in the radius of curvature over a short distance. A somewhat longer fairing could also be used, but should be completed by about $\xi - \xi_{SLOT} = .01$ to match the measured wall pressure values in $.01 < \xi - \xi_{SLOT} < .02$. Such a fairing is still quite rapid to apply to the outer boundary conditions at the outer edge of the upstream boundary layer, so the procedure described in Section 5 was adopted. The actual fairing used does not seem significant in the downstream calculations.

The pressure in the separated region is in reasonable agreement. Kind's measured value for $C_{P_W}$ is .65, the calculated value for the lower surface is .47, and the calculated value for the upper surface is .27 for $C_\mu = .054$ ($= -.2$ for $C_\mu = .046$). The calculated value is taken as the value obtained on the last iteration, i.e., the iteration that determined a separated profile. However, it is somewhat difficult to get a precise value for the wall jet separation pressure. The pressure gradient is very large, and a small change in the location of the separation point can make a significant change in the calculated pressure. This is complicated by the expression used for $f(\xi)$ being crude, and can also be complicated by using a fairly large step size as was done in the present calculations.

Figs. 10 through 15 show calculated and measured wall jet profiles. The values of $\xi - \xi_{SLOT}$ given are for the corresponding sta-

tions in the wall jet grid. In some cases, the stations do not correspond exactly with the location of the measured profile, but the difference is small. Figs. 10 through 12 are for $C_\mu$ = .054 ( $C_{\dot{m}}$ = .0055) and Figs. 13 through 15 are for $C_\mu$ = .046 ( $C_{\dot{m}}$ = .0051). In Fig. 12, the calculated and measured profiles on the right are at somewhat different locations.

The agreement with experiment is good for either set of profiles, especially since measured profiles and pressures are not used in the calculations. Which set provides the best agreement is somewhat ambiguous since one set is better in some ways while the other is better in others. Comparing Figs. 10 and 13 shows that the solution for $C_\mu$ = .054 gives better agreement for station 9, while the solution for $C_\mu$ = .046 gives better agreement for the inner region at station 12. In either case, however, the agreement between measured and calculated values is within about 5%. For either set of profiles, the agreement at stations 15 and 18 is essentially the same as the agreement at station 12, although at station 18 there is a slight tendency for the maximum velocity to be too large. Direct comparison with experiment of either profile at station 22 is complicated by the fact that the calculated and measured outer edge velocities differ by about 10%. The solid lines represent the calculated profiles, while the dashed lines represent the profiles multiplied by the ratio of calculated to measured outer edge velocity. The dashed lines are thus probably more representative of the velocity for the inner region. If so, the solution at station 22 tends to follow the solution at station 18 except that the velocity at station 22 remains too

high very near the wall. For $C_\mu$ = .046, separation was calculated at station 25 ( $\xi - \xi_{SLOT}$ = .0681) and for $C_\mu$ = .054 separation was calculated at station 26 ( $\xi - \xi_{SLOT}$ = .0706). Kind experimentally determined separation at $\xi - \xi_{SLOT}$ = .0711, and the experimental profile given in Fig. 12 (on the right) is for $\xi - \xi_{SLOT}$ = .0706. Thus the calculated and measured separation points agree well, but there is no calculated profile to compare to experiment. The calculated profile in Fig. 12 is thus for station 25 (the last profile determined), but the step size is relatively large and agreement should not be expected. However, it is of some interest to indicate how rapidly the jet is changing, so the profiles are included. The calculated profile is multiplied by the ratio of the calculated to measured velocity.

Without additional comparisons with experiment, conclusions drawn from the above observations are somewhat tentative. However, during (numerous!) development calculations, some results occurred with such monotonous regularity that some effects seem clear. All calculations were started with a turbulent slot profile. The velocity profile at station 9 is only sensitive to the assumed $C_\mu$ and to the value of $K_c \epsilon_m^+$ [Eq. (5-19) or (5-21)]. Variations in the radius of curvature fairing and inner eddy viscosity model have little effect on the portion of the profile far enough from the wall to be compared to experiment. Until pressure gradient effects begin to become severe (at about station 18), the solution depends largely on the value of $K_c \epsilon_m^+$ . Between stations 9 and 12, there is a strong tendency for the maximum velocity to decrease too slowly and the thick-

ness of the outer region to remain too small. Also in this region, the value of $\epsilon_M^+$ tends to remain nearly constant. The curvature correction $K_c$ accounts for most of the change in $K_c \epsilon_M^+$ in this region, and before it was incorporated the discrepancy between calculated and measured values was about double that in the present results. This may be an indication of some difficulty in the expression for $\epsilon_M^+$ as the flow passes from a favorable to an adverse pressure gradient. From station 12 to station 18, calculated velocity profiles, pressure gradients and outer edge velocities follow measured values very well. Pressure gradient effects begin to become severe at about station 18, and tend to dominate calculations downstream. For the calculations for $C_\mu = .054$, for example, the shear stress variation over $0 \leq \eta \leq .2\,\eta_M$ is about 5% for station 15, 15% for station 18, 50% for station 22, 300% for station 24, and separation occurs at station 26. Thus pressure effects are comparable to shear stress effects for a considerable distance upstream of separation. If the wall pressure gradient is too mild, the velocity very near the wall tends (strongly) to remain too high. Fig. 9 shows that the wall pressure gradient is somewhat too mild between stations 18 and 22, and the velocity profiles at station 22 show some of this effect. Downstream of this the calculated wall pressure gradient becomes larger than the measured one, and this tends to compensate to some degree. Calculations over the latter portion of the jet require a reasonable wall pressure distribution if they are to have any hope of success.

# 7. CONCLUSIONS

A self-contained analysis for arbitrary circulation controlled airfoils in incompressible flow is developed and found to be capable of predictions that are in good agreement with experiment. The analysis requires calculations for potential flow, laminar and turbulent boundary layer flow, and turbulent wall jet flow.

The turbulent wall jet calculations are the most difficult and are subject to the most uncertainty. Accurate calculations require reasonably accurate predictions of the wall pressure distribution in the wall jet region. Conventional boundary layer approximations provide an accurate wall pressure distribution for much of the wall jet region, but require modification for the latter portion of the jet. An exact correction to account for this seems untenable since such a correction tends to produce stability problems in the calculations. Such stability problems might well be expected since the correction involves second order streamwise derivatives, which do not fit into boundary layer theory. A plausible approximate correction based on average values seems adequate and workable. Such a correction is used, and suggestions for improving it are offered.

The shear stress model for the wall jet is subject to some uncertainty because of a lack of detailed experimental data, or in some cases because of conflicting experimental data. However, the model does seem reasonable and is formulated using available information. It is possible that additional comparison of calculated and experimental results would lead to improvement of the model. Such compar-

isons would probably be more helpful if the flow were subject to less severe curvature and pressure gradients than in the present calculations.

# BIBLIOGRAPHY


1. Thwaites, B. (ed.), Incompressible Aerodynamics, Oxford University Press, London, England, 1960, Chap. V.

2. Newman, B. G., "The Deflection of Plane Jets by Adjacent Boundaries - Coanda Effect," Boundary Layer and Flow Control, G. V. Lachmann, Pergamon Press, Vol. 1, 1961, pp. 232-264.

3. Ness, N., Gibbs, E. H., Tseng, W. A. P., "Calculation of the Lift on Airfoils with Separated Boundary Layers," TR 31, May 1972, Department of Aerospace Engineering, West Virginia University, Morgantown, W. Va.

4. Kind, R. J.and Maull, D. J., "An Experimental Investigation of a Low-Speed Circulation-Controlled Aerofoil," The Aeronautical Quarterly, Vol. XIX, May 1968, pp. 170-182.

5. Kind, R. J., "A Calculation Method for Circulation Control by Tangential Blowing Around a Bluff Trailing Edge," The Aeronautical Quarterly, Vol. XIX, August 1968, pp. 205-223.

6. Ambrosiani, J. P.and Ness, N., "Analysis of a Circulation Controlled Eliptical Airfoil," TR 30, April 1971, Department of Aerospace Engineering, West Virginia University, Morgantown, W. Va.

7. Theodorsen, T. and Garrick, I. E., "General Potential Theory of Arbitrary Wing Sections," NACA TR 452, 1933.

8. Cebeci, T., Smith, A. M. O., and Wang, L. C., "A Finite-Difference Method for Calculating Compressible Laminar and Turbulent Boundary Layers," Douglas Aircraft Company Report DAC-67131, March 1969.

9. Gaster, M., "The Structure and Behavior of Laminar Separation Bubbles," NPL Aero Report 1181 (Revised), March 13, 1967.

10. Ref. 1, pp. 198-200.

11. Myer, D. P., "An Experimental Investigation of a Circulation Controlled Cambered Elliptical Airfoil with a Rounded Trailing Edge," Master's Thesis, Department of Aerospace Engineering, West Virginia University, 1972.

12. Tseng, W. A. P., "Lift on Airfoil Sections in Separated Flow," Master's Thesis, Department of Aerospace Engineering, West Virginia University, 1972.

13. Kline, S. J., et al., (ed.), Computation of Turbulent Boundary Layers - 1968 AFOSR-IFP - Stanford Conference, Vol. I, Stanford University, Ca.

14. Keller, H. B., Cebeci, T., "Accurate Numerical Methods for Boundary Layer Flows-II. Two-Dimensional Turbulent Flows," AIAA Paper No. 71-164, January 1971.

15. Kind, R. J., "A Proposed Method of Circulation Control," Ph.D. Dissertation, University of Cambridge, 1967.

16. Davis, R. T., Werle, M. J., Wornom, S. F., "A Consistent Formulation of Compressible Boundary-Layer Theory with Second-Order Curvature and Displacement Effects," AIAA Journal, Vol. 8, September 1970, pp. 1701-1703.

17. Kind, R. J., "Calculation of the Normal-Stress Distribution in a Curved Wall Jet," The Aeronautical Journal, Vol. 75, May 1971, p. 343.

18. Kind, R. J., "A Calculation Method for Boundary Layer Control by Tangential Blowing," C.A.S.I. Transactions, Vol. 4, No. 2, September 1971, pp. 88-98.

19. Gartshore, I. S., Newman, B. G., "The Turbulent Wall Jet in an Arbitrary Pressure Gradient," The Aeronautical Quarterly, Vol. XX, February 1969, pp. 25-26.

20. Kruka, V., Eskinazi, S., "The Wall Jet in a Moving Stream," Journal of Fluid Mechanics, Vol. 20, 1964, pp. 555-579.

21. Dvorak, F. A., "Calculation of Turbulent Boundary Layers and Wall Jets over Curved Surfaces," AIAA Journal, Vol. 11, April 1973, pp. 517-524.

22. Gartshore, I. S., "An Experimental Examination of the Large-Eddy Equilibrium Hypothesis," Journal of Fluid Mechanics, Vol. 24, 1966, pp. 89-98.

23. Townsend, A. A., The Structure of Turbulent Shear Flow, Cambridge University Press, 1956.

24. Jones, D. G., "Measurements of Wall Jet Development on a Circulation-Controlled Aerofoil," Mechanical Engineering Department, University of California, Davis, January 1971.

25. Cebeci, T., Mosinskis, G. J., "Computation of Incompressible Turbulent Boundary Layers at Low Reynolds Numbers," AIAA Journal, Vol. 9, August 1971, pp. 1632-1634.

26. Cebeci, T., " Kinematic Eddy Viscosity at Low Reynolds Numbers," AIAA Journal, Vol. 11, January 1973, pp. 102-104.

27. Cebeci, T., "Wall Curvature and Transition Effects in Turbulent Boundary Layers," AIAA Journal, Vol. 9, September 1971, pp. 1868-1870.

28. Cebeci, T., "Calculation of Three-Dimensional Boundary Layers I. Swept Infinite Cylinders and Small Cross Flow," AIAA Journal, Vol. 12, June 1974, pp. 779-786.

29. Schlichting, H., Boundary Layer Theory, Fourth Edition, McGraw-Hill Book Company, 1960, pp. 477-480.

30. Conte, S. D., Elementary Numerical Analysis, McGraw Hill Book Company, 1965, pp. 177-181.

31. Ref. 29, pp. 66-68.

32. Mei, J. S., "Application of a Simple Eddy Viscosity Model to Channel and Boundary Layer Flow," Ph.D. Dissertation, Department of Aerospace Engineering, West Virginia University, 1973.

33. Mei, J. S., Squire, W., "A Simple Eddy Viscosity Model for Turbulent Pipe and Channel Flow," AIAA Journal, Vol. 10, March 1972, pp. 350-352.

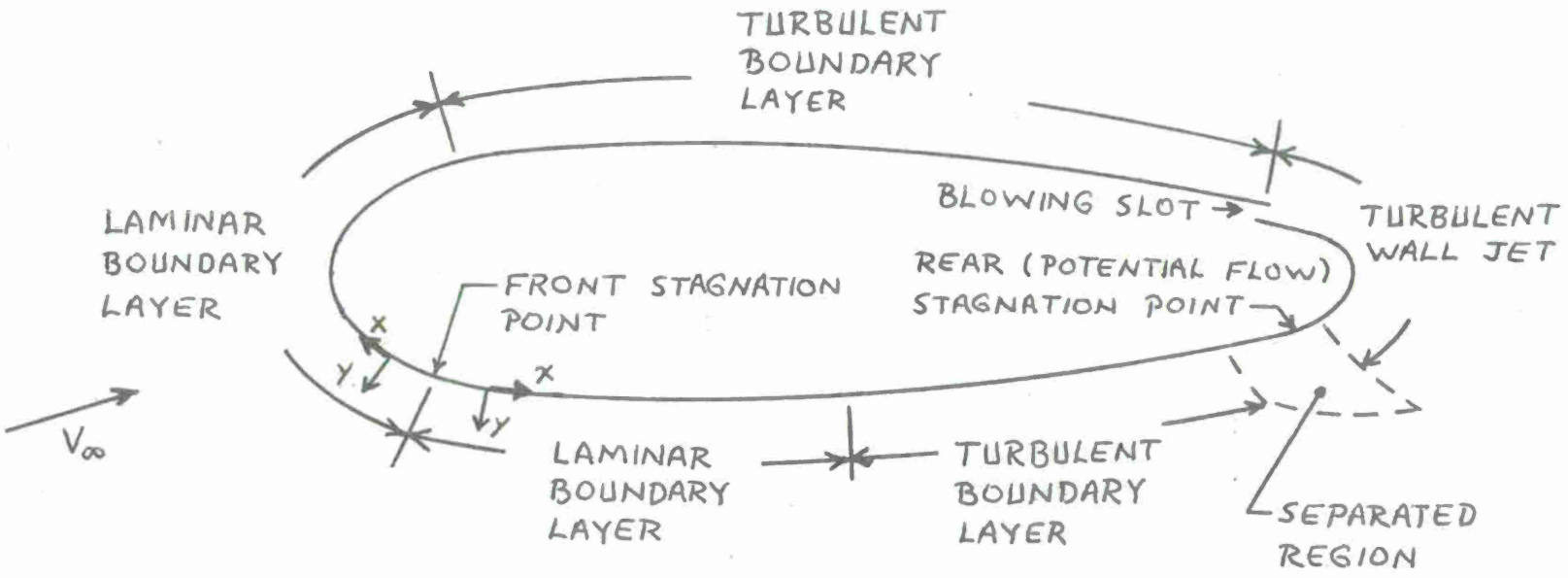


FIG. 1 FLOW CONDITIONS ON A CIRCULATION CONTROLLED AIRFOIL

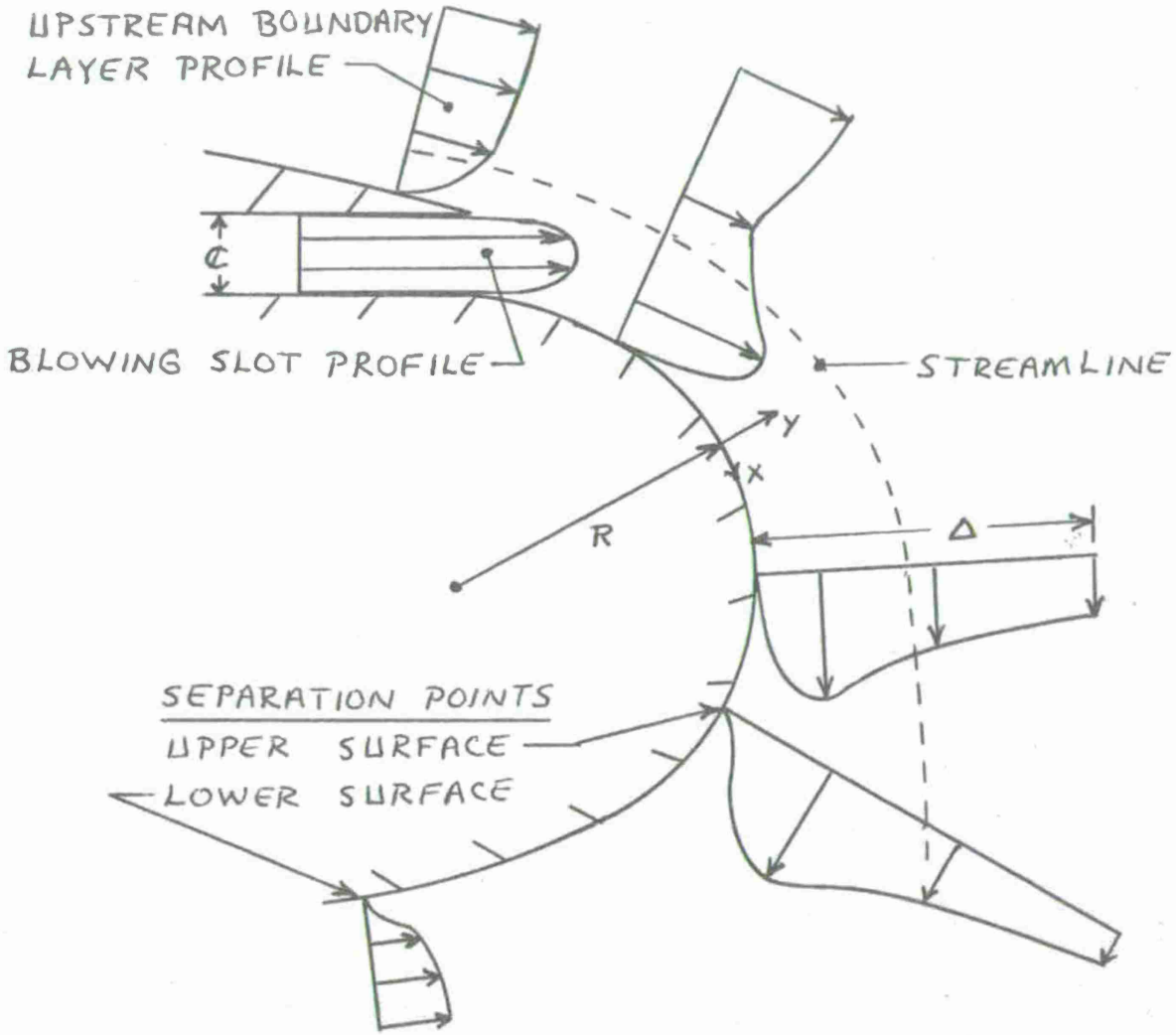


FIG. 2 TYPICAL WALL JET DEVELOPMENT

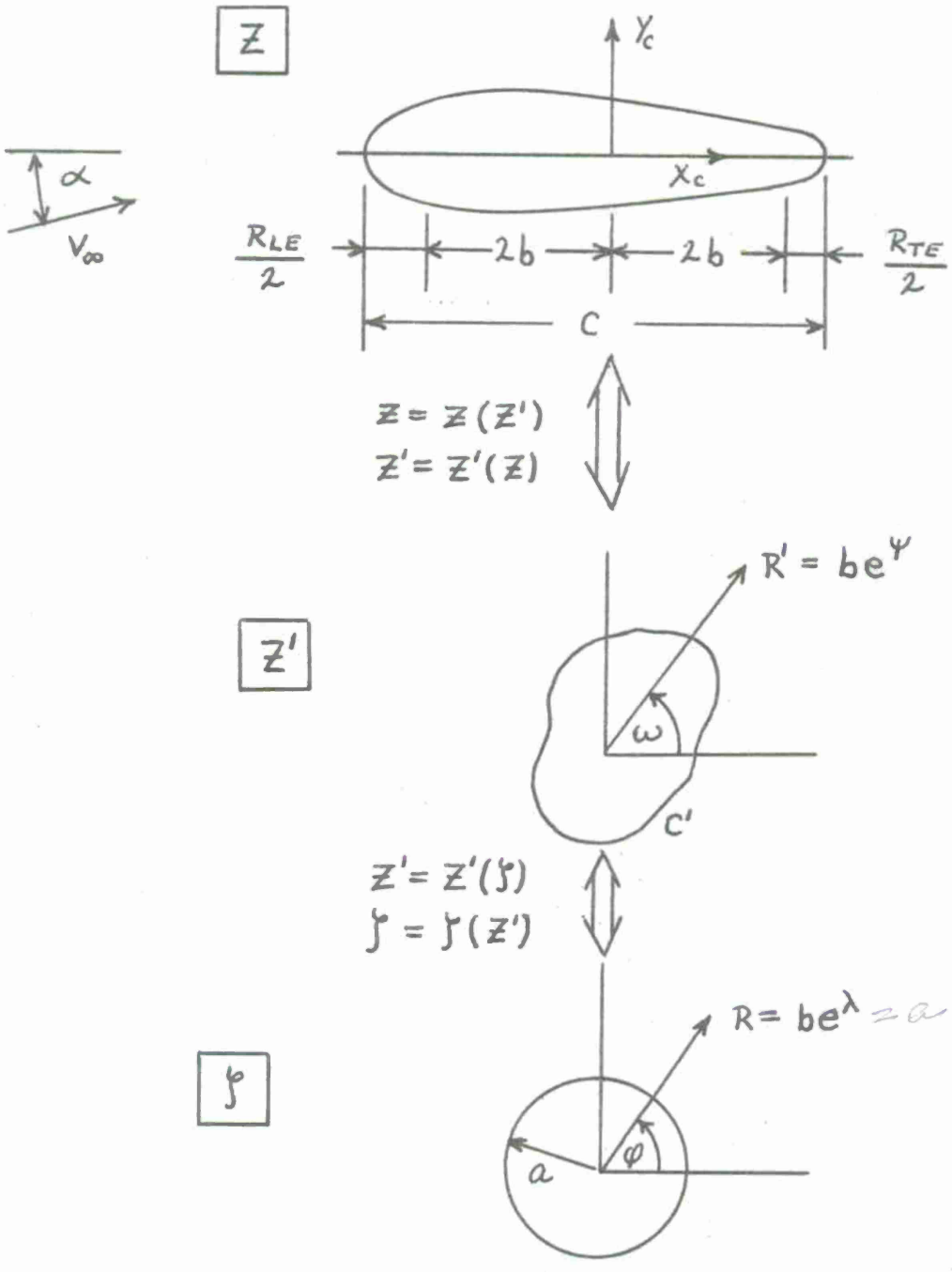


FIG. 3 TRANSFORMATIONS AND COORDINATE SYSTEMS FOR THE THEODORSEN METHOD

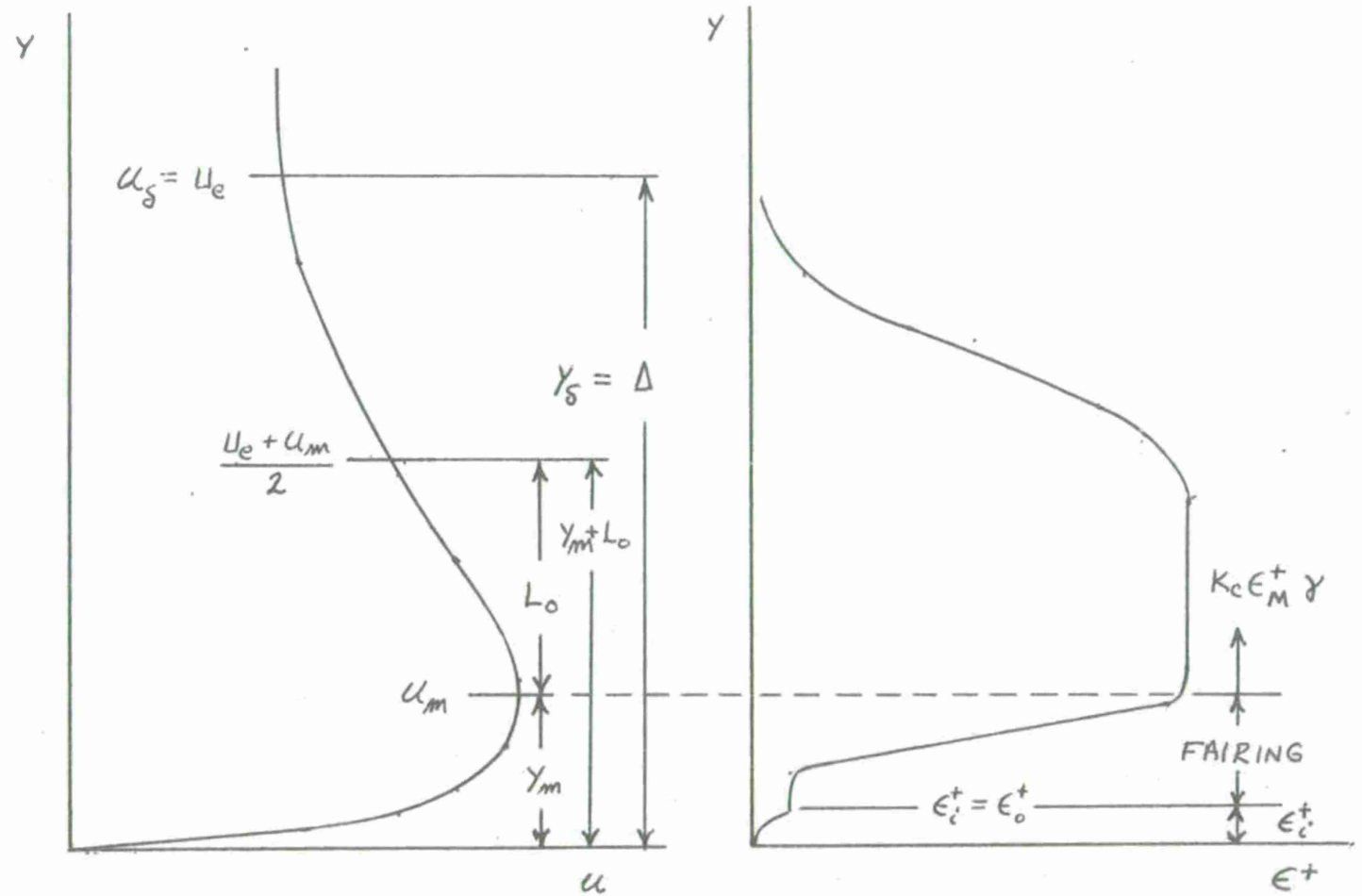


FIG. 4 NOTATION FOR A VELOCITY PROFILE WITHOUT A MINIMUM VELOCITY

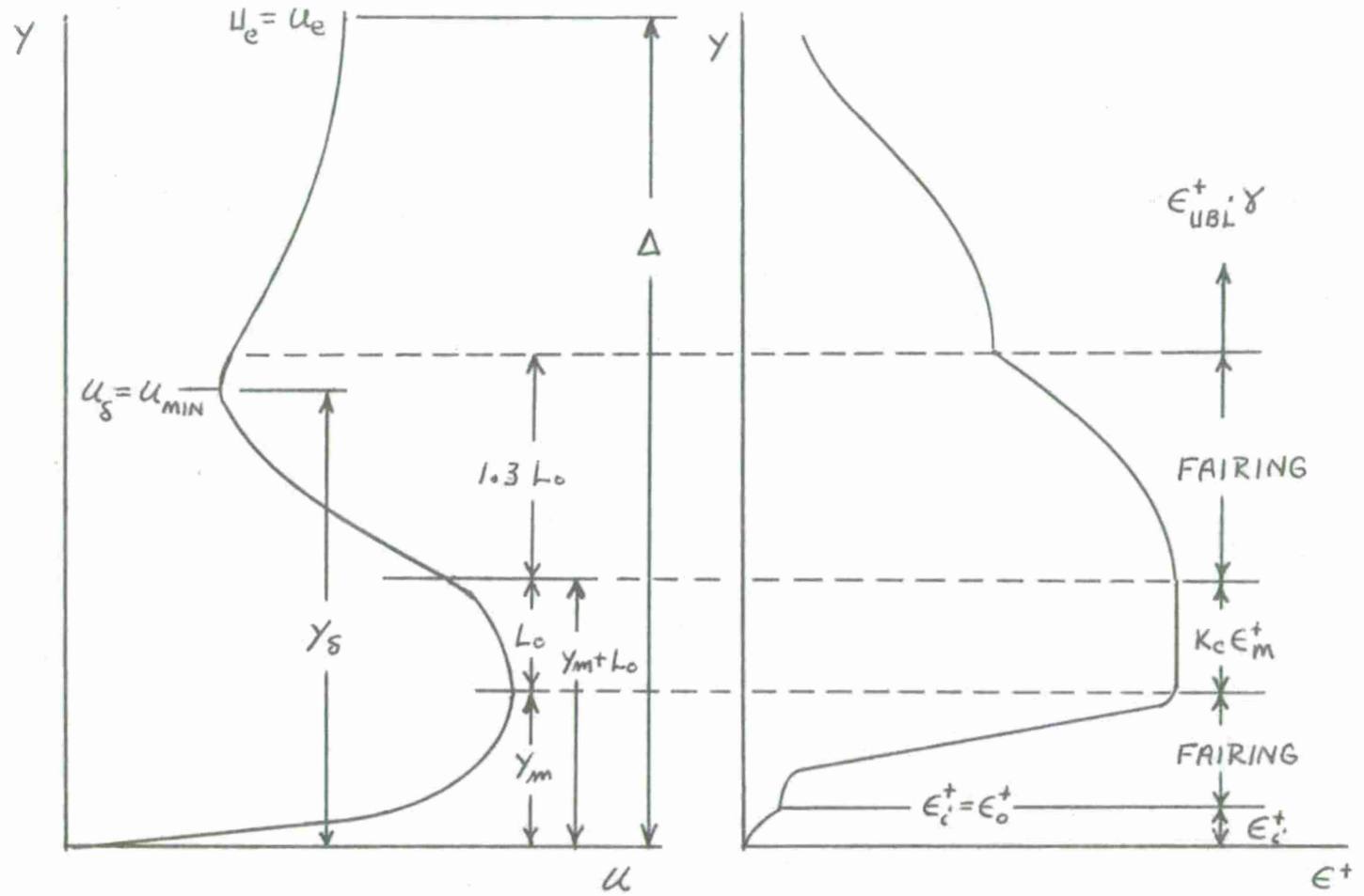


FIG. 5 NOTATION FOR A VELOCITY PROFILE WITH A MINIMUM VELOCITY

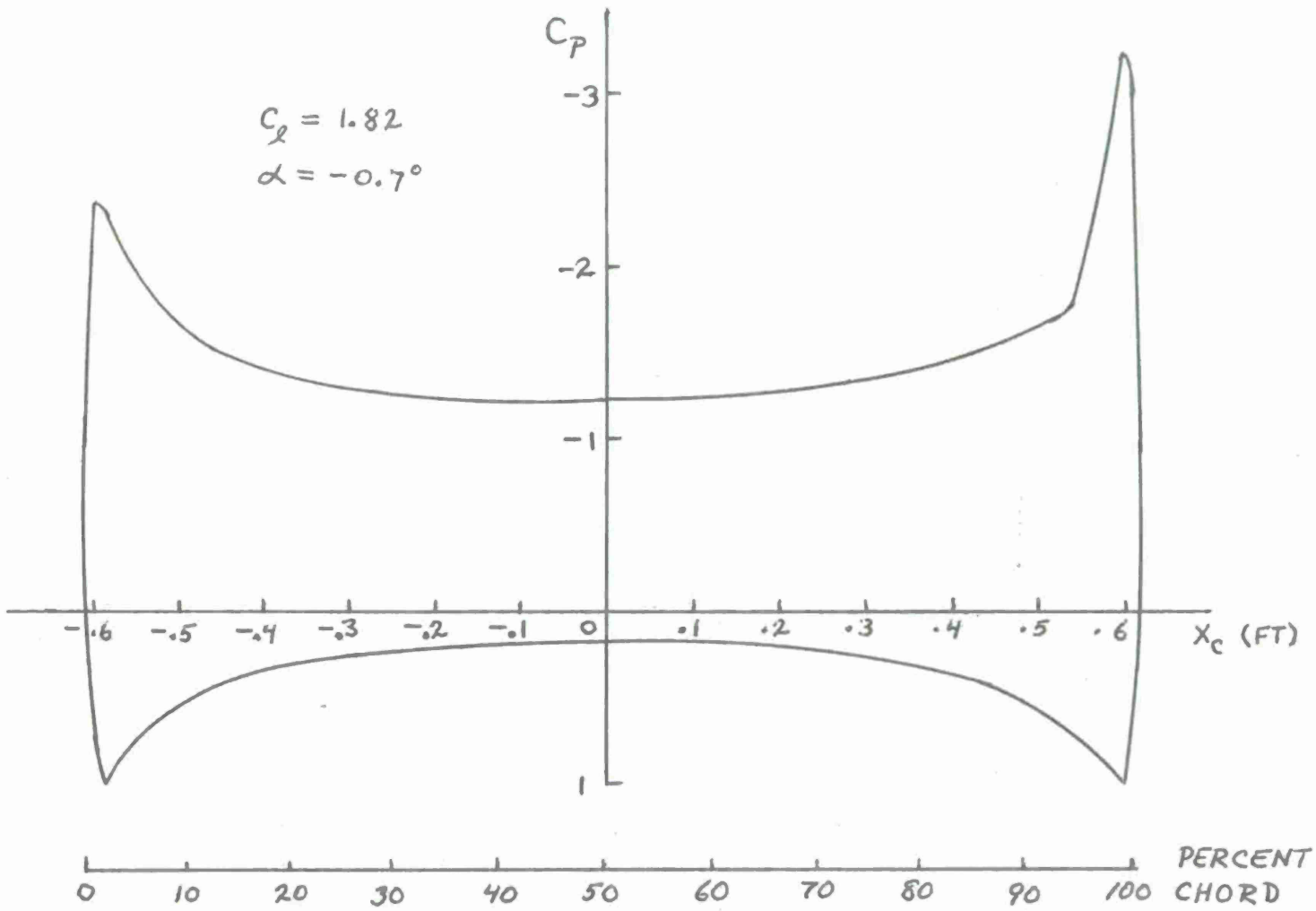


FIG. 6 CALCULATED POTENTIAL FLOW PRESSURE DISTRIBUTION

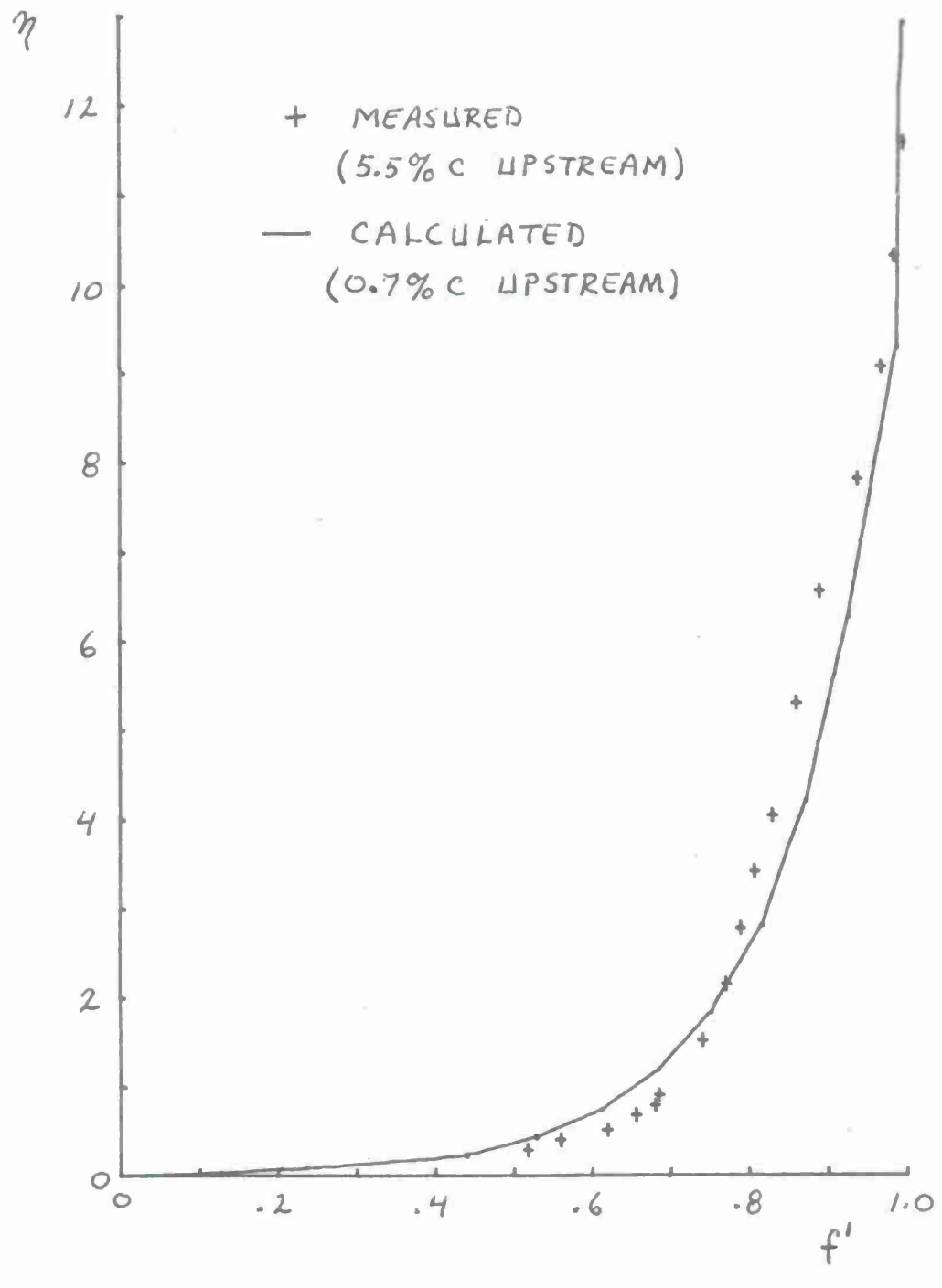


FIG. 7 COMPARISON OF CALCULATED AND MEASURED UPSTREAM BOUNDARY LAYER PROFILE

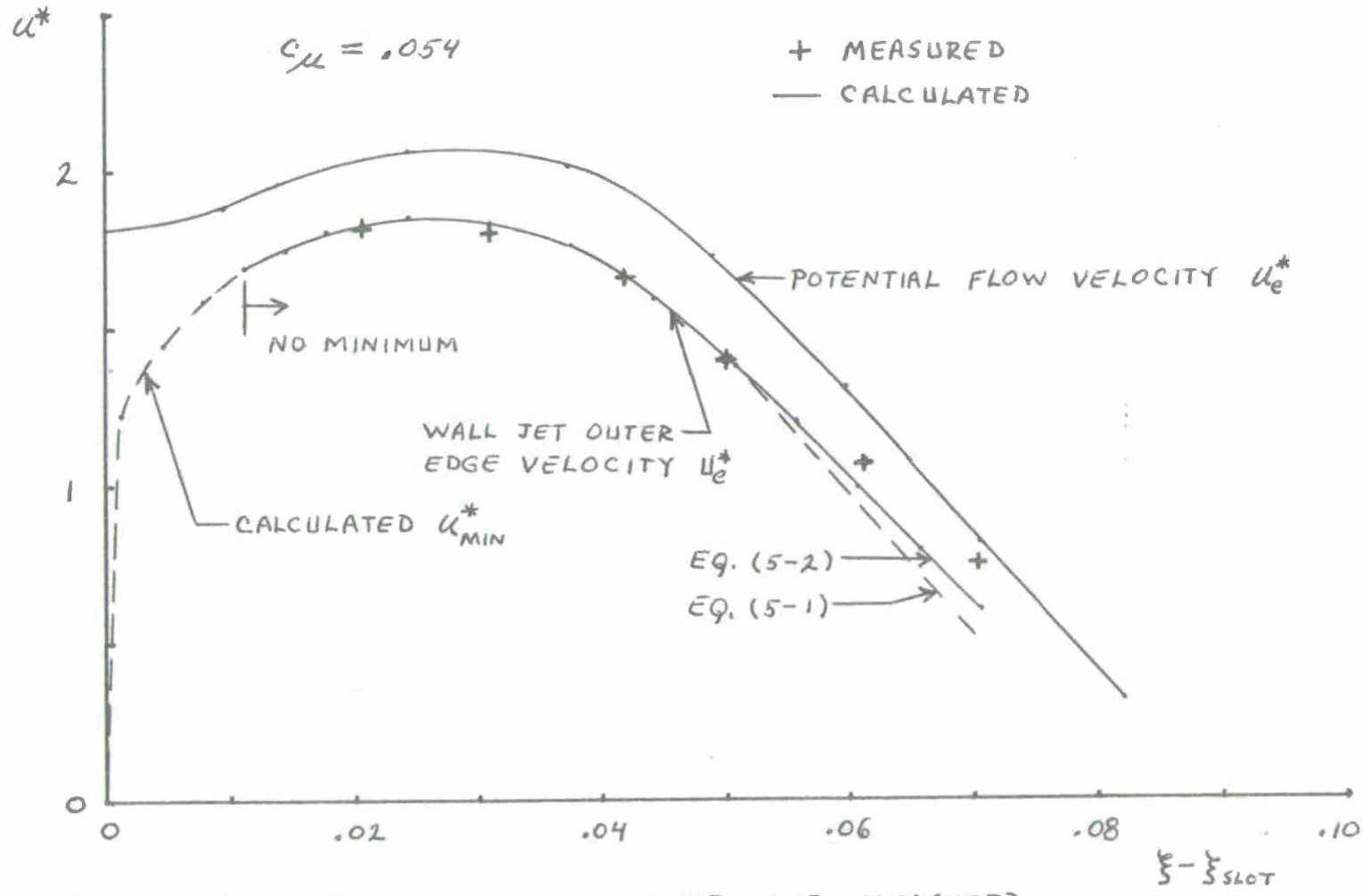


FIG. 8 COMPARISON OF CALCULATED AND MEASURED WALL JET OUTER EDGE VELOCITY

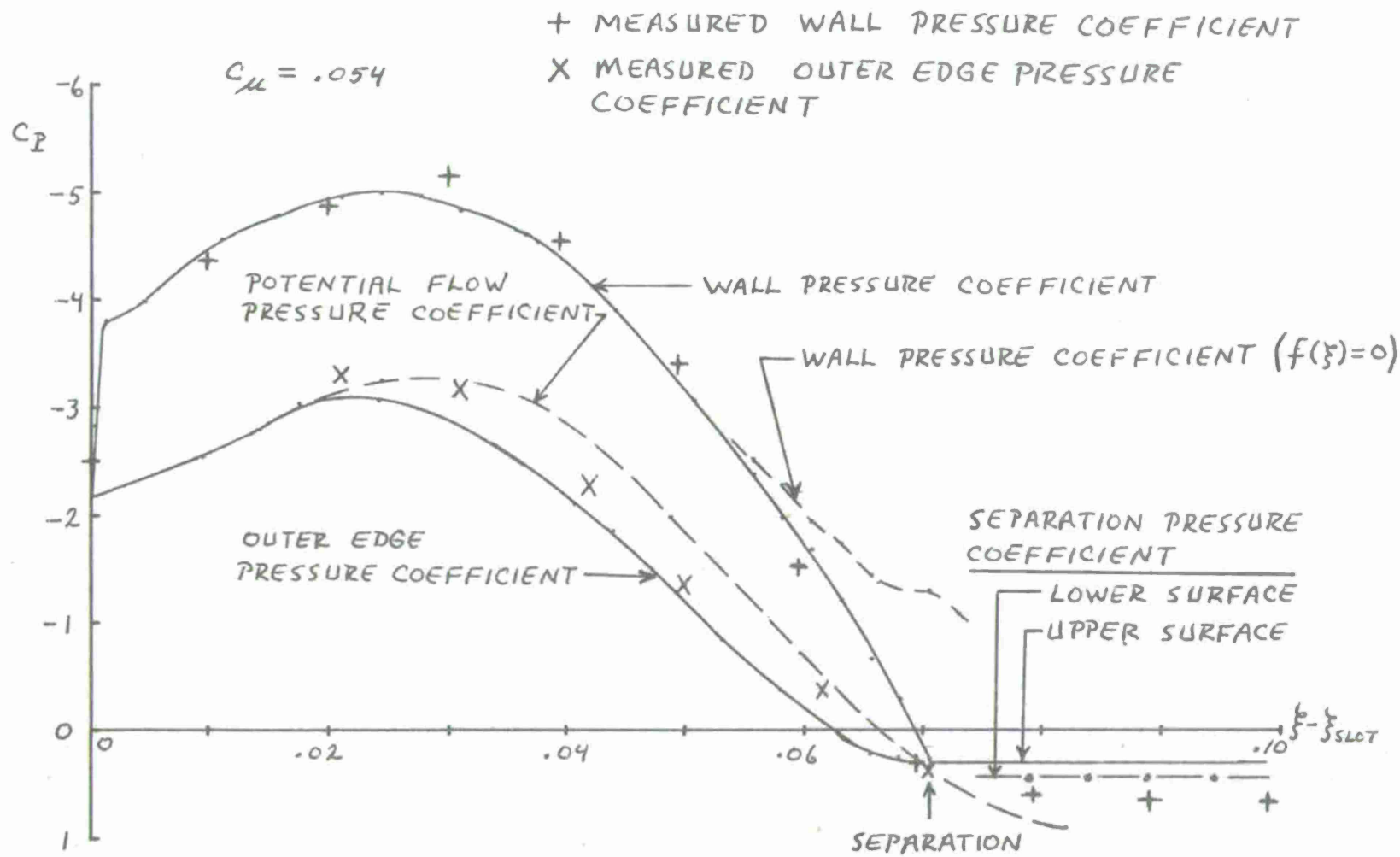


FIG. 9 COMPARISON OF CALCULATED AND MEASURED WALL JET PRESSURE DISTRIBUTION

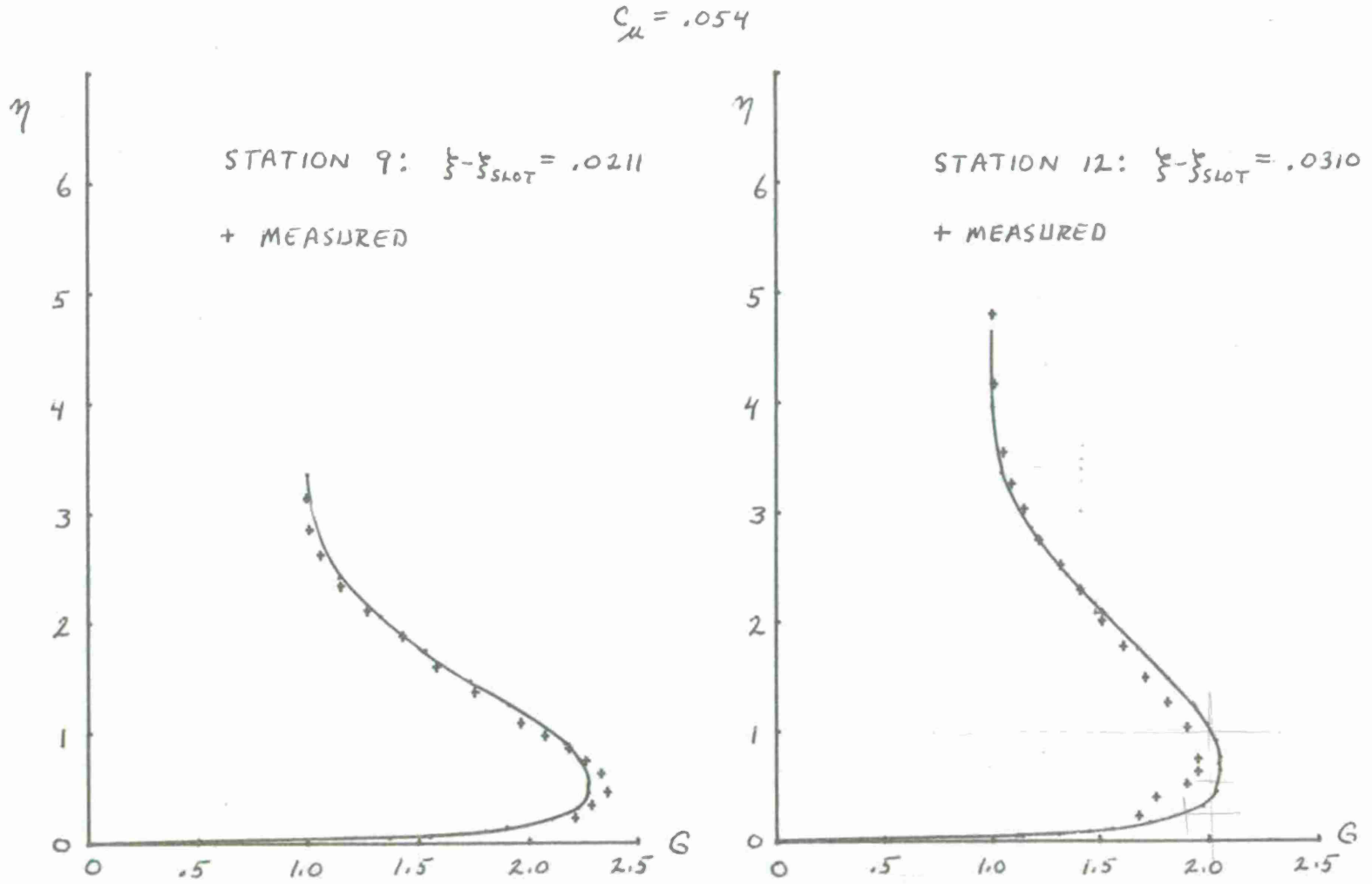


FIG. 10 COMPARISON OF CALCULATED AND MEASURED WALL JET PROFILES (STATIONS 9, 12 ; $C_\mu = .054$)

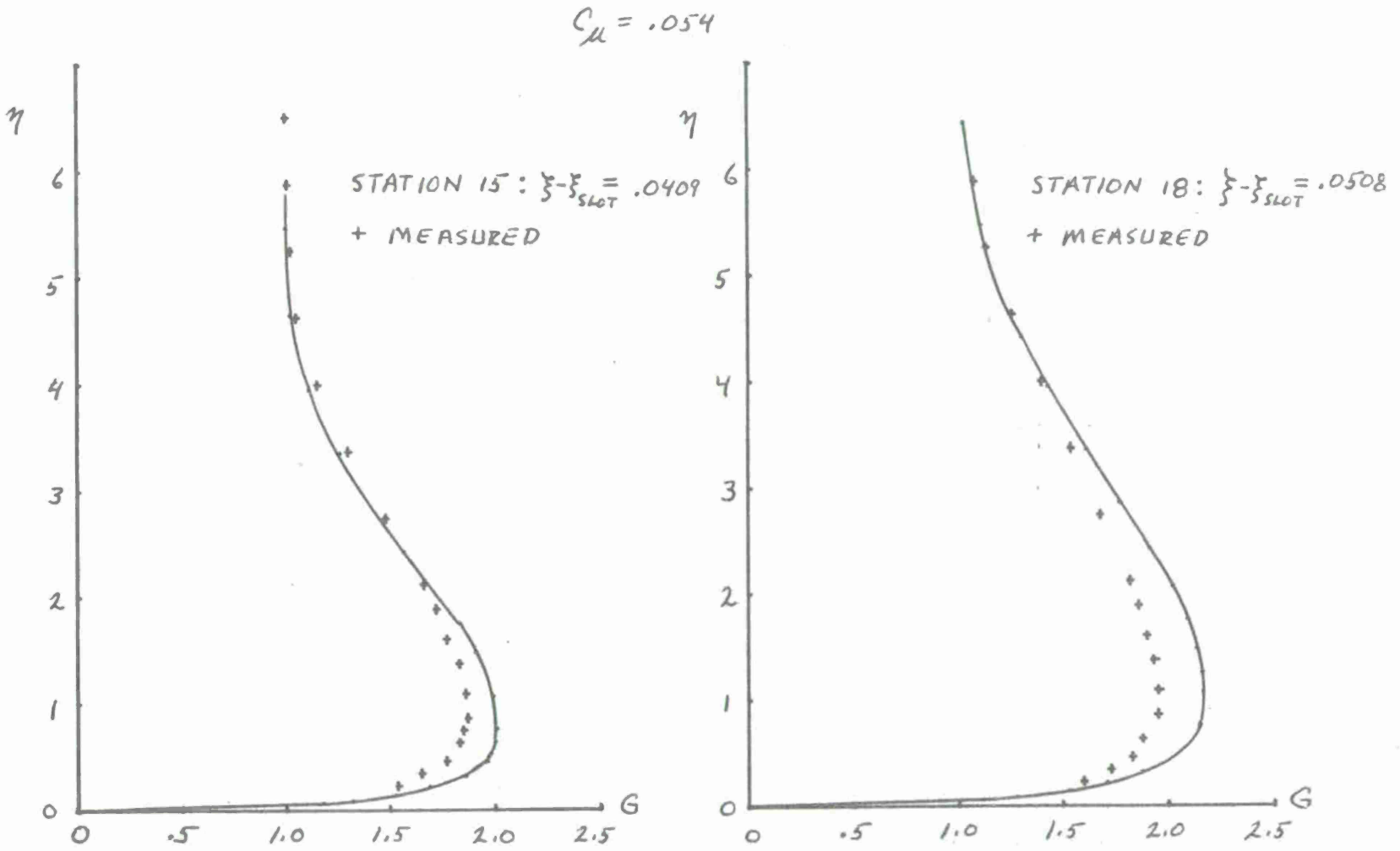


FIG. 11 COMPARISON OF CALCULATED AND MEASURED WALL JET PROFILES (STATIONS 15, 18 ; $C_\mu = .054$)

$C_\mu = .054$

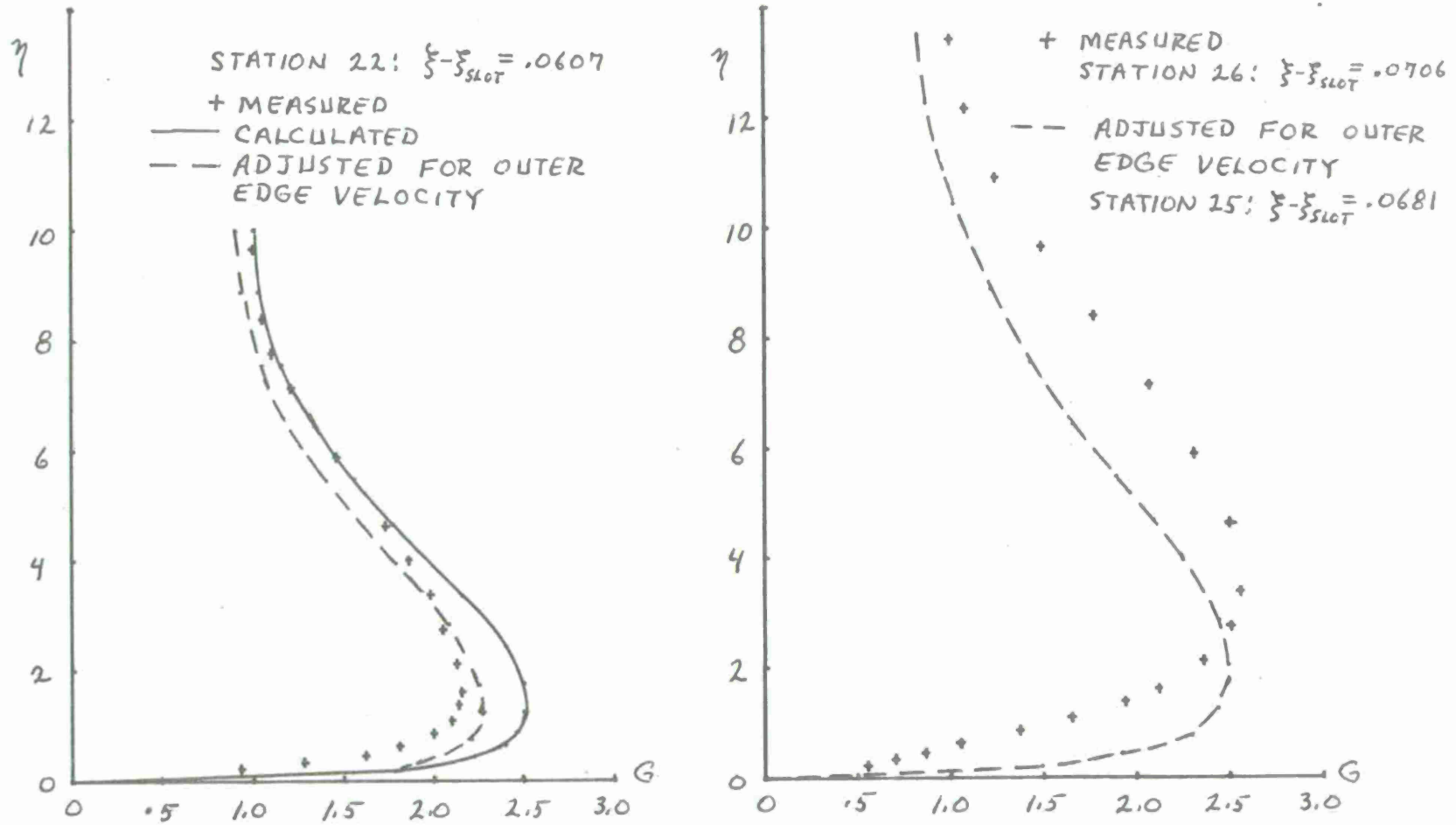


FIG. 12 COMPARISON OF CALCULATED AND MEASURED WALL JET PROFILES (STATIONS 22, 25 ; $C_\mu = .054$)

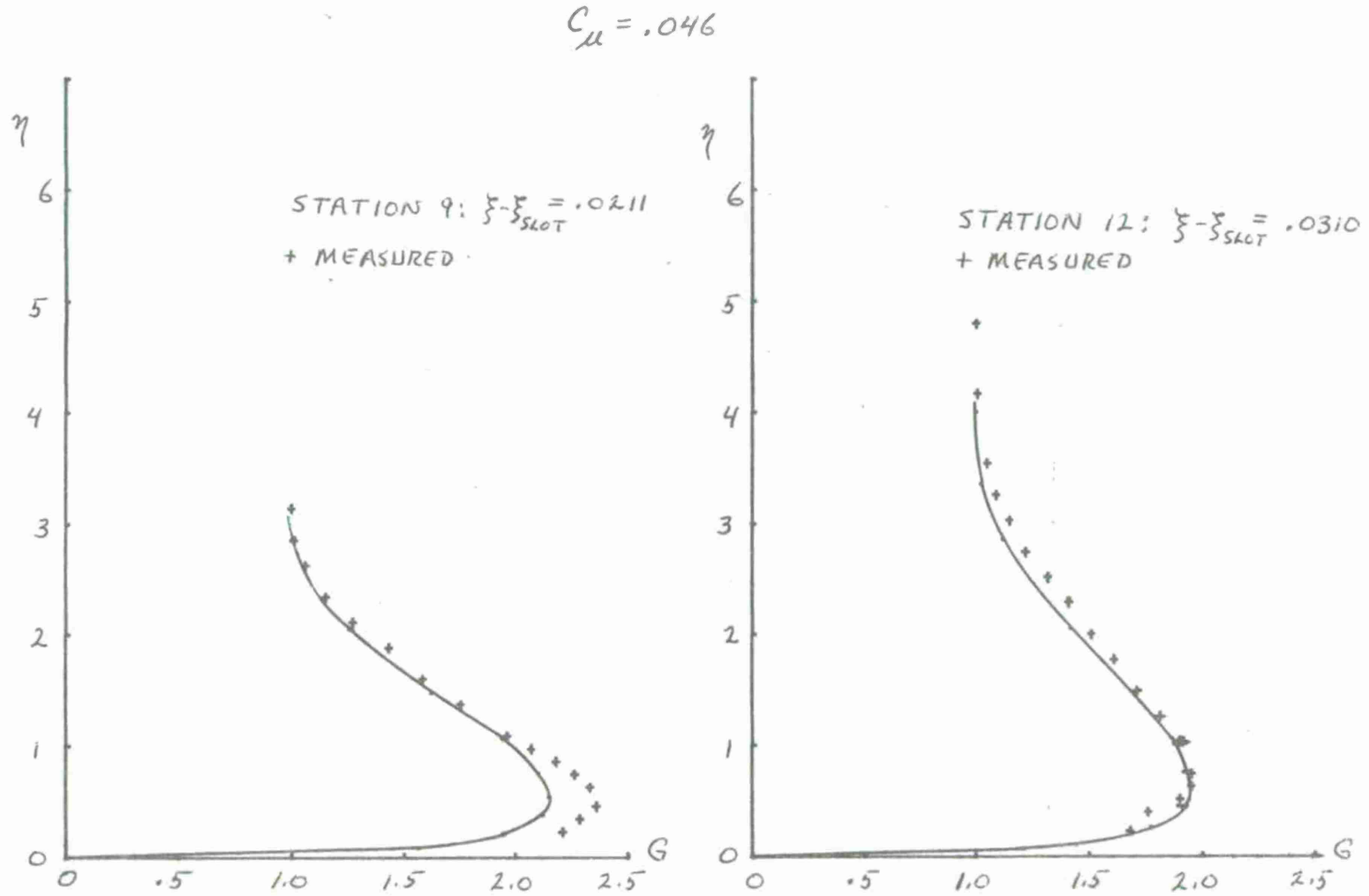


FIG. 13 COMPARISON OF CALCULATED AND MEASURED WALL JET PROFILES (STATIONS 9, 12 ; $C_\mu = .046$)

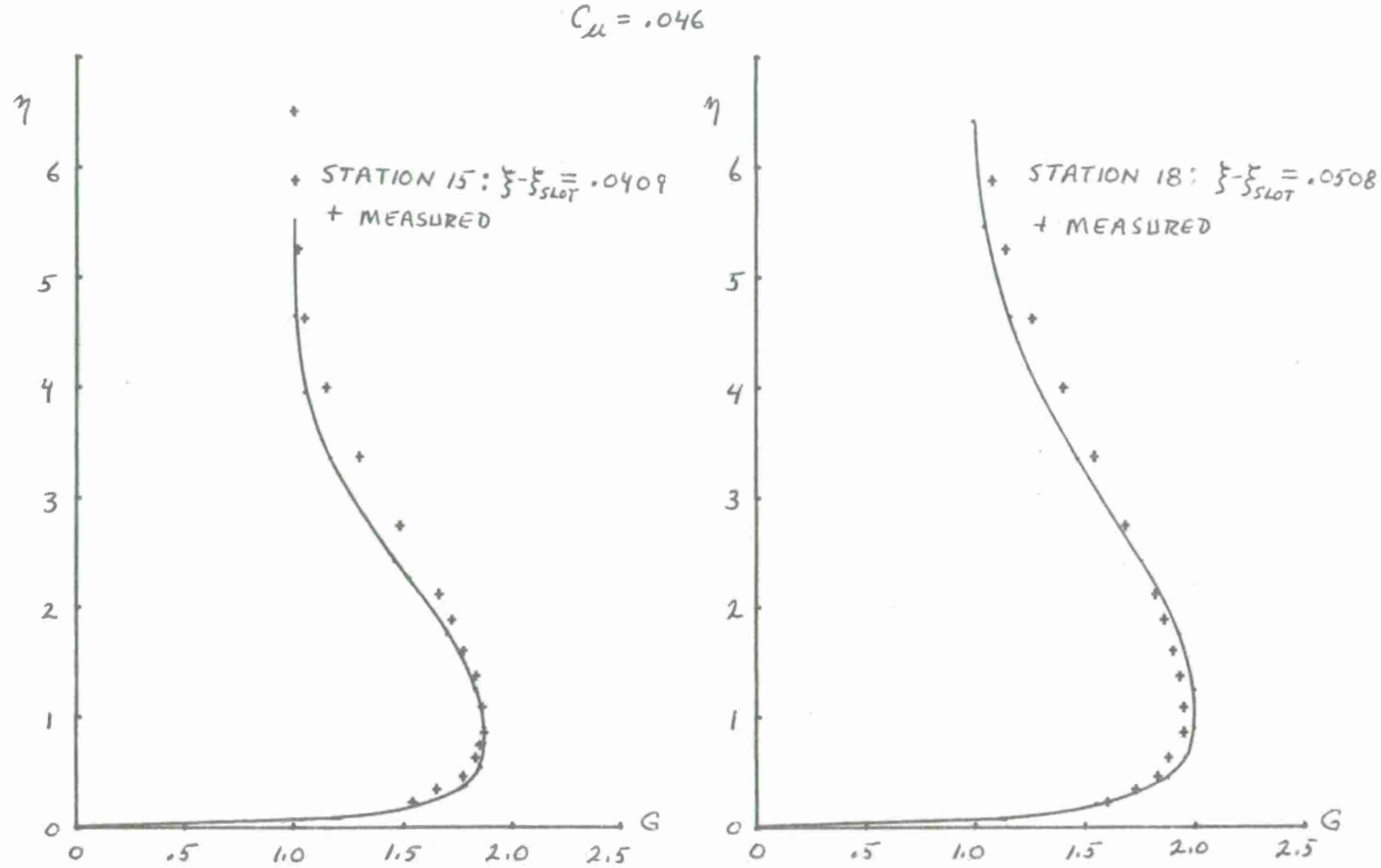


FIG. 14 COMPARISON OF CALCULATED AND MEASURED WALL JET PROFILES (STATIONS 15, 18 ; $C_\mu = .046$)

$C_\mu = .046$

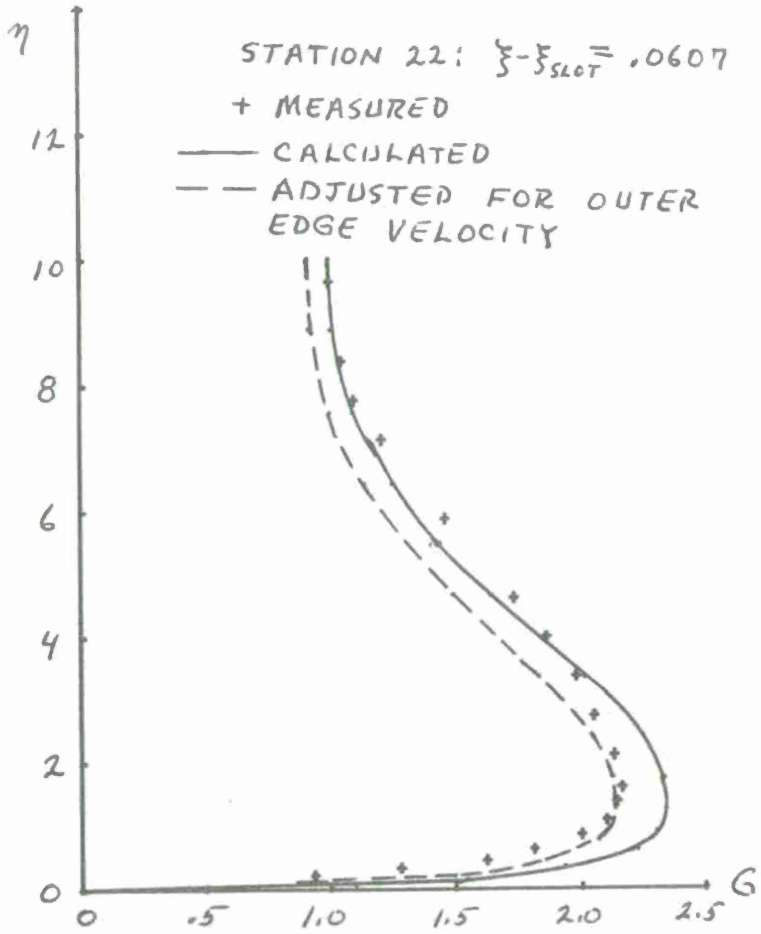


FIG. 15 COMPARISON OF CALCULATED AND MEASURED WALL JET PROFILES (STATION 22 ; $C_\mu = .046$)

# APPENDIX: COMPUTER PROGRAM

This appendix contains a listing of the computer program and a description of the program input and output. The program consists of the potential flow program described in Section 3, the boundary layer program described in Section 4, and the wall jet program described in Section 5. Only two dimensional flows ( $\epsilon = 0$) without suction ( $v_w = 0$) are considered here, and the boundary layer program is set up for this type of flow.

The program operates as follows. With the input given (Table A1), the potential flow is calculated and converted to the form required for boundary layer and wall jet use. Boundary layer calculations are performed first for the lower surface and then for the upper surface. Wall jet calculations are then performed for a prescribed number of assumed slot conditions. The initial assumed value of $u_t^*$ for the slot, and the increment $\Delta u_t^*$ for subsequent assumed values, are input. Drag and the change in $c_l$ caused by the pressure variation over the wall jet region could be calculated, but are not at present.

The input (Table A1) consists of three subroutine and three data cards. The subroutines provide the airfoil geometry as follows. Subroutine BODY provides the coordinates ( $x_c$, $y_c$ ) of the airfoil as required for the Theodorsen method. Subroutine SLOPE provides the values of $\frac{dy_c}{dx_c}$ required to convert to curvilinear coordinates. For convenience in cases where analytic expressions for $\frac{dy_c}{dx_c}$ are not available, an option in the program allows values of $dy_c/dx_c$ to be determined numerically. In this case, subroutine SLOPE is ignored,

and $\frac{dy_c}{dx_c}$ is automatically calculated numerically. An input integer tells the program which procedure to use. Subroutine RADIUS provides the surface radius of curvature in the wall jet region. The subroutines for Kind's airfoil are included in the program listing. The three data cards provide the rest of the input, including specifying options in the program. The form required for the data cards can be determined by inspection of the READ statements on the first page of the program listing.

Output from the program consists of the potential flow output (Table A2), the boundary layer output (Table A3), and the wall jet output (Table A4). The numbering system is different in the three sets of output. For the potential flow output, points are numbered in a counter-clockwise direction, with point 1 being the trailing edge. For the boundary layer output, point numbers are referenced from the front stagnation point. Point 1 is the first output point downstream of the stagnation point along the upper surface of the airfoil. The remaining upper surface points are numbered consecutively until the rear potential flow stagnation point is reached. If the last upper surface point is denoted by $j'_T$, the first point downstream of the front stagnation point along the lower surface of the airfoil is denoted by $(j'_T + 1)$. The remaining lower surface points are numbered consecutively. The wall jet points are numbered consecutively, with point 1 being at the blowing slot.

TABLE A1: COMPUTER PROGRAM INPUT

| Computer Symbol | Quantity & Units | Comments |
|---|---|---|
| CL | $C_\ell$ | Lift coefficient |
| ALPHA | $\alpha$ (degrees) | Angle of attack |
| REC | $Re_\infty$ | Free stream Reynolds number |
| NEPS | $N_\epsilon$ | Number of output points (must be even). Recommended: $40 \leq N_\epsilon \leq 80$ |
| NBPTS | $N_B$ | Number of body coordinates to be input (must be even). Recommended: $200 \leq N_B \leq 400$ |
| KUTTA | $K_U$ | $K_U$ = 0 if input $C_\ell$ is to be used. $K_U$ = 1 if Kutta condition is to be used. |
| NAEQN | $N_A$ | $N_A$ = 0 if airfoil slopes are to be calculated numerically. $N_A$ = 1 if subroutine SLOPE is to be used. |
| AK | K | Turbulent $\eta$ grid parameters |
| H1 | $h_1$ | See Table ~~I,~~ Ref. 8, p 26 |
| NT | N | |

(continued next page)

| | | |
|---|---|---|
| CHORD | c (feet) IN | Chord |
| BT | b (feet) IN | See Fig. 3 |
| XCJET | $x_{c_{slot}}$ | Cartesian coordinate of blowing slot |
| SLOTT | $\ell^* = \ell/c$ | Dimensionless slot thickness |
| UTSIG | $u_\tau^*$ | Initial value of $u_\tau^*$ for the blowing slot |
| UTSIN | $\Delta u_\tau^*$ | Increment of $u_\tau^*$ for the blowing slot |
| STEPS | $k_m / \ell^*$ | Maximum $\xi$ step size for wall jet grid |
| NWJIT | | Number of times wall jet calculations are to be performed. Assumed $u_\tau^*$ is incremeted by $\Delta u_\tau^*$ each time. |
| LAMSL | | LAMSL = 0 for a turbulent slot profile. LAMSL = 1 for a laminar slot profile |
| Subroutine BODY | | Subroutine BODY provides values for XX(J), YY(J) $(J=1,\ldots,N_B)$, c and b. XX $\rightarrow x_c$ and YY $\rightarrow y_c$ in Fig. 3. All dimensions are |

(continued on next page)

| | |
|---|---|
| | in feet. Points are numbered in counterclockwise order around the airfoil. The point J = 1 must be the trailing edge ($y_c = 0$, $x_c > 0$) and J=1/2$N_B$+1 must be the leading edge ($y_c = 0$, $x_c < 0$). It is desirable to have nearly equal arc lengths between points. |
| Subroutine SLOPE | Subroutine SLOPE provides the slopes of the upper and lower airfoil surfaces as functions of $x_c$. YPU = $\left(\frac{dy_c}{dx_c}\right)$ upper surface. YPL = $\left(\frac{dy_c}{dx_c}\right)$ lower surface. The function statement X = .5*(XUL-XLL)*XA+.5*(XUL+XLL) must be included. |
| Subroutine RADIUS | Subroutine RADIUS provides R* for a given X, where $X \rightarrow \xi - \xi_{slot}$. |

TABLE A2: POTENTIAL FLOW OUTPUT

| Computer Symbol | Quantity & Units | | Comments |
|---|---|---|---|
| PHI | $\varphi$ | (degrees) | Angle $\varphi$ defined in Fig. 3. |
| X | $x_c$ | (feet) | See Fig. 3 |
| Y | $y_c$ | (feet) | |
| U | $V_b/V_\infty$ | | Eq. (3-14) |
| CP | $C_p$ | | Eq. (3-16) |
| CL | $C_\ell$ | | Lift coefficient |
| ALPHA | $\alpha$ | (degrees) | Angle of attack |
| XSTAG | $x_{stag}$ | (feet) | Coordinates of front |
| YSTAG | $y_{stag}$ | (feet) | stagnation point. |

TABLE A3: BOUNDARY LAYER OUTPUT

| Computer Symbol | Quantity & Units | Comments |
|---|---|---|
| X | $x$ (feet) | Fig. 1 |
| XI | $\xi^*$ | Eq. (3-17a) |
| BETA | $\beta$ | Eq. (3-17b) |
| UE | $u_e^*$ | Eq. (3-14) |
| XC | $x_c$ (feet) | Fig. 3 |
| YC | $y_c$ (feet) | Fig. 3 |
| DELTA | $\delta$ (inches) | Eq. (4-23) |
| DELST | $\delta^*$ (inches) | Eq. (4-21) |
| THETA | $\theta$ (inches) | Eq. (4-22) |
| CF | $C_f$ | Eq. (4-20) |
| H | H | $H = \delta^*/\theta$ |
| REC | $Re_\infty$ | |
| REDS | $Re_{\delta^*}$ | Eq. (4-24) |
| RET | $Re_\theta$ | Eq. (4-25) |
| ITERATION | | Maximum is 20 |
| DFW, DDS | | Iteration tolerances |
| | | For laminar flow, DDS = 0. |

(continued next page)

| | | |
|---|---|---|
| NEDGE | | NEDGE must be $<$ NT (Table A1). If NEDGE = NT, the $\eta$ grid should be changed to allow for a thicker boundary layer. |
| FW" | $f''_w$ | Values of $f''_w$ indicate appropriate values of $h_1$ (Ref. 8). |

TABLE A4: WALL JET OUTPUT

| Computer Symbol | Quantity & Units | Comments |
|---|---|---|
| CMU | $C_\mu$ | Eq. (5-49) |
| CM | $C_m$ | Eq. (5-50) |
| UAVE | $u^*_{AVE}$ | Average velocity in blowing slot. |
| UMAX | $u^*_m$ | Maximum velocity in blowing slot. |
| HW | $H_w$ | |
| XI | $\xi = \frac{x}{c}$ | Eq. (5-7) |
| DELXI | $\xi - \xi_{SLOT}$ | |
| UE | $u^*_e$ | Eq. (5-12a) or Eq. (5-13) |
| CPW | $C_{p_w}$ | |
| CPE | $C_{p_e}$ | Eq. (5-12b) or Eq. (5-13) |
| CP (POT) | $C_{p_e}$ | $1 - u_e^{*2}$ |
| TAUW | $\tau^*_w$ | $2 u_e^* H_w / (C^* Re_\infty)$ |
| DELTA | $\Delta^*$ | |
| GMAX | $G_m$ | |
| GMIN | $G_{min}$ | $G_{min} \equiv 0$ for profiles without a minimum velocity |
| ITERATION | | Maximum is 10 |
| ETAMAX | $\eta_m$ | |
| ETAMIN | $\eta_{min}$ | |
| DHW, DCPW | | Iteration tolerances |
| JDELTA | | $\eta = \eta_\Delta$ at $j$ = JDELTA |

```
      DIMENSION ZP(401),ZO(401),L(100)
      DIMENSION A(100),B(101),C(100),D(100),E(100),F(100)
      DIMENSION XU(100),YU(100),U(100),P(200)
      COMMON/MAINWJ/PF(3,25),NPF,STEPS
      COMMON/MAINSL/STFT(7),LAMSL
      COMMON/HBDBMB/XI(100),BETA(100),UE(100),FW(100),CPHI(100),RWC(100)
     $,CF(100),XC(100),YC(100),X(100),CHORD,EPS,TVC,REC,NT,AK,H1,ETAET,
     $LAM,NPRNT,JMAX,JMIN,JJET,JSEPP
      COMMON/HBDBBO/XX(400),YY(400)
      EQUIVALENCE (U(1),UE(1)),(XU(1),XC(1)),(YU(1),YC(1))
C
C     CALCULATE POTENTIAL FLOW
C
      READ 908,CL,ALPHA,REC,NEPS
      READ 909,AK,H1,NT,NBPTS,KUTTA,NAEQN
      READ 911,XCJET,SLOTT,UTSIG,UTSIN,STEPS,NWJIT,LAMSL
      CHORD = 14.625
      THICK = .2
      CAMB = .05
C     INPUT BODY COORDINATES
      CALL BODY (CHORD,THICK,CAMB,NBPTS,BT,RLE,RTE)
C     INPUT SHOULD BE COMPLETE
      NPRNT = 0
      NLE = NBPTS/2 + 1
      PI = 3.141593
      TOPI = 6.283185
      RADEG = 360./TOPI
      B2 = 2.*BT
C     CALCULATE PSI AND OMEGA
      DO 1 J=1,NBPTS
      HXY = 1. - (XX(J)/B2)**2 - (YY(J)/B2)**2
      SR = (HXY**2 + (YY(J)/BT)**2)**.5
      IF (HXY .LT. 0. .AND. SR .LT. ABS(HXY)) SR = ABS(HXY)
      SO = (.5*(HXY+SR))**.5
      ZO(J) = ARSIN(SO)
      IF (XX(J) .LT. 0. .AND. J .LE. NLE) ZO(J) = PI - ZO(J)
      IF (XX(J) .LT. 0. .AND. J .GT. NLE) ZO(J) = PI + ZO(J)
      IF (XX(J) .GE. 0. .AND. J .GT. NLE) ZO(J) = TOPI - ZO(J)
      SHS = .5*(SR-HXY)
      IF (SHS .LT. 0.) SHS = 0.
      SH = SHS**.5
      IF (J .LT. NLE .AND. YY(J) .LT. 0.) SH = -SH
      IF (J .GT. NLE .AND. YY(J) .GT. 0.) SH = -SH
    1 ZP(J) = ALOG(SH + (1.+SHS)**.5)
      IF (NPRNT .EQ. 0) GO TO 3
```

=> no print

```
      DO 2 J=1,NBPTS
    2 PRINT 901,J,XX(J),YY(J),ZP(J),ZO(J)
    3 DPHI = TOPI/NEPS
      DO 4 J=1,NEPS
      P(J) = (J-.5)*DPHI
    4 P(NEPS+J) = (J-1)*DPHI
C     CALCULATE EPSILON
      DO 5 J=1,NEPS
      LL = 1
      IF (J .GT. 1) LL = L(J-1)
      DO 5 JJ=LL,NBPTS
      IF (ZO(JJ) .GT. P(J)) GO TO 5
      L(J) = JJ
    5 CONTINUE
      DO 6 J=1,NEPS
    6 F(J) = 0.
      JL = L(NEPS)
      JM = 1
      JU = L(1)
      D1 = TOPI - ZO(JL)
      D2 = ZO(JU)
      D3 = D1 + D2
      D(1) = -ZP(JL)*D2/D1/D3 + ZP(JM)*(1./D1-1./D2) + ZP(JU)*D1/D3/D2
      DO 7 J=JL,NBPTS
    7 F(1) = F(1) + ZP(J)
      DO 8 J=1,JU
    8 F(1) = F(1) + ZP(J)
      F(1) = F(1)/(NBPTS-JL+JU+1)
      DO 10 J=2,NEPS
      JU = L(J)
      JL = L(J-1)
      JM = (JU + JL)/2
      D1 = ZO(JM) - ZO(JL)
      D2 = ZO(JU) - ZO(JM)
      D3 = ZO(JU) - ZO(JL)
      D(J) = -ZP(JL)*D2/D1/D3 + ZP(JM)*(1./D1-1./D2) + ZP(JU)*D1/D3/D2
      DO 9 JJ=JL,JU
    9 F(J) = F(J) + ZP(JJ)
   10 F(J) = F(J)/(JU-JL+1)
      SO = PI/(2*NEPS)
      JM = NEPS/2 - 1
      DO 11 J=1,JM
      SR = SIN(SO*(2*J+1))/SIN(SO*(2*J-1))
   11 C(J) = ALOG (ABS(SR))
      DO 13 J=1,NEPS
```

```
      E(J) = DPHI*D(J)
      DO 12 JJ=1,JM
      JU = J + JJ
      IF (JU .GT. NEPS) JU = JU - NEPS
      JL = NEPS + J - JJ
      IF (JL .GT. NEPS) JL = JL - NEPS
   12 E(J) = E(J) + (F(JU)-F(JL))*C(JJ)
   13 E(J) = E(J)/PI
      IF (NPRNT .EQ. 0) GO TO 16
      DO 14 J=1,NEPS
   14 PRINT 902,J,F(J),D(J),E(J)
      DO 15 J=1,JM
   15 PRINT 903,J,C(J)
C     CALCULATE PHI
   16 DO 17 J=1,NEPS
      P(J) = P(NEPS+J) - E(J)
      A(J) = DPHI*(J-1) + E(J)
      IF (A(J) .LT. 0.) A(J) = A(J)+TOPI
      IF (A(J) .GT. TOPI) A(J) = A(J)-TOPI
      IF (P(J) .LT. 0.) P(J) = TOPI + P(J)
      IF (P(J) .GT. TOPI) P(J) = P(J) - TOPI
   17 CONTINUE
C     CALCULATE EPSILON PRIME
      F(1) = .1*(-2.*E(NEPS-1)-E(NEPS)+E(2)+2.*E(3))/DPHI
      F(2) = .1*(-2.*E(NEPS)-E(1)+E(3)+2.*E(4))/DPHI
      F(NEPS-1) = .1*(-2.*E(NEPS-3)-E(NEPS-2)+E(NEPS)+2.*E(1))/DPHI
      F(NEPS) = .1*(-2.*E(NEPS-2)-E(NEPS-1)+E(1)+2.*E(2))/DPHI
      LL = NEPS-2
      DO 18 J=3,LL
   18 F(J) = .1*(-2.*E(J-2)-E(J-1)+E(J+1)+2.*E(J+2))/DPHI
      DO 20 J=1,NEPS
      LL = 1
      DO 19 JJ=LL,NBPTS
      IF (ZO(JJ) .GT. A(J)) GO TO 20
   19 L(J) = JJ
   20 C(J) = 0.
      IF (L(1) .LT. L(NEPS)) LL=1
      IF (L(1) .LT. L(NEPS)) GO TO 22
      DO 21 J=2,NEPS
      IF (L(J) .LT. L(J-1)) LL=J
      IF (L(J) .LT. L(J-1)) GO TO 22
   21 CONTINUE
   22 JM = LL - 1
      IF (JM .EQ. 0) JM = NEPS
      JL = L(JM)
```

PRINT 915, JM
915 FORMAT (10X, 4HJM = , I6)

```
      JU = NBPTS
      DO 23 J=JL,JU
   23 C(LL) = C(LL) + ZP(J)
      JU = L(LL)
      DO 24 J=1,JU
   24 C(LL) = C(LL) + ZP(J)
      C(LL) = C(LL)/(NBPTS-JL+JU+1)
      AO = C(LL)*DPHI
      DO 26 J=1,NEPS
      IF (J .EQ. LL) GO TO 26
      JU = L(J)
      JM = J-1
      IF (JM .EQ. 0) JM = NEPS
      JL = L(JM)
      DO 25 JJ=JL,JU
   25 C(J) = C(J) + ZP(JJ)
      C(J) = C(J)/(JU-JL+1)
      AO = AO + C(J)*DPHI
   26 CONTINUE
      AO = AO/TOPI
      IF (NPRNT .EQ. 0) GO TO 28
      PRINT 903,LL,AO
      DO 27 J=1,NEPS
      SO = P(NEPS+J)*RADEG
      SR = P(J)*RADEG
   27 PRINT 901,J,SO,SR,C(J),F(J)
   28 ELK = EXP(AO)
C     FIND FRONT STAGNATION POINT
      ALF = ALPHA
      ALPHA = ALPHA/RADEG
      IF (KUTTA .EQ. 1) CL = 8./CHORD*PI*BT*ELK*SIN(E(1)+ALPHA)
      AR = CL/8.*CHORD/BT/ELK/PI
      SR = ARSIN(-AR)
      PHIST = ALPHA + PI - SR
      PRINT 900
      PRINT 907
      L(1) = 1
      DO 30 J=2,NEPS
      LL = L(J-1)
      DO 29 JJ=LL,NBPTS
      IF (ZO(JJ) .GT. P(NEPS+J)) GO TO 30
   29 L(J) = JJ
   30 CONTINUE
      LL = 1
      IF (PHIST .GT. PI) LL = NEPS/2-1
```

```
      DO 31 J=LL,NEPS
      SO=P(NEPS+J)-E(J)
      IF (SO .GT. PHIST) GO TO 32
   31 JSAVE = J
   32 ESTAG = E(JSAVE) + ((E(JSAVE+1)-E(JSAVE))/DPHI)*
     $(PHIST-P(JSAVE))
      WSTAG = PHIST + ESTAG
      LL = 1
      IF (WSTAG .GT. PI) LL=NLE
      DO 33 J=LL,NBPTS
      IF (ZO(J) .GT. WSTAG) GO TO 34
   33 JM = J
   34 PSIST = ZP(JM) + ((ZP(JM+1)-ZP(JM))/(ZO(JM+1)-ZO(JM)))*
     $(WSTAG-ZO(JM))
      EP = EXP(PSIST)
      EM = EXP(-PSIST)
      XSTAG = BT*COS(WSTAG)*(EP+EM)
      YSTAG = BT*SIN(WSTAG)*(EP-EM)
C     CALCULATE U AND CP
      PRINT 904,CL,ALF,XSTAG,YSTAG
      PRINT 905
      DO 36 J=1,NEPS
      IF (J .NE. 51) GO TO 35
      PRINT 900
      PRINT 907
      PRINT 904,CL,ALF,XSTAG,YSTAG
      PRINT 905
   35 SP = P(J)
      LL = L(J)
      SO = DPHI*(J-1)
      PSI = ZP(LL) + ((ZP(LL+1)-ZP(LL))/(ZO(LL+1)-ZO(LL)))*(SO-ZO(LL))
      EP = EXP(PSI)
      EM = EXP(-PSI)
      TS = SIN(SO)
      TC = COS(SO)
      SHS = .5*(EP-EM)
      SR = ((1. + D(J)**2)*(SHS**2 + TS**2))**.5
      IF (J .EQ. 1 .AND. KUTTA .EQ. 1) SR = 1.E-8
      SO = SIN(SP-ALPHA) + AR
      U(J) = ELK*ABS(SO*(1.-F(J)))/SR
      P(J) = 1. - U(J)**2
      SP = SP*RADEG
      XU(J) = BT*TC*(EP+EM)
      YU(J) = BT*TS*(EP-EM)
   36 PRINT 906,J,SP,XU(J),YU(J),U(J),P(J)
```

```
C
C     BYE, TEDDY
C
C     CHANGE TO BOUNDARY LAYER COORDINATES
C
      IF (NAEQN .EQ. 0) GO TO 43
      JM = NEPS/2
      B(1) = .34785485
      B(2) = .65214515
      B(3) = B(2)
      B(4) = B(1)
      C(1) = -.86113631
      C(2) = -.33998104
      C(3) = -C(2)
      C(4) = -C(1)
      DO 42 J=1,JM
      A(J) = 0.
      A(JM+J) = 0.
      IF (J .GT. 1 .AND. J .LT. JM) GO TO 39
      XLL = XU(J)
      XUL = XU(J+1)
      DO 37 JJ=1,4
      CALL SLOPE (XLL,XUL,C(JJ),YPU,YPL)
      SR = .5/YPU
   37 A(J) = A(J) + B(JJ)*SR
      A(J) = ABS(.5*(XUL-XLL)*A(J) + YU(J+1) - YU(J))
      XLL = XU(JM+J)
      JL = JM+J+1
      IF (JL .GT. NEPS) JL=1
      XUL = XU(JL)
      DO 38 JJ=1,4
      CALL SLOPE (XLL,XUL,C(JJ),YPU,YPL)
      SR = .5/YPL
   38 A(JM+J) = A(JM+J) + B(JJ)*SR
      A(JM+J) = ABS(.5*(XUL-XLL)*A(JM+J) + YU(JL) - YU(JM+J))
      GO TO 42
   39 XLL = XU(J)
      XUL = XU(J+1)
      DO 40 JJ=1,4
      CALL SLOPE (XLL,XUL,C(JJ),YPU,YPL)
      SR = (1.+YPU**2)**.5
   40 A(J) = A(J) + B(JJ)*SR
      A(J) = ABS(.5*(XUL-XLL)*A(J))
      XLL = XU(JM+J)
      XUL = XU(JM+J+1)
```

Gauss Quadrature Weights

```
      DO 41 JJ=1,4
      CALL SLOPE (XLL,XUL,C(JJ),YPU,YPL)
      SR = (1.+YPL**2)**.5
   41 A(JM+J) = A(JM+J) + B(JJ)*SR
      A(JM+J) = ABS(.5*(XUL-XLL)*A(JM+J))
   42 CONTINUE
      GO TO 52
   43 LL = NEPS/2
      L(1) = 1
      DO 45 J=2,LL
      SO = XU(J)
      JL = L(J-1)
      DO 44 JJ=JL,NLE
      IF (XX(JJ) .LT. SO) GO TO 45
   44 L(J) = JJ
   45 CONTINUE
      LM = NEPS/2
      LL = LM + 1
      L(LL) = NLE
      DO 47 J=LL,NEPS
      SO = XU(J)
      JL = L(J-1)
      DO 46 JJ=JL,NBPTS
      IF (XX(JJ) .GT. SO) GO TO 47
   46 L(J) = JJ
   47 CONTINUE
      LL = NEPS/2-2
      LM = NEPS/2+3
      LU = NEPS-2
      DO 51 J=1,NEPS
      IF (J .GT. 3 .AND. J .LT. LL) GO TO 49
      IF (J .GT. LM .AND. J .LT. LU) GO TO 49
      SO = 0.
      JL = L(J)
      JM = J+1
      IF (J .EQ. NEPS) JM = 1
      JU = L(JM)
      IF (J .EQ. NEPS) JU = NBPTS-1
      DO 48 JJ=JL,JU
   48 SO = SO + (XX(JJ+1)-XX(JJ))/(YY(JJ+1)-YY(JJ))
      SR = SO/(JU-JL+1)
      SO = (1.+SR**2)**.5
      JM = J+1
      IF (JM .GT. NEPS) JM=1
      A(J) = ABS(SO*(YU(JM)-YU(J)))
```

```
      GO TO 51
   49 SO = 0.
      JL = L(J)
      JU = L(J+1)
      DO 50 JJ=JL,JU
   50 SO = SO + (YY(JJ+1)-YY(JJ))/(XX(JJ+1)-XX(JJ))
      SR = SO/(JU-JL+1)
      SO = (1.+SR**2)**.5
      A(J) = ABS(SO*(XU(J+1)-XU(J)))
   51 CONTINUE
   52 IF (WSTAG .GE. PI) GO TO 54
      JL = 2
      JU = NEPS/2
      DO 53 J=JL,JU
      JSAVE = J
      IF (XU(J+1) .LT. XSTAG .AND. XU(J) .GE. XSTAG) GO TO 56
   53 CONTINUE
   54 JL = NEPS/2+1
      JU = NEPS-1
      DO 55 J=JL,JU
      JSAVE = J
      IF (XU(J+1) .GT. XSTAG .AND. XU(J) .LE. XSTAG) GO TO 56
   55 CONTINUE
C     REINITIAL U AND P
   56 PSR = ALPHA + ARSIN(-AR)
      IF (PSR .LT. 0.) PSR = TOPI+PSR
      DO 57 J=1,NEPS
      B(J) = DPHI*(J-1) - E(J)
      IF (B(J) .LT. 0.) B(J) = TOPI+B(J)
   57 CONTINUE
      IF (B(1) .LT. B(NEPS)) JM = NEPS
      IF (B(1) .LT. B(NEPS)) GO TO 59
      JU = NEPS-1
      DO 58 J=1,JU
      IF (B(J+1) .LT. B(J)) JM = J
      IF (B(J+1) .LT. B(J)) GO TO 59
   58 CONTINUE
   59 JU = JM+1
      IF (JU .GT. NEPS) JU = 1
      SR = B(JU) + TOPI
      SO = B(JM)
      IF (PSR .GE. SO .AND. PSR .LT. SR) JREAR = JM
      IF (PSR .GE. SO .AND. PSR .LT. SR) GO TO 61
      DO 60 J=1,NEPS
      IF (J .EQ. JM) GO TO 60
```

```
      JU = J+1
      IF (J .EQ. NEPS) JU=1
      IF (PSR .GE. B(J) .AND. PSR .LT. B(JU)) JREAR = J
      IF (PSR .GE. B(J) .AND. PSR .LT. B(JU)) GO TO 61
   60 CONTINUE
   61 IF (JREAR .LT. JSAVE) JTOP = JSAVE- JREAR
      IF (JREAR .GE. JSAVE) JTOP = JSAVE+NEPS-JREAR
      JBOT = NEPS-JTOP
      DO 62 J=1,JTOP
      JM = JSAVE+1-J
      IF (JM .LE. 0) JM = NEPS+JM
      B(J) = U(JM)
      C(J) = P(JM)
      D(J) = XU(JM)
   62 F(J) = YU(JM)
      DO 63 J=1,JBOT
      JL = JTOP+J
      JM = JSAVE + J
      IF (JM .GT. NEPS) JM = JM-NEPS
      B(JL) = U(JM)
      C(JL) = P(JM)
      D(JL) = XU(JM)
   63 F(JL) = YU(JM)
      D1 = XU(JSAVE) - XU(JSAVE-1)
      D2 = XU(JSAVE+1) - XU(JSAVE)
      D3 = D1+D2
      D4 = XSTAG - XU(JSAVE-1)
      D5 = XSTAG - XU(JSAVE)
      D6 = XSTAG - XU(JSAVE+1)
      SR = -A(JSAVE-1)*D4/D1*D6/D2 + (A(JSAVE)+A(JSAVE-1))*D4/D3*D5/D2
      SR = SR - A(JSAVE-1)
      JU = NEPS/2+1
      IF (JSAVE .EQ. JU) SR = A(JU)*(XSTAG-XU(JU))/(XU(JU+1)-XU(JU))
      X(1) = SR
      JU = JTOP-1
      DO 64 J=1,JU
      JM = JSAVE-J
      IF (JM .LE. 0) JM = NEPS+JM
   64 X(J+1) = X(J) + A(JM)
      X(JTOP+1) = A(JSAVE)-SR
      JU = JBOT-1
      DO 65 J=1,JU
      JL = JTOP+J
      JM = JSAVE +J
      IF (JM .GT. NEPS) JM = JM - NEPS
```

```
   65 X(JL+1) = X(JL) + A(JM)
      DO 66 J=1,NEPS
      U(J) = B(J)
      P(J) = C(J)
      XU(J) = D(J)
   66 YU(J) = F(J)
C     CALCULATE XI AND BETA
      XI(1) = .5*X(1)*U(1)/CHORD
      XI(JTOP+1) = .5*X(JTOP+1)*U(JTOP+1)/CHORD
      JU = JTOP-1
      DO 67 J=2,JU
      X1 = X(J-1)/CHORD
      X2 = X(J)/CHORD
      X3 = X(J+1)/CHORD
      C1 = U(J-1)/(X2-X1)/(X3-X1)
      C2 = -U(J)/(X2-X1)/(X3-X2)
      C3 = U(J+1)/(X3-X1)/(X3-X2)
      D1 = C1+C2+C3
      D2 = -C1*(X2+X3) - C2*(X1+X3) - C3*(X1+X2)
      D3 = C1*X2*X3 + C2*X1*X3 + C3*X1*X2
   67 XI(J) = XI(J-1) + (X2-X1)*(D1*X1*X2+.5*D2*(X1+X2)+D3)
     $     +D1*(X2-X1)**3/3.
      XI(JTOP) = XI(JTOP-1) + (X3-X2)*(D1*X2*X3+.5*D2*(X2+X3)+D3)
     $     + D1*(X3-X2)**3/3.
      JL = JTOP+2
      JU = NEPS-1
      DO 68 J=JL,JU
      X1 = X(J-1)/CHORD
      X2 = X(J)/CHORD
      X3 = X(J+1)/CHORD
      C1 = U(J-1)/(X2-X1)/(X3-X1)
      C2 = -U(J)/(X2-X1)/(X3-X2)
      C3 = U(J+1)/(X3-X1)/(X3-X2)
      D1 = C1+C2+C3
      D2 = -C1*(X2+X3) - C2*(X1+X3) - C3*(X1+X2)
      D3 = C1*X2*X3 + C2*X1*X3 + C3*X1*X2
   68 XI(J) = XI(J-1) + (X2-X1)*(D1*X1*X2+.5*D2*(X1+X2)+D3)
     $     + D1*(X2-X1)**3/3.
      XI(NEPS) = XI(NEPS-1) + (X3-X2)*(D1*X2*X3+.5*D2*(X2+X3)+D3)
     $     + D1*(X3-X2)**3/3.
      DO 69 J=1,NEPS
   69 B(J) = X(J)/CHORD
      D1 = (2.*B(1)*U(1)+2.*B(2)*U(2)-B(1)*U(2)-B(2)*U(1))/
     $(B(1)**2+B(2)**2-B(1)*B(2))
      BETA(1) = XI(1)*D1/U(1)**2
```

```
      D2 = 3.*(U(1)*B(1)+U(2)*B(2)+U(3)*B(3))-(U(1)+U(2)+U(3))*(B(1)
     $    +B(2)+B(3))
      D3 = 3.*(B(1)**2+B(2)**2+B(3)**2)-(B(1)+B(2)+B(3))**2
      D1 = 2.*D2/D3
      BETA(2) = XI(2)*D1/U(2)**2
      D1 = (2.*B(JTOP+1)*U(JTOP+1)+2.*B(JTOP+2)*U(JTOP+2)-B(JTOP+1)*
     $U(JTOP+2)-B(JTOP+2)*U(JTOP+1))/(B(JTOP+1)**2+B(JTOP+2)**2-
     $B(JTOP+1)*B(JTOP+2))
      BETA(JTOP+1) = XI(JTOP+1)*D1/U(JTOP+1)**2
      JL = JTOP+1
      JM = JTOP+2
      JU = JTOP+3
      D2 = 3.*(U(JL)*B(JL)+U(JM)*B(JM)+U(JU)*B(JU))
     $    -(U(JL)+U(JM)+U(JU))*(B(JL)+B(JM)+B(JU))
      D3 = 3.*(B(JL)**2+B(JM)**2+B(JU)**2)-(B(JL)+B(JM)+B(JU))**2
      D1 = 2.*D2/D3
      BETA(JTOP+2) = XI(JTOP+2)*D1/U(JTOP+2)**2
      JU = NEPS-2
      JL = JTOP-1
      JM = JTOP+3
      DO 73 J=3,JU
      IF (J .GE. JL .AND. J .LT. JM) GO TO 72
      DO 70 JJ=1,9
   70 C(JJ) = 0.
      LL = J-2
      LU = J+2
      HXY = .25*(B(LU)-B(LL))
      X1 = B(LL)
      DO 71 JJJ = LL,LU
      DX = (B(JJJ)-X1)/HXY
      P1 = 1.-.5*DX
      P2 = 1.-2.*DX+.5*DX**2
      C(1) = C(1) + P2**2
      C(2) = C(2) + P1**2
      C(3) = C(3) + 1.
      C(4) = C(4) + P1*P2
      C(5) = C(5) + P2
      C(6) = C(6) + P1
      C(7) = C(7) + U(JJJ)*P2
      C(8) = C(8) + U(JJJ)*P1
   71 C(9) = C(9) + U(JJJ)
      D1 = C(7) - C(5)*C(9)/C(3)
      D2 = C(2) - C(6)**2/C(3)
      D3 = C(4) - C(5)*C(6)/C(3)
      D4 = C(8) - C(6)*C(9)/C(3)
```

```
      D5 = C(1) - C(5)**2/C(3)
      D6 = D5*D2 - D3**2
      C1 = (D1*D2-D3*D4)/D6
      C2 = (D4*D5-D1*D3)/D6
      DX = (C1*((B(J)-X1)/HXY-2.)-.5*C2)/HXY
      BETA(J) = 2.*XI(J)*DX/U(J)**2
   72 IF (J .NE. JL) GO TO 73
      DX = (C1*((B(J)-X1)/HXY-2.)-.5*C2)/HXY
      BETA(J) = 2.*XI(J)*DX/U(J)**2
      DX = (C1*((B(J+1)-X1)/HXY-2.)-.5*C2)/HXY
      BETA(J+1) = 2.*XI(J+1)*DX/U(J+1)**2
   73 CONTINUE
      DX = (C1*((B(NEPS-1)-X1)/HXY-2.)-.5*C2)/HXY
      BETA(NEPS-1) = 2.*XI(NEPS-1)*DX/U(NEPS-1)**2
      DX = (C1*((B(NEPS)-X1)/HXY-2.)-.5*C2)/HXY
      BETA(NEPS) = 2.*XI(NEPS)*DX/U(NEPS)**2
      DO 74 J=1,5
      JJ = JTOP+J
      IF (BETA(J) .GT. 1.) BETA(J) = 1.
      IF (BETA(JJ) .GT. 1.) BETA(JJ) = 1.
   74 CONTINUE
      J = JTOP+1
      JJ = JTOP+2
      IF (BETA(1) .LT. BETA(2)) BETA(1) = 1.+X(1)*(BETA(2)-1.)/X(2)
      IF (BETA(J) .LT. BETA(JJ)) BETA(J) = 1.+X(J)*(BETA(JJ)-1.)/X(JJ)
C
C     CALCULATE BOUNDARY LAYER FLOW
C
      DO 80 J=1,NEPS
      FW(J) = 0.
      CPHI(J) = 0.
   80 RWC(J) = 1.
      DO 81 J=1,JTOP
      IF (XC(J) .GT. XCJET) GO TO 82
   81 JJET = J
   82 NPF = JTOP-JJET+1
      DO 83 J=1,NPF
      JJ = JJET-1+J
      PF(1,J) = X(JJ)/CHORD
      PF(2,J) = U(JJ)
   83 PF(3,J) = BETA(JJ)*U(JJ)**2/(2.*XI(JJ))
      XJET = X(JJET)+(X(JJET+1)-X(JJET))*(XCJET-XC(JJET))/
     $ (XC(JJET+1)-XC(JJET))
      XJET = XJET/CHORD
      EPS = 0.
```

```
      TVC = 0.
      ETAET = 100.
      NPRNT = 0
      LAM = 1
      JMAX = NEPS
      JMIN = JTOP+1
      CALL BLAYER
      LAM = 1
      JMAX = JTOP
      JMIN = 1
      CALL BLAYER
C
CC    CALCULATE WALL JET FLOW
C
      STFT(1) = SLOTT
      STFT(2) = REC
      STFT(3) = PF(2,1)
      STFT(4) = 1.-PF(2,1)**2
      STFT(5) = XI(JJET)
      STFT(6) = UTSIG-UTSIN
      STFT(7) = XJET
      DO 90 J=1,NWJIT
      STFT(6) = STFT(6)+UTSIN
      PRINT 912,J
      CALL WALJET
   90 CONTINUE
  900 FORMAT (1H1)
  901 FORMAT (I6,4E20.8)
  902 FORMAT (I6,3E20.8)
  903 FORMAT (I6,E20.8)
  904 FORMAT (6X,4HCL =,F6.3,6X,7HALPHA =,F6.2,8H DEGREES,6X,7HXSTAG =,
     $E16.8,6X,7HYSTAG =,E16.8)
  905 FORMAT (//7H  POINT,7X,3HPHI,14X,1HX,19X,1HY,19X,1HU,19X,2HCP)
  906 FORMAT (I6,5X,F7.2,4E20.8)
  907 FORMAT (100X,14HPOTENTIAL FLOW)
  908 FORMAT (F6.3,F6.2,E10.3,I3)
  909 FORMAT (F9.6,F6.3,I4,I4,I2,I2)
  911 FORMAT (F7.3,F8.5,F6.3,F7.4,F6.2,I3,I2)
  912 FORMAT (1H1,19H WALL JET ITERATION,I4)
      STOP
      END
```

```
      SUBROUTINE BODY (CHORD,THICK,CAMB,NBPTS,BT,RLE,RTE)
      COMMON/HBDBBO/XX(400),YY(400)
C     KIND AIRFOIL
      C1 = .5*CHORD
      C2 = C1*THICK
      N1 = NBPTS/2
      DTHET = 3.141593/N1
      A = .065
      RTE = C1*THICK**2
      JTE = 0
      XX(1) = C1+A
      XX(N1+1) = -C1+A
      YY(1) = 0.
      YY(N1+1) = 0.
      DO 1 J=2,N1
      JJ = NBPTS+2-J
      G = (J-1)*DTHET
      XX(J) = A+C1*COS(G)
      YY(J) = C2*SIN(G)
      XX(JJ) = XX(J)
      YY(JJ) = -YY(J)
      IF (JTE .EQ. 0 .AND. XX(J) .LT. 6.815) JTE=J-1
    1 CONTINUE
      IF (JTE .LT. 2) GO TO 3
      RTE = .5525
      CHORD = CHORD-.01
      XX(1) = 7.3675
      DTHET = 1.570796/(JTE-1)
      DO 2 J=2,JTE
      JJ = NBPTS+2-J
      G = (J-1)*DTHET
      XX(J) = 6.815+RTE*COS(G)
      YY(J) = RTE*SIN(G)
      XX(JJ) = XX(J)
    2 YY(JJ) = -YY(J)
    3 RLE = C1*THICK**2/12.
      RTE = RTE/12.
      CHORD = CHORD/12.
      DO 4 J=1,NBPTS
      XX(J) = XX(J)/12.
    4 YY(J) = YY(J)/12.
      BT = .25*(CHORD-.5*(RLE+RTE))
      RETURN
      END
```

Should be TE since RTE = .5525 vice .2926

CHORD = 14.625"

CHORD-.01 = 14.615

C1 =

```
      SUBROUTINE SLOPE (XLL,XUL,XA,YPU,YPL)
      X = .5*(XUL-XLL)*XA+.5*(XUL+XLL)
C     KIND AIRFOIL
      X = 12.*X
      IF (X .GE. 6.815) GO TO 1
      XS = X-.065
      SR = ABS(2.13890625-.04*XS**2)
      SR = SR**.5
      YPL = .04*XS/SR
      YPU = -YPL
      RETURN
    1 XS = X-6.815
      SR = ABS(.30525625-XS**2)
      SR = SR**.5
      YPL = XS/SR
      YPU = -YPL
      RETURN
      END
```

empirical input

```
      SUBROUTINE BLAYER
      DIMENSION E(5,241),B(241,4),Y(241),C(81),G(2,241)
      COMMON/BLSLBL/EDV(5,241),NBL,NEDGE
      COMMON/HBDBMB/XI(100),BETA(100),UE(100),FW(100),CPHI(100),RWC(100)
     $,CF(100),XC(100),YC(100),X(100),CHORD,EPS,TVC,REC,NT,AK,HI,ETAET,
     $LAM,NPRNT,JMAX,JMIN,JJET,JSEPP
      COMMON/HBDBEB/A(5,241),D(60),ETA(241)
      COMMON/HBDBMP/U(241,4),F(2,241),H(241)
      COMMON P(4,241)
      DOUBLE PRECISION A,E,P,U,B,Y,ETA,H,C,D,F,G
      PRINT 900
      JCOUNT = 0
      D(1) = EPS
      D(2) = TVC
      D(3) = REC
      D(4) = D(3)**.5
      D(5) = D(3)**.25
      D(40) = 0.
      D(47) = CHORD
      CALL PROFLE
      JU = 1
      JL = 1
      D(8) = 0.
      D(9) = 0.
      D(10) = 0.
      D(11) = 0.
      D(16) = 0.
      D(17) = 1.
      D(39) = 0.
      GO TO 2
    1 JU = JMAX
      JL = JMIN
    2 DO 99 JPT = JL,JU
      JCOUNT = JCOUNT+1
      IF (JCOUNT .NE. 1) GO TO 10
      IF (LAM .EQ. 0) GO TO 4
      N = 241
      LU = N-2
      D(6) = 6.
      D(7) = D(6)/(N-1)
      DO 3 J=1,N
      H(J) = D(7)
    3 ETA(J) = (J-1)*D(7)
      C(1) = 1.
      GO TO 6
```

```
4 N = NT
  LU = N-2
  C(1) = AK
  D(6) = ETAET
  D(7) = H1
  ETA(1) = 0.
  ETA(2) = D(7)
  H(1) = H1
  H(2) = C(1)*H1
  C(2) = C(1)
  DO 5 J=3,N
  C(2) = C(2)*C(1)
  ETA(J) = D(7)*(C(2)-1.)/(C(1)-1.)
5 H(J) = C(1)*H(J-1)
6 C(2) = C(1)**2
  C(3) = C(1)*C(2)
  C(4) = C(1)*C(3)
  C(5) = C(1)*C(4)
  C(6) = C(1)*C(5)
  C(7) = 1.+C(1)
  C(8) = C(7)+C(2)
  C(9) = C(8)+C(3)
  C(10) = 1./(C(7)*C(8)*C(9))
  C(11) = -1./(C(7)*C(8)*C(3))
  C(12) = 1./(C(7)**2*C(5))
  C(13) = -1./(C(7)*C(8)*C(6))
  C(14) = 1./(C(7)*C(8)*C(9)*C(6))
  C(15) = C(10)/C(14)
  C(16) = C(11)/C(14)
  C(17) = C(12)/C(14)
  C(18) = C(13)/C(14)
  C(19) = C(18)*C(9)/C(8)
  C(20) = C(17)*C(9)/C(7)
  C(21) = C(16)*C(9)
  C(22) = C(3)*C(7)*C(8) + C(2)*C(7)*C(9) + C(1)*C(8)*C(9) +
 $     C(7)*C(8)*C(9)
  C(23) = C(18)*C(7)*C(8)*C(9)/C(22)
  C(24) = C(17)*C(1)*C(8)*C(9)/C(22)
  C(25) = C(16)*C(2)*C(7)*C(9)/C(22)
  C(26) = C(15)*C(3)*C(7)*C(8)/C(22)
  C(27) = 6.*(C(7)+C(1)-C(2))
  C(28) = 2.*C(1)*(C(7)-C(7)*C(1)-C(2))
  C(29) = -C(3)*C(7)
  C(30) = 6.*(C(7)+C(1)-C(2)*C(7))
  C(31) = 2.*C(1)*C(7)*(1.-C(1)*C(7)-C(2))
```

```
      C(32) = -C(3)*C(7)**2
      C(33) = 6.*(C(7)+C(1)-C(2)-C(2)*C(7))
      C(34) = 2.*C(1)*
     $ (C(3)*C(7) - C(2)*C(7) - C(2) - C(1)*C(7)**2 - C(1)*C(7) + C(7))
      C(35) = C(3)*C(7)*(C(2) + C(1)*C(7) - C(7) - 1.)
      C(36) = 6.*(C(7) - C(2) - C(2)*C(7))
      C(37) = 2.*C(2)*C(7)*(C(2)-C(7)-1.)
      C(38) = C(4)*C(7)**2
      C(39) = 6.*C(1)*(1.-C(1)-C(1)*C(7))
      C(40) = 2.*C(3)*(C(1)*C(7)-C(7)-1.)
      C(41) = C(5)*C(7)
      C(42) = 6.*(C(8)+C(1)*C(7)+C(2))
      C(43) = 2.*C(1)*(C(7)*C(8)+C(8)*C(1)+C(7)*C(2))
      C(44) = C(3)*C(7)*C(8)
      C(45) = 6.*(C(8)+C(1)*C(7)+C(2)-C(3))
      C(46) = 2.*C(1)*
     $ (C(7)*C(8) + C(8)*C(1) - C(8)*C(2) + C(7)*C(2) - C(7)*C(3)-C(4))
      C(47) = -C(3)*(C(3)*C(7)+C(2)*C(8)+C(1)*C(7)*C(8)-C(7)*C(8))
      C(48) = 6.*(C(8)+C(1)*C(7)-C(3))
      C(49) = 2.*C(1)*(C(7)*C(8)-C(2)*C(8)-C(7)*C(3))
      C(50) = -C(4)*C(7)*C(8)
      C(51) = 6.*(C(8)+ C(2)-C(3))
      C(52) = 2.*C(2)*(C(8)-C(8)*C(1)-C(3))
      C(53) = -C(5)*C(8)
      C(54) = 6.*C(1)*(C(7)+C(1)-C(2))
      C(55) = 2.*C(3)*(C(7)-C(1)*C(7)-C(2))
      C(56) = -C(6)*C(7)
      C(57) = C(10)*(C(7)*C(8)*C(9) + C(8)*C(9) + C(7)*C(9) + C(7)*C(8))
      C(58) = C(11)*C(7)*C(8)*C(9)
      C(59) = C(12)*C(8)*C(9)
      C(60) = C(13)*C(7)*C(9)
      C(61) = C(14)*C(7)*C(8)
      C(62) = -C(10)*C(3)*C(7)*C(8)
      C(63) = C(11)*C(2)*(-C(1)*C(7)*C(8) + C(7)*C(8) + C(8) + C(7))
      C(64) = C(12)*C(2)*C(7)*C(8)
      C(65) = C(13)*C(2)*C(8)
      C(66) = C(14)*C(2)*C(7)
      C(67) = C(3)*C(7)
      C(68) = C(10)*C(2)
      C(69) = C(11)*C(1)*C(7)
      C(70) = C(12)*(C(2)+C(1)*C(7)-C(7)-1.)
      C(71) = -C(13)*C(7)
      C(72) = -C(10)*C(3)*C(7)
      C(73) = -C(11)*C(2)*C(8)
      C(74) = -C(12)*C(1)*C(7)*C(8)
```

```
      C(75) = -C(13)*(C(3)*C(7)+C(2)*C(8)+C(1)*C(7)*C(8)-C(7)*C(8))
      C(76) = C(14)*C(7)*C(8)
      C(77) = C(10)*C(3)*C(7)*C(8)
      C(78) = C(11)*C(2)*C(7)*C(9)
      C(79) = C(12)*C(1)*C(8)*C(9)
      C(80) = C(13)*C(7)*C(8)*C(9)
      C(81) = C(14)*(C(3)*C(7)*C(8) + C(2)*C(7)*C(9) + C(1)*C(8)*C(9) +
     $     C(7)*C(8)*C(9))
      DO 7 J=1,N
      G(1,J) = 0.
    7 G(2,J) = 0.
      IF (LAM .EQ. 0) GO TO 9
      DO 8 J=1,N
      F(1,J) = 0.
    8 F(2,J) = 0.
      GO TO 10
    9 CONTINUE
      CALL PTURB (N)
   10 IF (JU .EQ. 1) GO TO 16
      LU = JPT
      LM = JPT-1
      LL = JPT-2
      IF (JPT .GT. JL .AND. JCOUNT .EQ. 1) GO TO 14
      IF (LL .GE. JL) GO TO 13
      IF (LM .EQ. JL) GO TO 12
      D(8) = 1./XI(JL)
      D(9) = -D(8)
      D(10) = 0.
      GO TO 15
   12 D(8) = 1./(XI(JL+1)-XI(JL))+1./XI(JL+1)
      D(9) = -XI(JL+1)/XI(JL)/(XI(JL+1)-XI(JL))
      D(10) = (XI(JL+1)-XI(JL))/XI(JL)/XI(JL+1)
      GO TO 15
   13 D(8) = 1./(XI(LU)-XI(LM))+1./(XI(LU)-XI(LL))
      D(9) = -(XI(LU)-XI(LL))/(XI(LU)-XI(LM))/(XI(LM)-XI(LL))
      D(10) = (XI(LU)-XI(LM))/(XI(LM)-XI(LL))/(XI(LU)-XI(LL))
      GO TO 15
   14 D(8) = 1./(XI(LU)-XI(LM))
      D(9) = -D(8)
      D(10) = 0.
   15 D(11) = XI(JPT)
      D(12) = (2.*D(11))**.5
      D(13) = UE(JPT)
      D(14) = CPHI(JPT)
      D(15) = RWC(JPT)
```

```
      D(16) = 2.*D(1)*D(2)*D(12)*D(14)/D(15)**2/D(13)/D(4)
      D(17) = BETA(JPT)
      D(39) = D(15)
      IF (D(1) .LT. .5) D(39) = 1.
      D(39) = -D(12)/D(4)/D(13)/D(39)
      LU = N-2
   16 DO 40 JIT = 1,20
      TOL = .0001
      IF (JIT .GE. 10) TOL = .001
      IF (LAM .EQ. 0 .AND. JCOUNT .EQ. 1) TOL = .015
      JPR = JIT
      DO 17 J=1,N
      E(1,J) = 1. + D(16)*ETA(J)
      E(2,J) = D(16) + P(1,J) + ETA(J)
      E(3,J) = -D(17)*(P(2,J)+2.) - 2.*D(11)*D(8)*(P(2,J)+1.)
      E(4,J) = 2.*D(11)*P(3,J)*D(8)
   17 E(5,J) = -(E(3,J)*P(2,J)+E(4,J)*P(1,J)) + 2.*D(11)*((P(2,J)+1.)*
     $(D(9)*F(2,J)+D(10)*G(2,J))-P(3,J)*(D(9)*F(1,J)+D(10)*G(1,J)))
      IF (LAM .EQ. 1) GO TO 22
      DO 18 J=1,N
      A(1,J) = P(1,J)
      A(4,J) = P(2,J)
      A(2,J) = P(3,J)
   18 A(3,J) = P(4,J)
      CALL EDDIE (N)
      DO 19 J=1,N
      EDV(5,J) = 1.+A(1,J)
      E(1,J) = E(1,J)*(1.+A(1,J))
   19 E(2,J) = E(2,J)+D(16)*A(1,J)+A(2,J)*(1.+D(16)*ETA(J))
   22 DO 23 J=1,N
      E(5,J) = E(5,J)-(E(1,J)*P(4,J)+E(2,J)*P(3,J))
      E(2,J) = E(2,J)/E(1,J)
      E(3,J) = E(3,J)/E(1,J)
      E(4,J) = E(4,J)/E(1,J)
   23 E(5,J) = E(5,J)/E(1,J)
      A(1,2) = C(19)
      A(2,2) = C(20)
      A(3,2) = C(21)
      A(1,N) = C(23)
      A(2,N) = C(24)
      A(3,N) = C(25)
      A(4,N) = C(26)
      D(18) = E(2,N-1)*H(N-4)
      D(19) = E(3,N-1)*H(N-4)**2
      D(20) = C(42)+D(18)*C(43)+D(19)*C(44)
```

```
      A(1,N-1) = C(18)*(C(45)+D(18)*C(46)+D(19)*C(47))/D(20)
     $        +E(4,N-1)*H(N-4)**3/C(14)/D(20)
      A(2,N-1) = C(17)*(C(48)+D(18)*C(49)+D(19)*C(50))/D(20)
      A(3,N-1) = C(16)*(C(51)+D(18)*C(52)+D(19)*C(53))/D(20)
      A(4,N-1) = C(15)*(C(54)+D(18)*C(55)+D(19)*C(56))/D(20)
      A(5,N-1) = E(5,N-1)*H(N-4)**3/C(14)/D(20)
      DO 24 J=3,LU
      D(18) = E(2,J)*H(J-2)
      D(19) = E(3,J)*H(J-2)**2
      D(20) = C(27)+D(18)*C(28)+D(19)*C(29)
      D(21) = H(J-2)**3
      A(1,J) = C(18)*(C(30)+D(18)*C(31)+D(19)*C(32))/D(20)
      A(2,J) = C(17)*(C(33)+D(18)*C(34)+D(19)*C(35))/D(20)
     $        +E(4,J)*D(21)/C(14)/D(20)
      A(3,J) = C(16)*(C(36)+D(18)*C(37)+D(19)*C(38))/D(20)
      A(4,J) = C(15)*(C(39)+D(18)*C(40)+D(19)*C(41))/D(20)
   24 A(5,J) = E(5,J)*D(21)/C(14)/D(20)
      U(2,1) = A(3,2)
      U(2,2) = A(2,2)
      U(2,3) = A(1,2)
      U(2,4) = 1.
      B(3,1) = A(3,3)/U(2,1)
      U(3,1) = A(2,3)-B(3,1)*U(2,2)
      U(3,2) = A(1,3)-B(3,1)*U(2,3)
      U(3,3) = 1.-B(3,1)
      B(4,2) = A(4,4)/U(2,1)
      B(4,1) = (A(3,4)-B(4,2)*U(2,2))/U(3,1)
      U(4,1) = A(2,4)-B(4,2)*U(2,3)-B(4,1)*U(3,2)
      U(4,2) = A(1,4)-B(4,2)-B(4,1)*U(3,3)
      U(4,3) = 1.
      DO 25 J=5,LU
      B(J,2) = A(4,J)/U(J-2,1)
      B(J,1) = (A(3,J)-B(J,2)*U(J-2,2))/U(J-1,1)
      U(J,1) = A(2,J)-B(J,2)*U(J-2,3)-B(J,1)*U(J-1,2)
      U(J,2) = A(1,J)-B(J,1)
   25 U(J,3) = 1.
      B(N-1,3) = A(4,N-1)/U(N-4,1)
      B(N-1,2) = (A(3,N-1)-B(N-1,3)*U(N-4,2))/U(N-3,1)
      B(N-1,1) = (A(2,N-1)-B(N-1,3)-B(N-1,2)*U(N-3,2))/U(N-2,1)
      U(N-1,1) = A(1,N-1)-B(N-1,2)-B(N-1,1)*U(N-2,2)
      U(N-1,2) = 1.-B(N-1,1)
      B(N,4) = A(4,N)/U(N-4,1)
      B(N,3) = (A(3,N)-B(N,4)*U(N-4,2))/U(N-3,1)
      B(N,2) = (A(2,N)-B(N,4)-B(N,3)*U(N-3,2))/U(N-2,1)
      B(N,1) = (A(1,N)-B(N,3)-B(N,2)*U(N-2,2))/U(N-1,1)
```

```
      U(N,1) = 1.-B(N,2)-B(N,1)*U(N-1,2)
      Y(2) = 0.
      Y(3) = A(5,3)
      DO 26 J=4,LU
   26 Y(J) = A(5,J) - B(J,2)*Y(J-2) - B(J,1)*Y(J-1)
      Y(N-1) = A(5,N-1)-B(N-1,3)*Y(N-4)-B(N-1,2)*Y(N-3)-B(N-1,1)*Y(N-2)
      Y(N) = -B(N,4)*Y(N-4)-B(N,3)*Y(N-3)-B(N,2)*Y(N-2)-B(N,1)*Y(N-1)
      A(1,N) = Y(N)/U(N,1)
      A(1,N-1) = (Y(N-1)-U(N-1,2)*A(1,N))/U(N-1,1)
      DO 27 J=4,LU
      I = LU+4-J
   27 A(1,I) = (Y(I)-A(1,I+2)-U(I,2)*A(1,I+1))/U(I,1)
      A(1,3) = (Y(3)-U(3,3)*A(1,5)-U(3,2)*A(1,4))/U(3,1)
      A(1,2) = (Y(2)-A(1,5)-U(2,3)*A(1,4)-U(2,2)*A(1,3))/U(2,1)
      A(1,1) = 0.
      DO 28 J=2,3
      K = J-1
      A(J,1) = -(C(57)*A(K,1)+C(58)*A(K,2)+C(59)*A(K,3)+C(60)*A(K,4)
     $   +C(61)*A(K,5))/H(1)
      A(J,2) = (C(62)*A(K,1)+C(63)*A(K,2)+C(64)*A(K,3)+C(65)*A(K,4)
     $   +C(66)*A(K,5))/H(1)
      A(J,N-1) = C(3)*(C(72)*A(K,N-4)+C(73)*A(K,N-3)+C(74)*A(K,N-2)
     $   +C(75)*A(K,N-1)+C(76)*A(K,N))/H(N-4)
      A(J,N) = C(3)*(C(77)*A(K,N-4)+C(78)*A(K,N-3)+C(79)*A(K,N-2)
     $   +C(80)*A(K,N-1)+C(81)*A(K,N))/H(N-4)
      DO 28 JJ=3,LU
   28 A(J,JJ) = C(67)*(C(68)*A(K,JJ-2)+C(69)*A(K,JJ-1)+C(70)*A(K,JJ)
     $   +C(71)*A(K,JJ+1)-C(14)*A(K,JJ+2))/H(JJ-2)
      DO 29 J=1,N
   29 A(4,J) = E(5,J)-E(2,J)*A(3,J)-E(3,J)*A(2,J)-E(4,J)*A(1,J)
      IF (LAM .EQ. 1) GO TO 31
      IF (JIT .GT. 1) GO TO 31
      DO 30 J=1,N
      A(1,J) = .5*A(1,J)
      A(2,J) = .5*A(2,J)
      A(3,J) = .5*A(3,J)
   30 A(4,J) = .5*A(4,J)
   31 IF (JU .EQ. 1) GO TO 32
      D(22) = FW(JPT)
      P(1,1) = D(22)
   32 DO 33 J=1,N
      P(1,J) = P(1,J)+A(1,J)
      P(2,J) = P(2,J)+A(2,J)
      P(3,J) = P(3,J)+A(3,J)
   33 P(4,J) = P(4,J)+A(4,J)
```

```
      IF (P(3,1) .LE. 0.) JSEPP=JPT
      IF (P(3,1) .LE. 0.) PRINT 906,JPT
      IF (P(3,1) .LE. 0.) GO TO 104
      DO 34 J=2,N
      IF (P(2,J) .GT. 0.) GO TO 35
      IF (P(2,J-1) .GT. P(2,J)) GO TO 35
   34 JSAVE = J
      GO TO 37
   35 JLOW = JSAVE+1
      DO 36 J=JLOW,N
      P(1,J) = P(1,JSAVE)
      P(2,J) = 0.
      P(3,J) = 0.
   36 P(4,J) = 0.
   37 CONTINUE
      D(23) = (2.*A(3,1))/(2.*P(3,1)-A(3,1))
      DFW = D(23)
      DFW = ABS(DFW)
      JPRNT = JIT
      DDS = 0.
      IF (LAM .EQ. 1) GO TO 21
      IF (D(2) .GT. .5) GO TO 38
      D(24) = D(39)*(P(1,N)-P(1,1))
      GO TO 20
   38 D(24) = 0.
      DO 39 J=2,N
   39 D(24) = D(24) + .5*D(39)*H(J-1)*(P(2,J)+P(2,J-1))/
     $(1.+.5*D(16)*(ETA(J)+ETA(J-1)))
   20 D(40) = (D(24)-D(40))/D(24)
      DDS = D(40)
      DDS = ABS(DDS)
      D(40) = D(24)
   21 IF (DFW .LT. TOL .AND. DDS .LT. TOL) GO TO 41
   40 CONTINUE
   41 IF (JU .EQ. 1) GO TO 48
      D(24) = 1.
      IF (D(1) .GT. .5) D(24) = RWC(JPT)
      D(24) = 2.*D(24)*P(3,1)/D(4)/D(12)
      CF(JPT) = D(24)
      DO 42 J=1,N
      JM = J
      IF (P(2,J) .GT. -.005) GO TO 43
   42 CONTINUE
   43 IF (D(1) .GT. .5) GO TO 44
      D(41) = -D(39)*ETA(JM)
```

```
      D(42) = D(39)*(P(1,JM)-P(1,1))
      GO TO 46
   44 D(41) = 0.
      D(42) = 0.
      DO 45 J=2,JM
      D(43) = (ETA(J)-ETA(J-1))/(1.+.5*D(16)*(ETA(J)+ETA(J-1)))**.5
      D(41) = D(41)+D(43)
   45 D(42) = D(42) + .5*(P(2,J)+P(2,J-1))*D(43)
      D(41) = -D(39)*D(41)
      D(42) = D(39)*D(42)
   46 D(43) = 0.
      DO 47 J=2,JM
   47 D(43) = D(43) + .5*(ETA(J)-ETA(J-1))*(P(2,J)+P(2,J-1))*(1.+.5*
     $  (P(2,J)+P(2,J-1)))/(1.+.5*D(16)*(ETA(J)+ETA(J-1)))**.5
      D(43) = D(39)*D(43)
      D(44) = D(42)/D(43)
      D(45) = D(3)*D(13)*D(42)
      D(46) = D(3)*D(13)*D(43)
      IF (NPRNT .EQ. 1) PRINT 900
      PRINT 901,JPT,X(JPT),XI(JPT),BETA(JPT),UE(JPT),XC(JPT),YC(JPT)
      P1 = 12.*D(41)*D(47)
      P2 = 12.*D(42)*D(47)
      P3 = 12.*D(43)*D(47)
      P4 = CF(JPT)
      P5 = D(44)
      PRINT 902,P1,P2,P3,P4,P5
      P1 = D(3)
      P2 = D(45)
      P3 = D(46)
      PRINT 903,JPR,DFW,DDS,P1,P2,P3
      P1 = P(3,1)
      IF (NPRNT .EQ. 0) PRINT 909,JM,P1
      GO TO 50
   48 PRINT 904,JPR,DFW
      DO 49 J=1,N
      F(1,J) = P(1,J)
   49 F(2,J) = P(2,J)
   50 IF (NPRNT .EQ. 0) GO TO 52
      PRINT 905
      DO 51 J=1,N,10
      P1 = ETA(J)
      P2 = P(1,J) + ETA(J)
      P3 = P(2,J) + 1.
      P4 = P(3,J)
      P5 = P(4,J)
```

```
 51 PRINT 908,P1,P2,P3,P4,P5
 52 IF (JU .EQ. 1) GO TO 99
    IF (JPT .EQ. JJET) GO TO 101                                        JET
    DO 53 J=1,N
    G(1,J) = F(1,J)
    G(2,J) = F(2,J)
    F(1,J) = P(1,J)
 53 F(2,J) = P(2,J)
 54 IF (LAM .EQ. 1) GO TO 55
    GO TO 99
 55 IF (P(3,1) .GT. .2) GO TO 60
    IF (D(46) .LT. 125.) GO TO 99
    IF (JPT .EQ. JU) GO TO 99
    D(48) = -.001371*D(46)+.0817
    D(49) = D(47)*(UE(JPT+1)-UE(JPT))/(X(JPT+1)-X(JPT))
    D(49) = D(3)*D(43)**2*D(49)
    IF (D(49) .LT. D(48)) GO TO 60
    LAM = 0
    JCOUNT = 0
    PRINT 911
    GO TO 99
 60 D(48) = 640.
    IF (BETA(JPT) .LT. 0.) D(48) = 320.
    IF (D(46) .LT. D(48)) GO TO 99
    LAM = 0
    JCOUNT = 0
    PRINT 907,JPT
 99 CONTINUE
    IF (JU .EQ. 1) GO TO 1
100 CONTINUE
    GO TO 104
101 DO 102 J=1,N
    EDV(1,J) = ETA(J)
    EDV(2,J) = P(1,J)+ETA(J)
    EDV(3,J) = P(2,J)+1.
102 EDV(4,J) = P(3,J)
    NBL = NT
    NEDGE = JM
104 CONTINUE
900 FORMAT (1H1)
901 FORMAT (//,6H POINT,I3,1X,3HX =,E15.8,2X,4HXI =,E14.7,2X,6HBETA =,
   $E12.5,2X,4HUE =,E14.7,2X,4HXC =,E14.7,2X,4HYC =,E14.7)
902 FORMAT (10X,7HDELTA =,F8.4,3H IN,2X,7HDELST =,F8.4,3H IN,2X,
   $7HTHETA =,F8.4,3H IN,2X,4HCF =,E14.7,2X,3HH =,E14.7)
903 FORMAT (10X,9HITERATION,I3,8X,5HDFW =,E13.6,2X,5HDDS =,E13.6,2X,
```

```
     $5HREC =,E13.6,2X,6HREDS =,E12.5,2X,5HRET =,E13.6)
  904 FORMAT (18H STAGNATION POINT:,5X,9HITERATION,I3,5X,5HDFW =,E13.6)
  905 FORMAT(/,11X,3HETA,19X,1HF,19X,2HF',17X,3HF'',17X,4HF''')
  906 FORMAT (/,35H BOUNDARY LAYER SEPARATION AT POINT,I6)
  907 FORMAT (/,20H TRANSITION AT POINT,I6)
  908 FORMAT (5E20.7)
  909 FORMAT (10X,7HNEDGE =,I4,9X,6HFW'' =,E12.5)
  911 FORMAT(/54H 'SHORT BUBBLE' LAMINAR SEPARATION: TRANSITION ASSUMED)
  912 FORMAT (5E15.7)
      RETURN
      END
```

```
      SUBROUTINE PROFLE
      COMMON P(4,241)
      DOUBLE PRECISION P,ETAE,ETAD,ETA,ET,C1,C2,C3,C4,C5,C6,H
      N = 241
      ETAE = 6.
      ETAD = 3.
      C1 = 4./ETAD
      C2 = 12./ETAD**2
      C6 = -.2*ETAD
      H = ETAE/(N-1)
      DO 2 J=1,N
      ETA = (J-1)*H
      IF (ETA .GT. ETAD) GO TO 1
      ET = ETA/ETAD
      C3 = ET**2
      C4 = ET**3
      C5 = ET**4
      P(1,J) = ETA*(-.2*C5+C4-2.*C3+2.*ET-1.)
      P(2,J) = -C5+4.*C4-6.*C3+4.*ET-1.
      P(3,J) = C1*(-C4+3.*C3-3.*ET+1.)
      P(4,J) = C2*(-C3+2.*ET-1.)
      GO TO 2
    1 P(1,J) = C6
      P(2,J) = 0.
      P(3,J) = 0.
      P(4,J) = 0.
    2 CONTINUE
      RETURN
      END
```

```
      SUBROUTINE PTURB (N)
      DIMENSION D(7)
      COMMON P(4,241)
      COMMON/HBDBMP/U(241,4),F(2,241),H(241)
      DOUBLE PRECISION P,U,F,H,D
      JL = 1
      D(1) = 6.
      D(2) = 6./240.
      D(3) = 0.
      DO 3 J=2,N
      D(3) = D(3) + H(J-1)
      JS = J
      D(7) = P(1,J-1)
      IF (D(3) .GT. 6.) GO TO 4
      DO 1 JJ=JL,N
      JM = JJ
      D(4) = (JJ-1)*D(2)
      D(5) = JJ*D(2)
      IF (D(3) .GE. D(4) .AND. D(3) .LT. D(5)) GO TO 2
    1 CONTINUE
    2 D(6) = (D(3)-D(4))/(D(5)-D(4))
      JL = JM
      IF (JL .GE. 241) GO TO 4
      U(J,1) = P(1,JL)+D(6)*(P(1,JL+1)-P(1,JL))
      U(J,2) = P(2,JL)+D(6)*(P(2,JL+1)-P(2,JL))
      U(J,3) = P(3,JL)+D(6)*(P(3,JL+1)-P(3,JL))
      U(J,4) = P(4,JL)+D(6)*(P(4,JL+1)-P(4,JL))
    3 CONTINUE
    4 DO 5 J=JS,N
      U(J,1) = D(7)
      U(J,2) = 0.
      U(J,3) = 0.
    5 U(J,4) = 0.
      F(1,1) = P(1,1)
      F(2,1) = P(2,1)
      DO 6 J=2,N
      P(1,J) = U(J,1)
      P(2,J) = U(J,2)
      P(3,J) = U(J,3)
      P(4,J) = U(J,4)
      F(1,J) = P(1,J)
    6 F(2,J) = P(2,J)
      RETURN
      END
```

```
      SUBROUTINE EDDIE (N)
      COMMON/HBDBEB/A(5,241),D(60),ETA(241)
      DOUBLE PRECISION A,D,ETA
C     2D OR AS WITHOUT TVC
      D(31) = D(15)
      IF (D(1) .LT. .5) D(31) = 1.
      D(25) = .16*D(4)*D(12)/D(31)
      D(26) = -D(5)*(D(12)/D(31))**.5/26.
      D(27) = .0168*D(4)*D(12)/D(31)
      D(28) = A(2,1)
      D(29) = A(1,1)
      DO 1 J=1,N
      D(30) = A(1,J)
      IF (A(4,J) .GT. -.005) GO TO 2
    1 JSAVE = J
    2 JSAVE = JSAVE+1
      DO 3 J=1,N
      D(31) = A(2,J)
      IF (D(31) .LT. 0.) D(31) = -D(31)
    3 A(1,J) = D(31)
      D(30) = (D(29)-D(30))*D(27)
      D(31) = ETA(JSAVE)
      DO 4 J=1,N
      D(32) = D(28)-D(17)*ETA(J)
      IF (D(32) .LT. 0.) D(32) = -D(32)
      D(32) = D(32)**.5
      D(33) = DEXP(D(26)*ETA(J)*D(32))
      A(4,J) = D(25)*ETA(J)**2*A(1,J)*(1.-D(33))**2
      D(34) = 2.*A(2,J)+ETA(J)*A(3,J)
      IF (A(2,J) .LT. 0.) D(34) = -D(34)
      A(5,J) = D(25)*ETA(J)*(1.-D(33))*(D(34)*(1.-D(33))-2.*ETA(J)*
     $A(1,J)*D(26)*D(32)*D(33)*(1.-.5*D(17)*ETA(J)/D(32)**2))
      D(35) = D(30)/(1.+5.5*(ETA(J)/D(31))**6)
      IF (A(4,J) .GT. D(35)) GO TO 5
    4 JSAVE = J+1
      PRINT 10
    5 D(36) = -33./D(31)
      DO 6 J=JSAVE,N
      D(37) = ETA(J)/D(31)
      D(38) = 1.+5.5*D(37)**6
      A(4,J) = D(30)/D(38)
    6 A(5,J) = D(36)*D(37)**5*A(4,J)/D(38)
      A(1,1) = 0.
      A(2,1) = 0.
      A(1,2) = (A(4,2)+A(4,3))/3.
```

```
      A(2,2) = (A(5,2)+A(5,3))/3.
      LU = N-2
      DO 7 J=3,LU
      A(1,J) = .2*(A(4,J-2)+A(4,J-1)+A(4,J)+A(4,J+1)+A(4,J+2))
    7 A(2,J) = .2*(A(5,J-2)+A(5,J-1)+A(5,J)+A(5,J+1)+A(5,J+2))
      A(1,N-1) = A(1,N-2)
      A(1,N) = A(1,N-2)
      A(2,N-1) = A(2,N-2)
      A(2,N) = A(2,N-2)
   10 FORMAT (19H EDDIE'S IN TROUBLE)
      RETURN
      END
```

```
      SUBROUTINE WALJET
      DIMENSION CPWJ(50),CFWJ(50),UEWJ(50),XWJ(50),DELTA(50)
      DIMENSION ET(121),E(4,4,120),Z(4,121),DG(4,121)
      DIMENSION A(4,4),B(4,4),C(4,4),D(4,4),Q(4)
      COMMON/MAINWJ/PF(3,25),NPF,STEPS
      COMMON/JETMIX/HS(121),F(6,121),S(18)
      COMMON/HBDBJE/ETA(121),EPS(2,121),G(4,121),GG(7,121)
C     INPUT HERE
      CALL SLOTBL
      JU = 121
      S(6) = S(7)
      S(8) = STEPS*S(1)
      ET(1) = 0.
      ETA(1) = 0.
      UEP = S(4)
      NT = JU-1
      LU = JU
      LT = NT
      MXMN = 0
      NMAX = 50
C     INPUT INITIAL F,G,H,CP AND ETA GRID
      DO 1 J=1,JU
      G(1,J) = F(1,J)
      G(2,J) = F(2,J)
      G(3,J) = F(3,J)
      G(4,J) = F(4,J)
    1 EPS(1,J) = F(5,J)
      DO 2 J=2,JU
      ETA(J) = ETA(J-1)+HS(J)
    2 ET(J) = .5*(ETA(J)+ETA(J-1))
      REC = S(2)
      CS = S(1)
      CA = CS**2*REC
      CB = .5*CS*REC
      CPWJ(1) = G(4,1)
      UEWJ(1) = S(4)
      XSLOT = S(6)
      XWJ(1) = S(7)
      DX = S(8)
      DXM = .5*DX
      CFWJ(1) = 2.*S(4)*G(3,1)/(CS*REC)
      DELTA(1) = S(5)
      X = XWJ(1)-XSLOT
      CALL RADIUS (X,RC)
      GE = CS/RC
```

```
      DO 3 J=1,JU
    3 GG(3,J) = GE/(1.+GE*ET(J))
      C1 = DELTA(1)/CS
      JMAX = 1
      JMIN = 1
      DO 4 J=2,NT
      IF (G(2,J) .LT. G(2,J-1) .AND. JMAX .EQ. 1) JMAX=J-1
      IF (G(2,J) .LE. G(2,J-1) .AND. G(2,J) .LE. G(2,J+1)) JMIN=J
      IF (ETA(J) .GT. C1) GO TO 5
    4 JDEL = J
    5 IF (JMAX .EQ. 1) JMAX=JDEL
      IF (JMAX .GT. JDEL) JMAX=JDEL
      DO 6 J=1,4
      B(3,J) = 0.
      B(4,J) = 0.
      C(1,J) = 0.
    6 C(2,J) = 0.
      NL = 1
      NU = NPF-1
      N1 = 1
C     BEGIN SOLUTION FOR POINT N
      DO 75 N=2,NMAX
C     PICK X FOR STATION N
      UEPS = UEP
      JGOB = 0
      IF (N .LE. 3) JGOB=1
      DXT = DX
      IF (N .EQ. 2) DXT=CS/3.
      IF (N .EQ. 3) DXT=CS
      X = XWJ(N-1)+DXT
      DO 7 J=NL,NU
      IF (PF(1,J) .LE. X .AND. PF(1,J+1) .GE. X) GO TO 8
    7 N1 = J
    8 IF (N1 .GE. NU) N1=NU-1
      N2 = N1+1
      N3 = N2+1
      C4 = PF(1,N2)-PF(1,N1)
      C5 = PF(1,N3)-PF(1,N1)
      C6 = PF(1,N3)-PF(1,N2)
    9 C7 = X-PF(1,N1)
      C8 = X-PF(1,N2)
      C9 = X-PF(1,N3)
      C1 = C8*C9/C4/C5
      C2 = -C7*C9/C4/C6
      C3 = C7*C8/C5/C6
```

```
      UEP = C1*PF(2,N1)+C2*PF(2,N2)+C3*PF(2,N3)
      DUEP = C1*PF(3,N1)+C2*PF(3,N2)+C3*PF(3,N3)
      JGOB = JGOB+1
      IF (JGOB .EQ. 2) GO TO 10
      DELU = ABS(UEP-UEPS)
      IF (DELU .LT. .1) GO TO 10
      DXT = .1*DX/DELU
      IF (DXT .LT. DXM) DXT=DXM
      X = XWJ(N-1)+DXT
      GO TO 9
   10 XWJ(N) = X
      C0 = 3.
      C1 = PF(1,N1)+PF(1,N2)+PF(1,N3)
      C2 = PF(1,N1)**2+PF(1,N2)**2+PF(1,N3)**2
      C3 = PF(3,N1)+PF(3,N2)+PF(3,N3)
      C4 = PF(1,N1)*PF(3,N1)+PF(1,N2)*PF(3,N2)+PF(1,N3)*PF(3,N3)
      DDUEP = (C0*C4-C1*C3)/(C0*C2-C1**2)
      X = X-XSLOT
      CALL RADIUS (X,RC)
      GE = CS/RC
      DO 11 J=1,JU
      GG(1,J) = 1.+GE*ETA(J)
      GG(5,J) = GG(3,J)
      GG(2,J) = GE/(1.+GE*ETA(J))
      GG(3,J) = GE/(1.+GE*ET(J))
      GG(4,J) = 2.*GG(1,J)**2/CA/(1.+GE*ET(J))
   11 CONTINUE
C     STORE N-1 QUANTITIES
      DO 12 J=2,JU
      C1 = .5*(G(1,J)+G(1,J-1))
      C2 = .5*(G(2,J)+G(2,J-1))
      C3 = .5*(G(3,J)+G(3,J-1))
      C4 = .5*(G(4,J)+G(4,J-1))
      F(1,J) = UEWJ(N-1)*C1
      F(2,J) = C2
      F(3,J) = C3+GG(5,J)*C2
      F(4,J) = C4
   12 CONTINUE
C     ADJUST N-1 PROFILE FOR INITIAL GUESS AT N
      ETGE = 1.2*ETA(JDEL)
      IF (ETGE .GT. ETA(JU)) ETGE=ETA(JU)
      DO 13 J=JDEL,JU
      LU = J
      IF (ETA(J) .GE. ETGE) GO TO 14
   13 CONTINUE
```

```
   14 LT = LU-1
      DELTA(N) = DELTA(N-1)
      E7 = ETGE
      IF (JMIN .GT. 1) E7=1.1*ETA(JMIN)
      C1 = 1.+GE*E7
      USDU = DUEP/UEP
      C2 = -.5*RC**2*DDUEP*ALOG(C1)**2
      UWJS = (UEP+C2)/C1
      IF (MXMN .GT. 0) GO TO 15
      UEWJ(N) = UEP
      CPE = 1.-UEP**2
      GO TO 18
   15 UEWJ(N) = UWJS
      C1 = UEWJ(N)*G(1,LU)
      DO 16 J=JMAX,JU
      IF (F(5,J) .GT. C1) GO TO 17
   16 JM = J
   17 CPE = F(6,JM)-UEWJ(N)**2-(RC*DUEP*ALOG(GG(1,LU))/GG(1,LU))**2
   18 C1 = CPE-G(4,LU)
      DO 19 J=1,LU
   19 G(4,J) = G(4,J)+C1
      JM = LU+1
      IF (JM .GT. JU) JM=JU
      DO 20 J=JM,JU
      G(1,J) = G(1,J-1)+HS(J)*G(2,J-1)
      G(2,J) = 1.
      G(3,J) = 0.
   20 G(4,J) = CPE
C     BEGIN ITERATION
      DO 61 IT=1,10
      L = N
      IF (N .EQ. 2 .AND. IT .EQ. 1) L=1
      E4 = (G(4,1)-CPWJ(N-1))/DXT
      CALL EDDY (CS,REC,UEWJ(N),E4,X,RC,E7,JMAX,JMIN,JDEL,LU,L,IT)
      CO = MXMN
      DO 40 J=2,LU
      C1 = .5*(G(1,J)+G(1,J-1))
      C2 = .5*(G(2,J)+G(2,J-1))
      C3 = .5*(G(3,J)+G(3,J-1))
      C4 = .5*(G(4,J)+G(4,J-1))
      C5 = C3+GG(3,J)*C2
      C6 = UEWJ(N)*C1-F(1,J)
      C7 = UEWJ(N)**2*C2
      C9 = HS(J)/DXT
      C10 = F(4,J)+(UEWJ(N-1)*F(2,J))**2-C4-(UEWJ(N)*C2)**2
```

```
      C12 = 2.*HS(J)*GG(3,J)*UEWJ(N)**2*C2
      C12 = C12*(1.-.5*CS*RC*ETGE*USDU**2)
      IF (ETA(J) .GT. 1.2*E7) C12=0.
      S(1) = -.5*UEWJ(N)*C9*(UEWJ(N)*C5+UEWJ(N-1)*F(3,J))
      S(2) = C9*(C7-.5*UEWJ(N)*GG(3,J)*C6)+UEWJ(N)*EPS(2,J)*GG(2,J)
     $ -UEWJ(N)*EPS(2,J)*GG(6,J)
      S(3) = -UEWJ(N)*(.5*C9*C6+EPS(2,J))
      S(4) = .5*C9
      S(5) = -C12
      S(6) = C9*(C7-.5*UEWJ(N)*GG(3,J)*C6)-UEWJ(N)*EPS(2,J-1)*GG(2,J-1)
     $ +UEWJ(N)*EPS(2,J-1)*GG(6,J-1)
      S(7) = UEWJ(N)*(-.5*C9*C6+EPS(2,J-1))
      S(8) = -G(4,J)+G(4,J-1)+C12*C2
      S(9) = C9*(C10+C6*(UEWJ(N)*C5+UEWJ(N-1)*F(3,J)))+UEWJ(N)*
     $(EPS(2,J)*(G(3,J)-GG(2,J)*G(2,J)+GG(6,J)*(G(2,J)-1.))
     $-EPS(2,J-1)*(G(3,J-1)-GG(2,J-1)*G(2,J-1)+GG(6,J-1)*(G(2,J-1)-1.)))
      IF (J .EQ. 2) GO TO 25
      S(10) = -G(1,J-1)+G(1,J-2)+.5*HS(J-1)*(G(2,J-1)+G(2,J-2))
      S(11) = -G(2,J-1)+G(2,J-2)+.5*HS(J-1)*(G(3,J-1)+G(3,J-2))
   25 CONTINUE
      C11 = .5*HS(J-1)
      IF (J .GT. 2) GO TO 31
      DO 26 K=1,4
      A(1,K) = 0.
      A(2,K) = 0.
   26 A(4,K) = 0.
      A(1,1) = 1.
      A(2,2) = 1.
      A(4,4) = -1.
      A(3,1) = S(1)
      A(3,2) = S(6)
      A(3,3) = S(7)
      A(3,4) = S(4)
      A(4,2) = S(5)
      DO 27 K=1,4
      C(3,K) = A(3,K)
   27 C(4,K) = A(4,K)
      C(3,2) = S(2)
      C(3,3) = S(3)
      C(4,4) = 1.
      Q(1) = 0.
      Q(2) = 0.
      Q(3) = S(9)
      Q(4) = S(8)
      DO 28 K=1,4
```

```
      DO 28 KK=1,4
   28 D(K,KK) = A(K,KK)
      CALL INVERT (D)
      DO 29 K=1,4
      DO 29 KK=1,4
   29 E(K,KK,1) = D(K,1)*C(1,KK)+D(K,2)*C(2,KK)+D(K,3)*C(3,KK)
     $  +D(K,4)*C(4,KK)
      DO 30 K=1,4
   30 Z(K,1) = D(K,1)*Q(1)+D(K,2)*Q(2)+D(K,3)*Q(3)+D(K,4)*Q(4)
      GO TO 40
   31 DO 32 K=1,4
      A(1,K) = 0.
      A(2,K) = 0.
      A(4,K) = 0.
      B(1,K) = 0.
   32 B(2,K) = 0.
      A(1,1) = 1.
      A(1,2) = -C11
      A(2,2) = 1.
      A(2,3) = -C11
      A(3,1) = S(1)
      A(3,2) = S(6)
      A(3,3) = S(7)
      A(3,4) = S(4)
      A(4,2) = S(5)
      A(4,4) = -1.
      B(1,1) = -1.
      B(1,2) = -C11
      B(2,2) = -1.
      B(2,3) = -C11
      DO 33 K=1,4
      C(3,K) = A(3,K)
   33 C(4,K) = A(4,K)
      C(3,2) = S(2)
      C(3,3) = S(3)
      C(4,4) = 1.
      Q(1) = S(10)
      Q(2) = S(11)
      Q(3) = S(9)
      Q(4) = S(8)
      DO 34 K=1,4
      DO 34 KK=1,4
   34 D(K,KK) = A(K,KK)-B(K,1)*E(1,KK,J-2)-B(K,2)*E(2,KK,J-2)
     $  -B(K,3)*E(3,KK,J-2)-B(K,4)*E(4,KK,J-2)
      CALL INVERT (D)
```

```
      DO 35 K=1,4
      DO 35 KK=1,4
   35 E(K,KK,J-1) = D(K,1)*C(1,KK)+D(K,2)*C(2,KK)+D(K,3)*C(3,KK)
     $  +D(K,4)*C(4,KK)
      DO 36 K=1,4
   36 Q(K) = Q(K)-B(K,1)*Z(1,J-2)-B(K,2)*Z(2,J-2)-B(K,3)*Z(3,J-2)
     $  -B(K,4)*Z(4,J-2)
      DO 37 K=1,4
   37 Z(K,J-1) = D(K,1)*Q(1)+D(K,2)*Q(2)+D(K,3)*Q(3)+D(K,4)*Q(4)
   40 CONTINUE
      DO 41 K=1,4
      A(1,K) = 0.
      A(2,K) = 0.
      A(3,K) = 0.
      A(4,K) = 0.
      B(1,K) = 0.
      B(2,K) = 0.
   41 Q(K) = 0.
      A(1,1) = 1.
      A(1,2) = -.5*HS(LU)
      A(2,2) = 1.
      A(2,3) = A(1,2)
      A(3,2) = 1.
      A(4,4) = 1.
      B(1,1) = -1.
      B(1,2) = A(1,2)
      B(2,2) = -1.
      B(2,3) = A(1,2)
      Q(1) = -G(1,LU)+G(1,LT)+.5*HS(LU)*(G(2,LU)+G(2,LT))
      Q(2) = -G(2,LU)+G(2,LT)+.5*HS(LU)*(G(3,LU)+G(3,LT))
      DO 42 K=1,4
      DO 42 KK=1,4
   42 D(K,KK) = A(K,KK)-B(K,1)*E(1,KK,LT)-B(K,2)*E(2,KK,LT)
     $  -B(K,3)*E(3,KK,LT)-B(K,4)*E(4,KK,LT)
      CALL INVERT (D)
      DO 43 K=1,4
   43 Q(K) = Q(K)-B(K,1)*Z(1,LT)-B(K,2)*Z(2,LT)-B(K,3)*Z(3,LT)
     $  -B(K,4)*Z(4,LT)
      DO 44 K=1,4
   44 DG(K,LU) = D(K,1)*Q(1)+D(K,2)*Q(2)+D(K,3)*Q(3)+D(K,4)*Q(4)
      DO 45 JJ=1,LT
      J = LU-JJ
      DO 45 K=1,4
   45 DG(K,J) = Z(K,J)-E(K,1,J)*DG(1,J+1)-E(K,2,J)*DG(2,J+1)
     $  -E(K,3,J)*DG(3,J+1)-E(K,4,J)*DG(4,J+1)
```

```
      DG(1,1) = 0.
      DG(2,1) = 0.
      DO 48 J=1,LU
      DO 48 K=1,4
      IF (IT .GT. 1) GO TO 48
      DG(K,J) = .5*DG(K,J)
   48 G(K,J) = G(K,J)+DG(K,J)
C     TEST FOR SEPARATED PROFILE
      IF (G(3,1) .LE. 0.) PRINT 114,N,IT,G(4,1)
      IF (G(3,1) .LE. 0.) GO TO 86
C     FIND JMAX,JMIN,JDEL
      DO 49 J=2,JU
      JMAX = J
      IF (G(2,J) .LT. G(2,J-1)) GO TO 50
      IF (J .EQ. JDEL) GO TO 53
   49 CONTINUE
      GO TO 53
   50 DO 51 J=JMAX,JU
      JMIN = J
      IF (G(2,J) .GE. G(2,J-1)) GO TO 52
   51 CONTINUE
   52 IF (JMIN .GE. JDEL) GO TO 55
   53 IF (JMAX .GE. JDEL) JMIN=1
      DO 54 J=JMIN,LU
      JDEL = J
      IF (G(2,J) .GT. .99) GO TO 57
   54 CONTINUE
      GO TO 57
   55 JMIN = 1
      DO 56 J=JMAX,JU
      JDEL = J
      IF (G(2,J) .LT. 1.01) GO TO 57
   56 CONTINUE
   57 IF (JMAX .GT. JDEL) JMAX=JDEL
      IF (MXMN .GT. 0) JMIN=1
      IF (JDEL .EQ. JU) GO TO 60
      IF (JMIN .GT. 1) G(2,JDEL) = 1.
      G(1,JDEL) = G(1,JDEL-1)+.5*HS(JDEL)*(G(2,JDEL)+G(2,JDEL-1))
C     ADJUST SOLUTION FOR NEW DELTA
      JSAVE = JDEL+1
      DELTA(N) = CS*ETA(JDEL)
      DO 59 J=JSAVE,JU
      G(1,J) = G(1,J-1)+HS(J)*G(2,J-1)
      G(2,J) = 1.
      G(3,J) = 0.
```

```
   59 CONTINUE
      G(3,JDEL) = (G(2,JDEL+1)-G(2,JDEL-1))/(ETA(JDEL+1)-ETA(JDEL-1))
   60 G(3,JDEL-1) = (G(2,JDEL)-G(2,JDEL-2))/(ETA(JDEL)-ETA(JDEL-2))
      IF (JMAX .LT. JDEL) JMAX=JMAX-1
      IF (JMIN .GT. 1) JMIN=JMIN-1
C     TEST FOR CONVERGENCE
      IF (IT .EQ. 1) GO TO 61
      TOL = .005
      IF (IT .GT. 5) TOL=.01
      IF (IT .GT. 7) TOL=.015
      DHW = ABS(DG(3,1)/(G(3,1)+.5*DG(3,1)))
      DCPW = ABS(DG(4,1))
      IF (DHW .LT. TOL .AND. DCPW .LT. TOL) GO TO 62
   61 CONTINUE
   62 CONTINUE
C     OUTPUT AND STORAGE
      IF (N .LE. 3) GO TO 92
      IF (JMIN .EQ. 1) GO TO 92
      IF (G(2,JMIN)*UEP .LT. .98*UWJS) GO TO 92
      MXMN = MXMN+1
      UEWJ(N) = UEP*G(2,JMIN)
      DO 91 J=1,JU
      F(5,J) = UEP*G(1,J)
      F(6,J) = G(4,J)+(UEP*G(2,J))**2
      IF (J .GT. JMIN) GO TO 90
      G(1,J) = G(1,J)/G(2,JMIN)
      G(2,J) = G(2,J)/G(2,JMIN)
      G(3,J) = G(3,J)/G(2,JMIN)
      GO TO 91
   90 G(1,J) = G(1,J-1)+HS(J)
      G(2,J) = 1.
      G(3,J) = 0.
      G(4,J) = G(4,JMIN)
   91 CONTINUE
      JDEL = JMIN
      JMIN = 1
   92 CONTINUE
      CPWJ(N) = G(4,1)
      CFWJ(N) = 2.*UEWJ(N)*G(3,1)/(CS*REC)
      UMAX = G(2,JMAX)
      UMIN = G(2,JMIN)
      CPOT = 1.-UEP**2
      PRINT 100,N,XWJ(N),UEWJ(N),CPWJ(N),CPE,CPOT
      PRINT 101,CFWJ(N),X,DELTA(N),UMAX,UMIN
      PRINT 102,IT,ETA(JMAX),ETA(JMIN),DHW,DCPW
```

```
      PRINT 103,JDEL,G(3,1)
      NPRNT = 0
      IF (NPRNT .EQ. 0) GO TO 64
      PRINT 104
      C1 = 2.*UEWJ(N)/(CS*REC)
      DO 63 J=1,LU,3
      C2 = C1*EPS(1,J)*(G(3,J)-GG(2,J)*G(2,J)+GG(6,J)*(G(2,J)-1.))
   63 PRINT 105,ETA(J),G(1,J),G(2,J),G(3,J),G(4,J),EPS(1,J),C2
   64 CONTINUE
C     ADJUST GRID FOR DOWNSTREAM CALCULATIONS
      IF (N .NE. 3) GO TO 75
      PRINT 115
      DO 65 J=2,JU
      IF (ETA(J) .GT. .05) GO TO 66
   65 JK = J+1
   66 CONTINUE
      RS = 1.055
      GG(1,JK-1) = ETA(JK-1)
      JEO = JU
      DO 67 J=JK,JU
      HS(J) = HS(J-1)*RS
      IF (HS(J) .GT. 1.) HS(J)=1.
      GG(1,J) = GG(1,J-1)+HS(J)
      IF (GG(1,J) .GT. ETA(JDEL) .AND. GG(1,J-1) .LT. ETA(JDEL)) JEO=J
   67 CONTINUE
      JB = 1
      DO 70 J=JK,JEO
      DO 68 JJ=JB,NT
      JA = JJ-1
      IF (ETA(JJ) .GE. GG(1,J)) GO TO 69
   68 CONTINUE
   69 JB = JA+1
      C1 = (GG(1,J)-ETA(JA))/(ETA(JB)-ETA(JA))
      DO 70 JJJ=1,4
   70 F(JJJ,J) = G(JJJ,JA)+(G(JJJ,JB)-G(JJJ,JA))*C1
      DO 71 J=JK,JU
      ETA(J) = GG(1,J)
      ET(J) = .5*(ETA(J)+ETA(J-1))
      GG(3,J) = GE/(1.+GE*ET(J))
      DO 71 JJ=1,4
   71 G(JJ,J) = F(JJ,J)
      JDEL = JEO
      G(2,JDEL) = 1.
      JK = JDEL+1
      DO 72 J=JK,JU
```

```
      G(1,J) = G(1,J-1)+HS(J)*G(2,J-1)
      G(2,J) = 1.
      G(3,J) = 0.
      G(4,J) = 1.-UEP**2
   72 CONTINUE
      JMAX = JU
      DO 73 J=2,JDEL
      IF (G(2,J) .GE. G(2,J-1) .AND. G(2,J) .GE. G(2,J+1) .AND. JMAX
     $   .EQ. JU) JMAX=J
      IF (G(2,J) .LE. G(2,J-1) .AND. G(2,J) .LE. G(2,J+1)) JMIN=J
   73 CONTINUE
      IF (NPRNT .EQ. 0) GO TO 75
      DO 74 J=1,JU
   74 PRINT 106,ETA(J),G(1,J),G(2,J),G(3,J),G(4,J)
   75 CONTINUE
   86 CONTINUE
  100 FORMAT (/,10H JET POINT,I4,6X,4HXI =,E13.6,3X,4HUE =,E14.7,2X,
     $5HCPW =,E13.6,2X,5HCPE =,E13.6,2X,10HCP (POT) =,E11.4)
  101 FORMAT (20X,6HTAUW =,E12.5,2X,7HDELXI =,E12.5,1X,7HDELTA =,E11.4,
     $2X,6HGMAX =,E12.5,2X,6HGMIN =,E12.5)
  102 FORMAT (20X,9HITERATION,I4,7X,8HETAMAX =,F9.4,3X,
     $ 8HETAMIN =,F9.4,3X,5HDHW =,E13.6,2X,6HDCPW =,E14.7)
  103 FORMAT (20X,8HJDELTA =,I4,8X,4HHW =,E14.7)
  104 FORMAT (/,8X,3HETA,13X,1HF,15X,1HG,15X,1HH,14X,2HCP,14X,4HEPS+,
     $ 13X,3HTAU)
  105 FORMAT (7E16.7)
  106 FORMAT (5E16.7)
  110 FORMAT (6E13.6)
  114 FORMAT (//,40H SEPARATED PROFILE CALCULATED AT STATION,I4,5X,
     $12HON ITERATION,I4,5X,5HCPW =,E16.7)
  115 FORMAT (//,42H GRID ADJUSTED FOR DOWNSTREAM CALCULATIONS,//)
      RETURN
      END
```

```
      SUBROUTINE EDDY (E1,E2,E3,E4,E5,E6,E7,JMAX,JMIN,JDEL,LU,L,IT)
      DIMENSION S(4,50)
      COMMON/HBDBJE/ETA(121),EPS(2,121),G(4,121),GG(7,121)
      N = L
      JE = JDEL
      IF (JMIN .GT. 1) JE=JMIN
      S(1,N) = E3
      C1 = E1*E2*E3
      IF (N .GT. 1 .AND. IT .EQ. 1)C1=1.05*C1*S(1,N-1)/E3
      C2 = C1/15.
      C4 = 0.
      DO 4 J=2,JMAX
    4 C4 = C4+.5*(ETA(J)-ETA(J-1))*(G(2,J)+G(2,J-1))*(1.-.5*(G(2,J)
     $ +G(2,J-1))/G(2,JMAX))
      S(2,N) = C1*C4
      IF (N .GT. 1 .AND. S(2,N) .LT. S(2,N-1)) S(2,N)=S(2,N-1)
      RET = S(2,N)
      IF (RET .LT. 300.) RET=300.
      C4 = (RET*.001)**2
      CK1 = .4+.19/(1.+.49*C4)
      CK3 = 26.+14./(1.+C4)
      C4 = RET/425.-1.
      IF (C4 .LT. 0.) C4=0.
      C4 = 1.-EXP(-.243*C4**.5-.298*C4)
      CK2 = .0168*1.55/(1.+.55*C4)
      C3 = CK1**2*C1
      JWJ = 2
      IF (JMIN .EQ. 1) JWJ=1
      IF (JMIN .EQ. 1 .AND. JMAX .EQ. JDEL) JWJ=0
      IF (JWJ .EQ. 0) GO TO 8
      C4 = .5*(G(2,JMAX)+G(2,JE))
      DO 1 J=JMAX,JDEL
      IF (G(2,J) .LE. C4) GO TO 2
    1 JL = J+1
    2 SF = ETA(JL)-ETA(JMAX)
      GD = G(2,JMAX)-G(2,JE)
      GL = G(2,JE)/GD
      SL = .471
      IF (GL .LT. 3.04 .AND. GL .GT. 1.1) SL=.403+.035*(GL-1.1)
      IF (GL .LE. 1.1) SL=.541*(GL-.52)*(GL-1.1)-1.114*GL*(GL-1.1)
     $   +.632*GL*(GL-.52)
      SL = SL*SF
      EB = 1.4
      IF (GL .LT. 3.04 .AND. GL .GT. 1.1) EB=1.59-.098*(GL-1.1)
      IF (GL .LE. 1.1) EB=3.65*(GL-.52)*(GL-1.1)-5.71*GL*(GL-1.1)
```

```
     $   +2.49*GL*(GL-.52)
         EB = ETA(JMAX)+EB*SF
         S(3,N) = C2*GD*SL
         C4 = E1*ETA(JL)/E6
         CC1 = 1.34*C4**2
         CC = (1.+4.48*C4-CC1)**2/(1.+CC1)/(1.+.3*C4)
         S(3,N) = S(3,N)*CC
         IF (N .GT. 1) S(3,N)=.5*(S(3,N)+S(3,N-1))
         S(4,N) = S(3,N)
         IF (N .GT. 1) GO TO 5
         DO 3 J=2,LU
         JJ = LU+1-J
         IF (EPS(1,JJ) .LT. EPS(1,JJ+1)) GO TO 5
       3 EPEB = EPS(1,JJ+1)-1.
       5 C4 = 1.+S(4,N)
         C5 = .5*S(4,N)
         IF (JWJ .EQ. 1) GO TO 9
         C6 = ETA(JMAX)+2.3*SF
         DO 6 J=JL,LU
         IF (ETA(J) .GT. C6) GO TO 7
       6 JM = J
       7 C5 = .5*EPEB
         EB = .8*ETA(JDEL)
         SL = .127*ETA(JDEL)
         GO TO 9
       8 C5 = .5*CK2*C1*(ETA(JDEL)*G(2,JDEL)-G(1,JDEL))
         EB = .8*ETA(JDEL)
         SL = .127*ETA(JDEL)
         C4 = 1.+2.*C5
       9 SL = 1.414*SL
         EPO = 1.+CK2*C1*(ETA(JMAX)*G(2,JMAX)-G(1,JMAX))
         IF (N .GT. 1 .AND. IT .EQ. 1) C1=.95*E1*E2*E3
         C6 = (C1*G(3,1))**.5
         C7 = 11.8/C6
         C8 = 1.+E1**2*E2*E4*C7*(1.+.5*E1*C7/E6)/(E3*G(3,1))
         IF (C8 .LT. .7) C8=.7
         C8 = C8**.5*C6/(CK3*(1.+E1*C7/E6))
         DO 10 J=1,JMAX
         C6 = C8*ETA(J)
         C6 = CK1*ETA(J)*(1.-EXP(-C6))
         EPS(1,J) = 1.+C1*G(3,J)*C6**2
         IF (EPS(1,J) .GT. EPO) EPS(1,J)=EPO
         IF (EPS(1,J) .GE. EPO) GO TO 11
      10 JC = J
      11 CONTINUE
```

```
      JC = JC+1
      C6 = .5*(C4-EPS(1,JC))
      C7 = .175*ETA(JMAX)
      C8 = .65*ETA(JMAX)
      DO 12 J=JC,JMAX
   12 EPS(1,J) = EPS(1,JC)+C6*(1.+ERF((ETA(J)-C8)/C7))
      IF (JWJ .EQ. 1) JM=JMAX
   13 IF (JWJ .EQ. 0) JM=JC
      DO 14 J=JM,LU
   14 EPS(1,J) = 1.+C5*(1.-ERF((ETA(J)-EB)/SL))
      IF (JWJ .LE. 1) GO TO 17
      DO 15 J=JMAX,JL
   15 EPS(1,J) = C4
      C5 = EPS(1,JM)-C4
      C6 = 1.570796/(ETA(JM)-ETA(JL))
      DO 16 J=JL,JM
   16 EPS(1,J) = C4+C5*(1.-COS(C6*(ETA(J)-ETA(JL))))
   17 DO 18 J=1,LU
   18 EPS(2,J) = EPS(1,J)*GG(4,J)
      C7 = -.1387/SF
      C6 = ETA(JMAX)+.85*SF
      C5 = .6
      C4 = 1./C5**3/ETA(JMAX)
      C5 = C5*ETA(JMAX)
      DO 20 J=1,LU
      C8 = 0.
      IF (ETA(J) .LT. C5) C8=C4*ETA(J)
      IF (ETA(J) .GE. C5 .AND. J .LE. JMAX) C8=(ETA(JMAX)/ETA(J))**2
      IF (J .GT. JMAX .AND. ETA(J) .LE. C6) C8=1.-1.387*
     $ ((ETA(J)-ETA(JMAX))/SF)**2
   20 GG(6,J) = C7*C8
      RETURN
      END
```

```
      SUBROUTINE RADIUS (X,RC)
C     KIND AIRFOIL
      RC = .037777778
      IF (X .LT. .001) RC=.1
      IF (X .EQ. 0.) RC=.408
      RETURN
      END
```

```
      SUBROUTINE INVERT (D)
      DIMENSION D(4,4),U(4,4),UI(4,4)
C     INVERT A 4X4 MATRIX
      DO 1 J=1,4
    1 U(J,1) = D(J,1)
      DO 2 J=2,4
      U(1,J) = D(1,J)/U(1,1)
    2 U(J,2) = D(J,2)-U(J,1)*U(1,2)
      DO 3 J=3,4
      U(2,J) = (D(2,J)-U(2,1)*U(1,J))/U(2,2)
    3 U(J,3) = D(J,3)-U(J,1)*U(1,3)-U(J,2)*U(2,3)
      U(3,4) = (D(3,4)-U(3,1)*U(1,4)-U(3,2)*U(2,4))/U(3,3)
      U(4,4) = D(4,4)-U(4,1)*U(1,4)-U(4,2)*U(2,4)-U(4,3)*U(3,4)
      UI(1,1) = U(2,2)*U(3,3)*U(4,4)
      UI(2,1) = -U(2,1)*U(3,3)*U(4,4)
      UI(3,1) = U(2,1)*U(3,2)*U(4,4)-U(3,1)*U(2,2)*U(4,4)
      UI(4,1) = U(2,1)*U(4,2)*U(3,3)+U(3,1)*U(2,2)*U(4,3)
     $     -U(2,1)*U(3,2)*U(4,3)-U(2,2)*U(3,3)*U(4,1)
      UI(1,2) = -U(1,2)
      UI(2,2) = U(1,1)*U(3,3)*U(4,4)
      UI(3,2) = -U(1,1)*U(3,2)*U(4,4)
      UI(4,2) = U(1,1)*U(3,2)*U(4,3)-U(1,1)*U(4,2)*U(3,3)
      UI(1,3) = U(1,2)*U(2,3)-U(1,3)
      UI(2,3) = -U(2,3)
      UI(3,3) = U(1,1)*U(2,2)*U(4,4)
      UI(4,3) = -U(1,1)*U(4,3)*U(2,2)
      UI(1,4) = -U(1,2)*U(2,3)*U(3,4)+U(1,2)*U(2,4)+U(1,3)*U(3,4)-U(1,4)
      UI(2,4) = U(2,3)*U(3,4)-U(2,4)
      UI(3,4) = -U(3,4)
      UI(4,4) = U(1,1)*U(2,2)*U(3,3)
      DO 4 J=1,4
    4 D(4,J) = UI(4,J)
      DO 5 J=1,3
      D(J,4) = UI(J,4)*UI(4,4)
      D(3,J) = UI(3,J)+UI(3,4)*UI(4,J)
      D(2,J) = UI(2,3)*UI(3,J)+UI(2,4)*UI(4,J)
    5 D(1,J) = UI(1,3)*UI(3,J)+UI(1,4)*UI(4,J)
      D(2,2) = D(2,2)+UI(2,2)
      D(2,1) = D(2,1)+UI(2,1)
      D(1,2) = D(1,2)+UI(1,2)*UI(2,2)
      D(1,1) = D(1,1)+UI(1,1)+UI(1,2)*UI(2,1)
      C = U(1,1)*U(2,2)*U(3,3)*U(4,4)
      DO 6 J=1,4
      DO 6 K=1,4
    6 D(J,K) = D(J,K)/C
```

```
      C = ABS(C)
      IF (C .LT. 1.E-3) PRINT 7,C
    7 FORMAT (38H NEARLY SINGULAR MATRIX, DETERMINANT =,E18.7)
      RETURN
      END
```

```
      SUBROUTINE SLOTBL
      DIMENSION A(5,241),ETA(121)
      COMMON/JETMIX/HS(121),F(6,121),S(18)
      COMMON/BLSLBL/EDV(5,241),NBL,NEDGE
      COMMON/MAINSL/STFT(7),LAMSL
      EQUIVALENCE (A(1,1),EDV(1,1))
      DO 1 J=1,7
    1 S(J) = STFT(J)
      CS = S(1)
      UT = S(6)
      C1 = CS*S(2)*UT
      C2 = UT/S(3)
      HSJET = .0005
      RS = 1.13
      JU = 121
      HS(1) = HSJET/RS
      ETA(1) = 0.
      DO 2 J=2,JU
      HS(J) = HS(J-1)*RS
      IF (HS(J) .GE. .04) HS(J)=.04
      ETA(J) = ETA(J-1)+HS(J)
      IF (ETA(J) .GT. .006) RS=1.1
      IF (ETA(J) .GT. .1) RS=1.15
      JCL = J
      IF (ETA(J) .GT. .45) GO TO 3
    2 CONTINUE
    3 HCL = .5-ETA(JCL)
      HS(JCL+1) = 2.*HCL
      ETA(JCL+1) = ETA(JCL)+HS(JCL+1)
      DO 4 J=2,JCL
      K = JCL+J
      I = JCL+2-J
      HS(K) = HS(I)
    4 ETA(K) = ETA(K-1)+HS(K)
      JD = 2*JCL
      CI = 0.
      F(1,1) = 0.
      F(2,1) = 0.
      F(3,1) = C1*C2
      F(5,1) = 1.
      DO 5 J=2,JCL
      F(5,J) = 1.+.4*(C1*ETA(J))**3/((C1*ETA(J))**2+324.)
     $   /(1.+6.8*CS*ETA(J)/S(1))
      IF (LAMSL .EQ. 1) F(5,J) = 1.
      F(3,J) = F(3,1)/F(5,J)*(1.-2.*CS*ETA(J)/S(1))
```

```
      F(2,J) = F(2,J-1)+.5*HS(J)*(F(3,J)+F(3,J-1))
      F(1,J) = F(1,J-1)+.5*HS(J)*(F(2,J)+F(2,J-1))
    5 CI = CI+.5*HS(J)*(F(2,J)**2+F(2,J-1)**2)
      CI = 2.*CI+2.*HCL*F(2,JCL)**2
      F(1,JCL+1) = F(1,JCL)+2.*HCL*F(2,JCL)
      DO 7 J=1,JCL
      K = JCL+J
      I = JCL+1-J
      IF (J .EQ. 1) GO TO 6
      F(1,K) = F(1,K-1)+F(1,I+1)-F(1,I)
    6 F(2,K) = F(2,I)
      F(3,K) = -F(3,I)
    7 F(5,K) = F(5,I)
      CMU = 2.*CS*S(3)**2*CI
      UAVE = CS*S(3)*F(1,JD)/S(1)
      CJ = CS*S(3)*F(1,JD)
      UMAX = S(3)*F(2,JCL)
      PRINT 101
      PRINT 102,CMU,CJ,UAVE,UMAX,F(3,1)
      JBL = NEDGE+10
      IF (JBL .GT. NBL) JBL = NBL
      JLO = JU-JD
      JO = (6*JBL-3*JLO)/(2*JLO)+1
      JR = JLO/3
      JL = JD+1
      JR1 = JR+JL
      JR2 = 2*JR+JL
      C3 = (2.*S(5))**.5/(CS*S(2)**.5*S(3))
      K = 1
      LL = 0
      DO 8 J=JL,JU
      LL = LL+1
      IF (LL .EQ. 1 .AND. J .LE. JR1) GO TO 8
      K = K+1
      IF (J .GT. JR2) K=K+JO
      ETA(J) = ETA(JD)+C3*A(1,K)
      F(1,J) = F(1,JD)+C3*A(2,K)
      F(2,J) = A(3,K)
      F(3,J) = A(4,K)/C3
      F(5,J) = A(5,K)
    8 IF (LL .EQ. 1) LL=-1
      DO 9 J=JL,JR1,2
      ETA(J) = .5*(ETA(J-1)+ETA(J+1))
      F(1,J) = .5*(F(1,J-1)+F(1,J+1))
      F(2,J) = .5*(F(2,J-1)+F(2,J+1))
```

```
      F(3,J) = .5*(F(3,J-1)+F(3,J+1))
    9 F(5,J) = .5*(F(5,J-1)+F(5,J+1))
      DO 11 J=1,JU
      IF (J .GT. JD) HS(J)=ETA(J)-ETA(J-1)
   11 CONTINUE
      S(5) = 0.
      DO 12 J=1,JU
      IF (J .GT. JL .AND. F(2,J) .GT. .99 .AND. S(5) .EQ. 0.)
     $ S(5) = S(1)*ETA(J)
   12 F(4,J) = S(4)
      S(4) = S(3)
      NPRNT = 0
      IF (NPRNT .EQ. 0) GO TO 13
      DO 10 J=1,JU
   10 PRINT 104,ETA(J),F(1,J),F(2,J),F(3,J),F(4,J),F(5,J)
   13 CONTINUE
  101 FORMAT (///,10X,24H JET STARTING CONDITIONS)
  102 FORMAT (/,6H CMU =,F8.5,5X,4HCM =,F 9.6,5X,6HUAVE =,F7.3,5X,
     $ 6HUMAX =,F7.3,5X,4HHW =,F7.2)
  104 FORMAT (6E13.6)
      RETURN
      END
```

# DISTRIBUTION LIST

Chief of Naval Research
Department of the Navy
Arlington, Virginia 22217
ATTN: Vehicle Technology Program, Code 211 (7 cys)

Chief of Naval Development
Department of the Navy
Washington, D. C. 20360
ATTN: NAVMAT 0331 (1 cy)
NAVMAT 0334 (1 cy)

Naval Air Systems Command
Department of the Navy
Washington, D. C.
ATTN: NAVAIR 320D (1 cy)
NAVAIR 5301 (1 cy)
NAVAIR 53013 (1 cy)

Naval Ship Research and Development Center
Aviation and Surface Effects Department
Bethesda, Maryland 20084
ATTN: Director, Aviation Department, Code 16 (1 cy)
Library, Aviation Department, Code 5643 (1 cy)

Naval Research Laboratory
Washington, D. C. 20375
ATTN: Technical Information Office, Code 2627 (6 cys)
Library, Code 2629 (3 cys)

Superintendent
U. S. Naval Academy
Annapolis, Maryland 21402 (1 cy)

Superintendent
U. S. Naval Postgraduate School
Monterey, California 93940 (1 cy)

U. S. Naval Air Development Center
Johnsville, Warminster, Pennsylvania 18974
ATTN; Aeromechanics Department (1 cy)

Commandant of the Marine Corps.
Washington, D. C. 20380
ATTN: Dr. A. L. Slafkosky
Scientific Advisor (Code RD-1) (1 cy)

Defense Documentation Center
Cameron Station, Bldg 5
Alexandria, Virginia 22314 (12 cys)

Contract Administrator
Southeastern Area
2110 G. Street, N. W.
Washington, D. C. 20037 (1 cy)

ONR Residence Representative
Johns Hopkins University
Room 46, Garland Hall
39th and Charles St.
Baltimore, Maryland 21218 (1 cy)

Department of the Army
DCS for Research Development and Acquisition
Washington, D. C. 20310
ATTN: DAMA-WSA (Mr. R. L. Ballard) (1 cy)

U. S. Army Materiel Command
5001 Eisenhower Avenue
Alexandria, Virginia 22333 (1 cy)
ATTN: AMCRD-F

Director, Headquarters
U. S. Army Air Mobility R & D Lab
Ames Research Center
Moffett Field, California 94035 (1 cy)

Director, Ames Directorate
U. S. Army Air Mobility R & D Lab
Ames Research Center
Moffett Field, California 94035 (1 cy)

Director, Langley Directorate
U. S. Army Air Mobility R & D Lab
Langley Research Center
Hampton, Virginia 23665 (1 cy)

Director, Eustis Directorate
U. S. Army Air Mobility R & D Lab
Fort Eustis, Virginia 23604 (1 cy)

U. S. Air Force Flight Dynamics Laboratory
Wright-Patterson, AFB, OHIO 45433
ATTN: PT, Prototype Division (1 cy)
FGC, Control Criteria Branch (1 cy)
FXM, Aeromechanics Branch (1 cy)

Air Force Office of Scientific Research
1400 Wilson Boulevard
Arlington, Virginia 22209
ATTN: Mechanics Division (1 cy)

National Aeronautics and Space Administration
600 Independence Avenue, S. W.
Washington, D. C. 20546
ATTN: Code RAA (1 cy)
Code RAV (1 cy)

National Aeronautics and Space Administration
Ames Research Center
Moffett Field, California 94035
ATTN: Large-Scale Aerodynamics Branch (1 cy)

National Aeronautics and Space Administration
Langley Research Center
Hampton, Virginia 23665
ATTN: Subsonic-Transonic Aerodynamics Division (1 cy)